Studies on Measurement Time Reduction Techniques for Insulation Diagnostics in High Voltage Equipment

Thesis Submitted by
Soumya Chatterjee

Doctor of Philosophy (Engineering)

Electrical Engineering Department,
Faculty Council of Engineering & Technology
Jadavpur University
Kolkata, India

2019

JADAVPUR UNIVERSITY
KOLKATA-700032, INDIA

INDEX NO. 247/16/E

1. Title of the thesis

Studies on Measurement Time Reduction Techniques for Insulation Diagnostics in High Voltage Equipment

2. Name, Designation and Institution of the Supervisors

Dr. Sivaji Chakravorti
Professor,
Electrical Engineering Department
Jadavpur University
Kolkata 700032

Dr. Biswendu Chatterjee
Associate Professor,
Electrical Engineering Department
Jadavpur University
Kolkata 700032

3. List of Journal Publications:

- **S.Chatterjee,** A.K.Pradhan, S.Dalai, B.Chatterjee and S.Chakravorti, "Reducing Frequency Domain Spectroscopy Measurement Time for Condition monitoring of Oil-Paper Insulation using Non-sinusoidal Excitations", ***IET Science, Measurement & Technology*****,** vol.11, no.2, pp. 204–212, 2017.

- **S.Chatterjee**, S.Dalai, S.Chakravorti and B.Chatterjee "Use of Chirp Excitations for Frequency Domain Spectroscopy Measurement of Oil-paper Insulation", ***IEEE Transactions on Dielectrics and Electrical Insulation*****,** vol.25, no.2, pp. 1103–1111, 2018.

- **S.Chatterjee**, A.K.Pradhan, S.Dalai, S.Chakravorti and B.Chatterjee, "A Non-linear Model for Sensing Moisture Content in Transformers at Reduced Time", ***IEEE Sensors Journal***, vol.19, no.12, pp.4639-4646, 2019.

4. List of Presentations in International/National Conferences

- **S.Chatterjee,** A.K.Pradhan, B.Chatterjee and S.Chakravorti, "An Advanced Technique for Frequency Domain Spectroscopy of Oil-Paper Insulation at Reduced Time using Triangular Excitation" ***Proceedings of 1st IEEE International Conference on Energy Economics and Environment,*** **(*ICEEE*)**, Noida, Uttar Pradesh, India, pp.1-4, 2015.

- **S.Chatterjee**, S.Dalai, B.Chatterjee and S.Chakravorti, "A Method to Reduce FDS Measurement Time Using Logarithmic Chirp Excitation Voltage," ***Proceedings of 3rd IEEE International Conference on Condition Assessment Techniques in Electrical Systems (CATCON),*** Rupnagar, Punjab, India, pp. 248-252, 2017.

Certificate from the supervisors

This is to certify that the thesis entitled "***Studies on Measurement Time Reduction Techniques for Insulation Diagnosis in High Voltage Equipment***" submitted by Shri **Soumya Chatterjee**, who got his name registered on 18/04/2016 for the award of Ph.D (Engg.) degree of Jadavpur University is absolutely based upon his own work under the supervision of Prof. Sivaji Chakarvorti and Dr. Biswendu Chatterjee and that neither his thesis nor any part of the thesis has been submitted for any degree/diploma or any other academic award anywhere before.

_____

Signature of the Supervisor and Date
with Official Seal

_____

Signature of the Supervisor and Date
with Official Seal

Acknowledgment

The author would like to express his sincere gratitude and deep appreciation to his supervisors *Prof. Sivaji Chakravorti* and *Dr. Biswendu Chatterjee* of Electrical Engineering Department, Jadavpur University for their invaluable guidance in carrying out the thesis work. The author has been provided with necessary freedom during the course of the research work and at the same time the intense supervision by the supervisors has helped to enhance the quality of the research. Their moral support, amiable and amicable personality, encouragement and profound knowledge about the subject have made the research work possible. Besides, the author is also grateful to the supervisors for providing necessary mental support during difficult times helping him to become a better individual which led to his overall professional development.

The author would like to express his profound gratitude to Dr. Sovan Dalai, Associate Professor of Electrical Engineering Department, Jadavpur University for his active involvement, providing necessary suggestions and advice to carry out the research work.

The author is grateful to the Head of the Department of Electrical Engineering, Jadavpur University for providing necessary departmental facilities needed to carry out the research work.

The author would also like to acknowledge his respected teachers Prof. Abhijit Mukherjee and Prof. Kesab Bhattacharya for providing necessary advice and support in completing the research work.

The author would like thank his colleagues Dr. Arijit Baral, Dr. Arpan Pradhan, Dr. Riddhi Ghosh, Dr. Nasirul Haque, Mr. Suhas Deb, Mr. Biswajit Chakraborty and Mr. Subhajit Maur for providing support in various ways and making the laboratory an interesting place in carrying out the research work.

The author would also like to extend thanks to all the existing and past graduate students of the High Tension Laboratory of Electrical Engineering Department, Jadavpur University for making it possible to work in a homely atmosphere.

The author would specially like to express his heart-felt gratitude to Ms. Subhasree Raha for supporting him mentally, emotionally and helping him to

complete his research work. The author would also like to thank all of his beloved students for providing necessary mental support and help needed to carry out the research work.

The author would like to convey his deep love and respect towards his parents Mr. Swapan Chatterjee and Mrs. Shanta Chatterjee for their never ending support and encouragement during difficult times. Without their support, this work could never have been completed.

Finally, as it is impossible to mention everybody by name, the author would like to convey his gratitude to all who have contributed in one way or another, in making this work possible.

Dedicated to-
My parents

Abstract

Over the past few decades electrical power utilities all around the globe are primarily interested in asset management and proper utilization of resources. Among the different electrical equipment transformer is the most important asset to an electrical utility. This is because not only transformers are most expensive of all electrical equipment but also their failure leads to severe interruption of power supply, incurring huge financial loss to an electrical utility. One of the primary reasons behind the failure of a transformer is the degradation of oil-paper insulation. Therefore condition assessment of transformer insulation at periodic intervals is necessary to prevent premature failure of transformers. In this context, dielectric spectroscopy measurement in frequency domain also known as frequency domain spectroscopy (FDS) is a major non-invasive technique that is widely used to assess the condition of oil-paper insulation. In conventional FDS test, series of sine waves at distinct measurement frequency points starting from 0.1mHz to 1kHz are applied on the insulation under test, which makes conventional FDS test lengthy and very time consuming. The overall measurement time can go up to 10-11 hours which is practically problematic. This practical problem has been addressed in this thesis work and several methods to reduce FDS measurement time have been proposed which were not used in practice till date.

Chapter 1 of this thesis provides a comprehensive overview of existing techniques for condition monitoring of transformer oil-paper insulation and also introduces the research problem.

Chapter 2 presents a method to accelerate FDS measurement using regression approach. For this purpose both sinusoidal and non-sinusoidal waveforms are used for the purpose of experiment and reduction in FDS test time is determined using both sinusoidal and triangular excitation voltages.

Chapter 3 presents a method to reduce FDS measurement time using chirp signals. For this work, broadband excitation signals in the form of chirp waveforms with linear and logarithmic frequency sweeps are used for the purpose of experiment. The overall reduction in FDS measurement time is computed for both types of chirp signals.

Chapter 4 presents a non-linear model of oil-paper insulation using logarithmic chirp signal. Different parameters of non-linear model are found

to be sensitive to change in moisture content. A comparative study of the proposed model with the linear model is also presented.

Chapter 5 concludes the thesis by summarizing the main findings of the present work and also gives some idea of possible extension of the research work.

List of Symbols and abbreviations

Symbol	Description
ρ_v	Volume resistivity
$^\circ C$	Degree centigrade
$m.c\ (\%)$	Moisture content expressed in percentage
DP_t	Degree of polymerization at t^{th} instant
T	Operating temperature
E	Activation energy
R	Universal Gas constant
ppm	Parts per million
$\bar{I}_R$	Resistive component of current
$\bar{I}_c$	Capacitive component of current
C	Capacitance
ω	Angular frequency
δ	Loss angle
C_{HL}	Capacitance between high voltage and low voltage winding of the transformer
$E(t)$	Electric field at t^{th} instant
$D(t)$	Electric flux density at t^{th} instant
$J(t)$	Current density at t^{th} instant
$P(t)$	Polarization vector at t^{th} instant
σ_0	DC conductivity
ε_0	Permittivity of free space
$\delta(t)$	Dirac delta function
C_0	Geometric capacitance
V_c	Charging voltage
$i_{pl}(t)$	Polarization current at t^{th} instant
$i_{dpl}(t)$	Depolarization current at t^{th} instant
T_c	Charging time

$f(t)$	Dielectric response function
T_{d}	Discharging time
V_{R}	Recovery voltage
$\overline{\chi}(\omega)$	Complex susceptibility
$\chi'(\omega)$	Real part of complex susceptibility
$\chi''(\omega)$	Imaginary part of complex susceptibility
$\overline{C}(\omega)$	Complex capacitance
$C'(\omega)$	Real part of complex capacitance
$C''(\omega)$	Imaginary part of complex capacitance
$\tan\delta$	Dielectric dissipation factor
$\tan\delta_{\min}$	Minimum value of dielectric dissipation factor
e_k	Error at k^{th} point
$\hat{y}_k$	Fitted value at k^{th} point
$\overline{y}$	Mean of data points
SS_{res}	Summed square of residuals
SS_{tot}	Total sum of squares
R^2	Goodness of fit
$f_i(t)$	Instantaneous frequency
$\phi(t)$	Instantaneous phase
β	Chirp rate
T_{ch}	Time duration of the chirp signal
f_F	Final frequency of the chirp signal
f_I	Initial frequency of the chirp signal
A	Amplitude of the chirp signal
E_{ch}	Energy of the chirp signal
$G(n)$	Impulse response in time domain
S_{cr}	Cross correlation between output and input sequence
S_{rr}	Auto correlation of the input sequence

$\tan\delta_{Ch_i}$	Dielectric dissipation factor obtained using chirp signal at i^{th} measurement frequency
$\tan\delta_{cFDS_i}$	Dielectric dissipation factor obtained using conventional FDS measurement at i^{th} measurement frequency
MAE (%)	Mean absolute error percentage
$\hat{c}(n)$	Output of the Wiener model
$g(n)$	Added noise
$e(n)$	Error
$v(n)$	Output of the static non-linearity
$G(z)$	Discrete time transfer function
p	Order of the numerator coefficients of $G(z)$
q	Order of the denominator coefficients of $G(z)$
m	Order of static non-linearity
α	Numerator coefficient of the modified discrete time transfer function
β	Denominator coefficient of the modified discrete time transfer function
$\tan\delta_{M_j}$	Dielectric dissipation factor obtained from the proposed model using chirp signal at j^{th} measurement frequency
cFDS	Conventional frequency domain spectroscopy
CF	Crest factor
DP	Degree of polymerization
DAC	Digital to analog converter
DGA	Dissolved gas Analysis
FFA	Furfuraldehyde
FDS	Frequency domain spectroscopy
FFT	Fast Fourier Transform
GI	Galvanized iron
HV	High voltage
IR	Insulation resistance
LC	Linear chirp

LM	Linear model
LV	Low voltage
LGC	Logarithmic chirp
PI	Polarization index
PDC	Polarization depolarization current
RVM	Return voltage measurement
SNR	Signal to noise ratio
Trf	Transformer
WM	Wiener model

Contents

List of Figures

List of Tables

Chapter 1

Introduction

1.1 Introduction

Transformer is an important electrical equipment installed in power transmission and distribution network. For reliable power transmission and distribution, transformer plays a major role. Failure of transformer leads to interruption of power supply due to complete or partial shutdown of a substation, which incurs significant amount of financial loss to electric power utilities, involving huge cost of repair or replacement. In order to prevent such catastrophe, condition monitoring is of utmost importance, so that the premature failure of a transformer can be prevented. Condition monitoring of transformer can actually render reliable and uninterrupted power transmission and distribution, thereby facilitating the power network to be more resilient. Besides, most of the transformers, which are operating worldwide, are either nearing the end of their designed service life or have surpassed it [1]. Direct replacement of aged and degraded transformers with the new ones is not an economical and pragmatic solution as transformers are the costliest of all electrical equipment. Therefore, from a power utility point of view, maximizing the operating life of a transformer through condition based maintenance is a more feasible option. It is believed that the service life of a transformer can be increased if the condition assessment is done at periodic intervals [2]. Regular condition monitoring can impart knowledge regarding the state of the electrical equipment before a power utility can take corrective measures and schedule maintenance program, which is important from the point of view of asset management and proper utilization of resources. Therefore, electric power utilities all around the globe are making attempts to develop different diagnostic tools for reliable monitoring of transformers so that the outage of power supply can be reduced and at the same time the service life of a transformer can be increased substantially.

The insulation is the most important part of the transformer because majority of the transformers fail due to the degradation of their insulation condition [1-5]. The insulation system of the transformer is subjected to various transient and steady state electrical, chemical and thermal stresses throughout their service life. As a consequence, the insulation condition deteriorates substantially over the period of operation of the transformer from the date of

commissioning, which leads to the failure of the transformers in the long run. Before going into the details of the mechanism of insulation degradation, the basic components of the transformer insulation system and their dielectric properties are briefly elucidated below.

1.2 Brief overview of transformer insulation

The bulk insulation of the transformer consists of mineral oil and paper, together known as composite oil-paper insulation. The mineral oil in transformer is used as an insulating medium as well as coolant. The mineral oil is obtained from crude petroleum through fractional distillation. New transformer oil is a clear and transparent liquid composed of a mixture of mainly three types of hydrocarbon compounds, viz. alkane, naphthalene and aromatic hydrocarbons. The dielectric strength of new untreated transformer oil is about 30 kV_{rms} and after treatment it is 60 kV_{rms} measured using spherical electrode arrangement with diameter of 12.5mm-13mm with a gap spacing of 2.5mm [6]. The minimum flash point and the maximum pour point of transformer oil are 140°C and –6°C, respectively [6]. The minimum volume resistivity (ρ_v) and the dielectric dissipation factor (tanδ) at 90°C is of the order of 35×10^{12} Ω.cm and 0.2%, respectively [6]. However, transformer oil is hygroscopic in nature. Hence, moisture can easily get into oil during transportation, storage, refilling etc. The dielectric properties of the transformer oil change with both moisture ingress and aging (degradation) of the oil condition.

Paper in transformers is used to provide insulation as well as mechanical support. Paper is wrapped around the copper conductors (windings) to provide insulation between high voltage (HV) and low voltage (LV) windings. The paper insulation of transformer mainly consists of 90% cellulose, which is made from wood pulp and processed by kraft chemical process [7-8]. Cellulose is a polymer of glucose molecule linked together in a long polymeric chain. The presence of long chain length provides greater mechanical strength. The chemical formulae of cellulose is $(C_6H_{10}O_5)_n$, where 'n' is the degree of polymerization (DP). The DP value is an indicator of the mechanical strength of the paper insulation [8]. The volume resistivity is of the order of 10^{15}-10^{17} Ω.cm and the (tanδ) at power frequency varies between 3%-4%, respectively [9]. Besides offering good mechanical and electrical insulation properties, paper is also widely used in transformer insulation due to its low cost. However, the paper insulation being porous, it is hygroscopic in nature. Therefore, it is impregnated with mineral oil, which

fills up the small air pockets, reducing moisture affinity and at the same time increasing the dielectric strength. But, even after treatment or impregnation, it can still absorb moisture from the neighboring medium, i.e. oil, which reduces the dielectric properties of paper insulation significantly. Besides, having high affinity for moisture, paper insulation is also very reactive in the presence of oxygen and is thermally unstable at higher temperatures. The deterioration of the insulation system is a major concern and the main factors responsible for the degradation are discussed in the next section.

1.3 Degradation of oil-paper insulation system

It is well known that once the transformer is energized, the composite oil-paper insulation suffers an irreversible and slow degradation process, due to electrical, thermal and chemical stresses imposed upon it. The presence of high temperature, oxygen and moisture are three key factors that contribute to the degradation of insulation system of the transformer. The degradation of oil-paper insulation is the cumulative effect of all of these factors, which are explained below.

1.3.1 Degradation of oil

At elevated temperature, thermal degradation of mineral oil occurs. The rate of oil degradation becomes almost double for an increase in temperature of about 8°C-10°C. Due to decomposition of mineral oil at high temperature, varieties of by-products are formed, which affect the insulating properties of oil. The presence of oxygen at high temperature leads to oxidation of mineral oil. The main by-products of oxidation of oil include moisture (water), carbon dioxide (CO_2), carbon monoxide (CO), ethylene (C_2H_4), acids and sludge [10-11]. Different types of acids are formed due to oxidation of mineral oil among which low molecular weight and polar carboxylic acids (R-COOH) and phenol (C_6H_5OH) are very common [12]. Acids formed in oil cause damage to the insulation and corrosion of metals coming in contact with oil. Sludge is another by-product of oxidative aging of mineral oil. Sludge is a semi-solid insoluble substance that remains suspended in oil and gradually settle at the bottom and on other oil-immersed parts to form a thick layer. Sludge being bad conductor of heat impairs transfer of heat from the components where the heat is generated. Besides several other polar chemical compounds like alcohols (-OH), aldehydes (-CHO), ketones (RCR´) etc are generated due to oxidation process of oil [11]. The presence of these chemical contaminants increases the conductivity of the oil and decreases the

dielectric strength considerably. Moreover, due to oxidative aging highly reactive peroxide groups (R-O-O-R) are formed by breaking the hydrocarbon chain of the oil insulation, which further accelerates the oxidation mechanism and hence degradation of the oil insulation [11]. Along with oxygen, presence of moisture in mineral oil in any state (either in free or bonded) is detrimental to the insulation. Moisture is generated inside a transformer due to thermal degradation of mineral oil and cellulosic paper. Besides, some moisture can also seep into the transformer via breather or oil-drain valve in moisture rich environment. Moisture inside the transformer always remains in a dynamic state [13]. At very high temperature, moisture migrates from paper to the oil. However, it does not impose any serious threat as the solubility of moisture in mineral oil also increases with the increase of temperature, and the oil can absorb excess moisture. But the situation aggravates as the temperature goes down, when the excess amount moisture present in the oil tries to go back to the paper slowly, leaving the mineral oil to be saturated with moisture. This results in the presence of excess amount of moisture to be present in the oil which leads to partial discharges, flashover or even short circuit due to insulation failure.

1.3.2 Degradation of paper

Like mineral oil, the cellulosic paper insulation also undergoes gradual degradation due to thermal, oxidative and hydrolytic effects. During degradation, the cellulose undergoes depolymerization which is caused due to breakage of higher molecular weight cellulosic chain [8, 14]. The consequence is the loss of mechanical and dielectric strength of paper insulation, which can be identified by a marked reduction in DP value. The DP value of new paper insulation lies between 1200 to1300 after processing which reduces to about 200-300 with the degradation of insulation condition [15]. The tensile strength of the paper insulation decreases and it becomes brittle, until it falls off form the copper conductor indicating extreme aging condition of the insulation. Thermal degradation of paper insulation occurs due to chemical reactions in the presence of oxygen and moisture, the latter being more responsible for hydrolysis. The life of paper insulation is reduced by almost 50% for an increase in temperature rise by 6°C-8°C in the hot spot temperature range of 80 °C to 100 °C [16]. Increased temperature also leads to shortening of polymeric chains, which is responsible for mechanical failure of the paper insulation, which can no longer withstand the mechanical forces created inside the transformer during through fault. At very high temperature, the glycosidic linkage of the cellulose breaks with the

liberation of CO_2, CO, hydrogen (H_2), moisture and traces of methane (CH_4). Besides, thermal degradation of paper results in the formation of aldehydes (-CHO) and carboxyl (R-COOH) groups [11]. The presence of oxygen is also fatal to the paper insulation, since it results in oxidation that accelerates the breakage of polymeric chains leading to rapid depolymerization [18]. The oxidative depolymerization of cellulose results in the formation of hydrogen peroxide (H_2O_2) and several other highly reactive peroxide (R-O-O-R) groups. Moreover, in the presence of oxygen the hydroxyl (–OH) groups are oxidized to form carboxyl (R-COOH) and carbonyl groups (C=O), which again attack the cellulose chain and further contribute to the mechanism of insulation degradation. Presence of positive ions from metals like (Fe^{+}/Fe^{2+}/Cu^{2+}/Cu^{3+}) also acts as catalyst for oxidation [11]. Besides oxygen, the degradation of cellulosic insulation is highly influenced by the presence of moisture [18-20]. As mentioned earlier that the cellulose insulation being hygroscopic in nature, significant amount of moisture tends to reside within the cellulose. Although during manufacturing process of transformer, relatively dry kraft paper is used, yet some amount of moisture still remains within the insulation due to inappropriate factory drying out process (heating at very high temperature for several hours to wipe out any residual moisture). When a transformer is new, the paper insulation is almost dry containing about 0.5% moisture or even less. However, over the period of operation, the paper moisture content can increase up to 3%-4%, or even more depending on the operating condition of the transformer. The presence of moisture leads to hydrolysis by breaking the glycosidic chains liberating free glucose molecule. The rate of chain scission also increases with the increase in moisture content [21]. The number of chain break up can provide an idea about the degree of hydrolytic degradation. The degradation of wet cellulose is also accelerated at elevated temperature. Therefore, a very wet transformer is generally operated at reduced load in order to maximize their operating life.

The dynamics of moisture migration between paper and oil is a relatively complex phenomenon. The differences in vapour pressure play a key role in moisture migration from paper to oil and vice-versa [22-23]. Throughout the period of operation of the transformer, the moisture diffusion process continues and sometimes it may take several days for moisture to reach equilibrium between paper and oil insulation. Hence, estimation of paper moisture from oil using moisture equilibrium curve seldom delivers accurate results [24]. Therefore electrical utilities are trying to use different techniques for proper estimation of moisture content and aging status of the transformer insulation. A brief review of the state of the art condition monitoring

techniques for diagnosis of transformer insulation is presented in the following section.

1.4 Chemical Diagnostic Tests

As highlighted in section 1.2, the condition of the oil-paper insulation of the transformer degrades substantially over the period of operation resulting in the formation of several organic chemical compounds as well as gases. Therefore, condition of the insulation can be assessed using chemical diagnostic techniques. Some of the common chemical tests used for insulation diagnosis include dissolved gas analysis (DGA), degree of polymerization (DP) measurement and furan Analysis. A brief overview of the different chemical tests used for insulation diagnosis is given below.

1.4.1 Dissolved gas analysis (DGA)

Dissolved gas analysis is an important testing method to determine the condition of transformer insulation. During the operation of transformer, several gases are generated due to excess thermal and electrical stresses, partial discharge, arcing and overheating of oil and cellulosic paper insulation. The gases generated inside the transformer can be classified into two types, viz. (a) gases liberated due to thermal and electrical faults, which include mainly hydrogen (H_2), hydrocarbons (CH_4, C_2H_6, C_2H_4, C_2H_2) and oxides of carbon (CO_2, CO), (b) no fault gases which comprises Nitrogen (N_2) and Oxygen (O_2) [17]. Table 1.1 shows the key gases generated in a transformer along with the related fault types according to IEEE Std. C57.104-2008 [25]. These gases remain dissolved in mineral oil till the solubility limit is reached after which they come out of the oil and gets collected in gas collecting devices like gas blanket, Buchholz relay etc.

In general, there are three steps involved in a DGA test. The first step is the procurement of oil sample. A small volume of oil is extracted from either bottom or top drain valve of a transformer and is subsequently sampled using glass syringe as recommended in IEC 60567 [26]. The gases are extracted from the oil in vacuum and identification of the extracted gases is done using gas chromatographic analysis. The next step is to determine if a fault exists or not. During the normal operating condition of a transformer, some amount of gases always remains dissolved in mineral oil. For the safe operation of a transformer, the gases dissolved in oil should be below some threshold value. An increase in gas level beyond the threshold value indicates the inception of

Table 1.1 Generated gases with respective fault type [25]

Gases	Fault type
H_2	Corona in oil and cellulosic paper
CH_4 ,C_2H_6	Thermal degradation of oil at low temperature
C_2H_4, C_2H_2 and traces of CH_4 and C_2H_6	Thermal degradation of oil at low temperature
CO_2	Thermal degradation at low temperature and corona in cellulosic paper
CO_2, CO	Thermal degradation at high temperature and corona in cellulosic paper
H_2, CH_4 and traces of C_2H_4 and C_2H_6	Low energy electrical discharge
H_2, C_2H_2 and traces of CH_4 and C_2H_4	Electrical arcing

a fault. The final step is the interpretation of the DGA test result to determine the type of fault. The most commonly used DGA interpretation techniques based on IEEE Std. C57.104-2008 and IEC 60599-2007 [27] are as follows.

i) Total dissolved combustible gas (TDCG) concentration method
ii) Permissible gas concentration method
iii) Key gas method
iv) Gas ratio method
    a) Dornenburg ratio method
    b) Roger's ratio method
    c) IEC Gas ratio method
v) Duval's triangle
vi) Duval's pentagon

All of the above mentioned interpretation techniques can provide an approximate idea about the type of fault occurring inside a transformer. However, pin pointing the exact location and the type of fault is not plausible by using any of these techniques. The evaluation of integrity of the transformer insulation system cannot be provided by the DGA test result solely, for which the detailed information regarding the manufacturing details of the transformer, maintenance log, loading conditions etc. are necessary. Besides, a lot of ambiguity still persists regarding the choice of correct gas ratios to be considered for accurate interpretation of DGA results. It is reported in [28] that the effect of stray gas and especially low gas concentrations [29] can influence the efficacy of DGA measurement. Besides, DGA results cannot provide any information regarding the moisture content and the aging state of the cellulosic paper insulation.

1.4.2 Degree of Polymerization Measurement

Degree of polymerization is an invasive measurement technique, commonly used to assess the aging or the progress of aging of the paper insulation of a transformer. As mentioned in section 1.2, the basic building block of the paper insulation is cellulose, which has a linear polymeric structure. The polymeric structure is formed by combination of large number of monomer units linked together in a long chain that provides the desired mechanical strength to the paper insulation. The number of monomer units that combine to form the polymeric chain is known as degree of polymerization (DP). Due to thermal, oxidative and hydrolytic degradation (as reported in Section 1.2.1) the polymeric chain of the paper insulation breaks [30]. As a consequence, the paper insulation loses its tensile strength, becomes brittle and the DP value decreases. However, as reported in [15], the dielectric strength of the brittle paper is still sufficiently high, not to trigger the breakdown of a transformer. The main reason behind the failure of a transformer is the inability of the degraded paper insulation to withstand the mechanical forces created inside a transformer under short circuit conditions. The kinetics of the cellulose degradation is monitored by the change in DP value. Hence, it is important to measure the DP value of the paper insulation to have an idea regarding the mechanical strength of the kraft paper. The steps involved in DP measurement are as follows.

Strips of paper sample from either bushing or winding leads of a transformer are meticulously removed for the purpose of measurement. After collection of paper strips, the molecular weight of the same samples is measured. A comprehensive guideline for DP measurement of paper insulation is provided in IEC 60450:2004 [31] and ASTM D4243 [32]. Two popular methods of DP measurement are (a) Viscometric method and (b) Gel permeation chromatography (GPC). Viscometric method provides an idea about the average molecular weight of the cellulose chain, whereas the GPC method provides the full molecular weight distribution of the cellulose chain inside the paper insulation. After measurement, the next step is the interpretation of the measured DP value. The interpretations of DP values, as well as necessary recommendations for safe operation of a transformer are shown in Table 1.2 [33].

DP value is well correlated to the relative moisture (water) content of the paper insulation [15]. The variation of the paper moisture content (*m.c*) with DP is shown in Figure 1.1.

Table 1.2 Interpretations of DP values and recommendation [33]

Measured DP value	**Remarks**	**Recommendation**
< 200	Extensive paper degradation exceeding the critical point.	Transformer must be taken out of service immediately for visual inspection
200-250	The paper has attained the critical condition.	The transformer needed to be taken out of service as quickly as possible for thorough inspection.
260-350	The paper is approaching the critical condition.	Inspection and/or re-sampling within 1 year
360-450	The paper is starting to approach the critical condition	Resampling within 1-2 years of time
460-600	Significant paper deterioration but still well away from the critical point	No action necessary
610-900	Mild to minimal paper aging	No action necessary
> 900	No detectable paper degradation	No action necessary

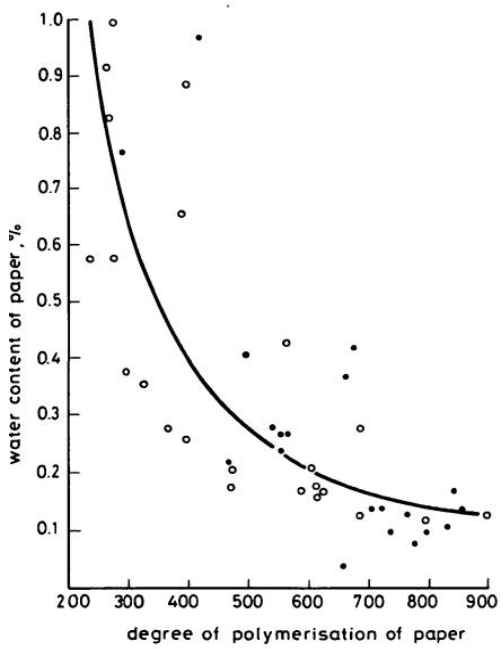

Figure 1.1: Variation of *m.c* (%) with DP [15]

The relative paper *m.c* (%) is empirically related to DP, by the following relationship [34]

$$m.c(\%) = C_1.e^{-DP_t.C_2} \tag{1.1}$$

In the above equation, C_1 and C_2 are the constants to be derived from experimentally obtained data and DP_t is the measured DP value at any time *t*. The DP value can also be used to predict the remaining life of the transformer insulation. The relationship between the remaining transformer life and the DP value is given by [34]

$$\frac{1}{DP_f} - \frac{1}{DP_i} = C \times Life \tag{1.2}$$

Here, DP_f and DP_i indicates the final and the initial DP value of the paper insulation, respectively, and *C* is a constant, which is related to the temperature and other parameters by the following relationship [34]

$$C = A.e^{-\left(\frac{E}{R(T+273)}\right)} \tag{1.3}$$

Here, *T*= operating temperature (°C)
E =activation energy=113kJ mol^{-1}
R=universal gas constant=8.31J $mol^{-1}K^{-1}$
A is a pre-exponential factor derived from the covariance analysis of degradation rate and is dependent on the condition of paper insulation.

The advantages and disadvantages of DP measurement are as follows. DP measurement is relatively easy. The paper *m.c* and transformer remaining life can be estimated using the empirical relationships. However, the main limitation of DP measurement is that it is an invasive technique, which can only be performed during shutdown or overhauling period of transformer. Besides, as the paper insulation is impregnated with oil, special drying process is necessary to remove oil from paper sample, otherwise, an error may creep in during measurement of DP value of paper. Also, as the degradation of paper insulation is different along the thickness of the insulation [35-36], the DP value measured from the paper samples extracted from the different regions of the transformer will also be different. Moreover, in order to predict the insulation condition from DP measurement, it is

necessary to know the initial DP value, which is difficult information to gather for in service units. In the event of any wrong information, the predicted life of the insulation based on DP value will be different from the actual end of life of the insulation.

1.4.3 Furan analysis

Furan analysis is an indirect method of assessing the degradation of the paper insulation. At very high temperature, the thermal degradation of paper insulation takes place with the liberation of CO and CO_2. However, these two gases are also generated during thermal decomposition of mineral oil. Hence, measuring the concentration of CO and CO_2 from DGA analysis cannot be used as an efficient marker to indicate the degradation of paper insulation. Furan analysis on the other hand, measures the concentration of Furfuraldehyde (FFA)-a chemical compound specific to the thermal decomposition of paper insulation and not generated by degradation of mineral oil [37]. The monitoring of the furanic compounds provides an indication about the degradation of paper insulation. Different types of furans are found to be present in oil due to thermal decomposition of paper as follows: 2-furfuraldehyde (2FAL), 5-hydroxy-methyl 2-furfuraldehyde (5H2F), 2-acetylfuran (2ACF), 5-methyl 2-furfuraldehyde (5M2F), and 2-furfuryl-alcohol (2FOL) etc. Among different furanic compounds, it was reported that the concentration of 2FAL is always found to be highest [38] and measuring the concentration of 2FAL can be used as a marker for paper degradation.

Unlike DP measurement, the furan analysis can be done online by collecting oil sample from an in-service transformer through the oil drain valve. The measurement of FFA is done by high performance liquid chromatography (HPLC) which is a well-known technique used to determine the concentration of FFA in mineral oil. The tests are carried out in accordance with IEC-611198 specifications [39]. Table 1.3 shows the interpretations of furan levels as reported in [40].

Table 1.3 Interpretation of Furan levels [40]

Furan Concentration (mg/l)	**Interpretation**
< 0.1	Acceptable
> 0.1	Questionable
> 0.25	Not acceptable

The concentration of 2FAL can be empirically correlated with the DP value and the *m.c* of the paper insulation. Figure 1.2 shows the variation of furan concentration with DP.

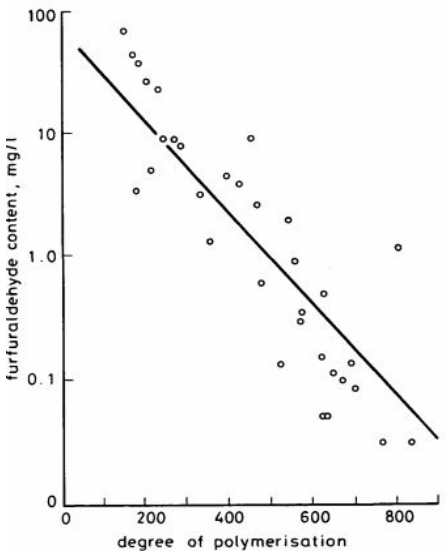

Figure 1.2: Variation of 2FAL content with DP [15]

The empirical relationship between 2FAL and DP is given by [41]

$$\log_{10}(2FAL_{ppm}) = 1.5655 - 0.0035 \times DP \tag{1.4}$$

Attempts have also been made to correlate 2FAL with *m.c* in [42]. Although highly stable 2FAL compound concentration in mineral oil can act as a potential indicator of paper degradation, yet one common problem is that the 2FAL concentration in mineral oil is affected during oil resampling and reclamation process of transformer. Moreover as reported in [43], the furan compounds can move to and fro i.e. from oil to paper and vice versa, which inadvertently change the concentration of furanic compounds in oil. Besides, in some literatures, it has been reported that the thermally upgraded kraft paper (TUK) has lower furan content in mineral oil compared to ordinary kraft paper [44]. Such ambiguity of 2FAL concentrations for different kraft papers is also not well understood.

1.5 Conventional Electrical Diagnostic Tests

In addition to chemical tests, monitoring of the insulation condition is also done by several electrical based diagnostic techniques. The dielectric properties of the oil paper insulation degrade substantially throughout the service life of transformer, (due to electrical, thermal and chemical stresses) which can be detected by several electrical tests. Some of the widely used electrical based diagnostic techniques are (i) insulation resistance (IR) measurement (ii) polarization index (PI) test (iii) capacitance and dielectric dissipation factor (DDF) measurement, also known as C-tanδ test (iv) dielectric spectroscopy measurement. A distinct advantage of electrical based diagnostics is that, these are non-invasive testing methods which require access to transformer bushing only. A brief overview of different electrical tests commonly used for insulation diagnosis is given below. In the following section, only first three electrical tests are discussed. The dielectric spectroscopy measurement is explained separately in Section 1.6.

1.5.1 Insulation resistance test

Insulation resistance (IR) measurement is an age old electrical testing method to investigate the condition of transformer insulation. During IR test, a DC voltage (up to 5kV depending on the transformer rating) is applied across the oil-paper insulation system [45]. Upon application of DC voltage, three types of current generally flow through the insulation. The capacitive current, which decreases sharply after 10-15 seconds, flows due to the charging of geometric capacitance. The absorption current which generally takes from 10 minute to several hours to decay flows due to the polarization of the dipoles. The third component is the leakage current, which is a steady state current due to the volume resistance of the insulation [45]. The total current measured during IR test is the combination of all three current components. The IR value at any instant of time is subsequently determined from the applied excitation voltage and the corresponding response current using Ohm's Law at a particular instant. The absolute value as well as the shape of the IR curve versus time is used to assess the insulation condition.

IR measurement is done either in between the two windings or between each winding with the ground. During IR test, it is recommended that the tank and the core of the transformer should be grounded and the windings should be kept short circuited at the respective bushing ends. Even after conducting the IR measurement, the windings should be kept short circuited to eliminate the

effect of any absorbed charge during measurement. Moreover, as IR is influenced by the change in temperature, therefore the measured IR value at any temperature is usually corrected by using temperature correction factor for the purpose of comparison [46]. Although IR measurement can provide some insight into the insulation problems, yet localization of the problem is not possible using IR measurement only. Besides, IR measurement fails to provide a comprehensive idea regarding the aging state and *m.c* of the cellulosic insulation.

1.5.2 Polarization index test

Polarization index (PI) test is a ratio based measurement and is generally conducted on transformers either prior to installation or as a part of maintenance schedule. The PI measurement is done in accordance with IEEE Std. 62-1995 [45]. The PI is defined as the ratio of the IR value measured after 10 minutes to the IR value measured after one minute, respectively. The PI test is generally done by applying same voltage as that of IR test, but instead for a period of 10 minutes. This allows the absorption (polarization) component of current to decay for a sufficient time, thereby providing a better insight to insulation condition (contamination, moisture ingress etc.) compared to IR test. Table 1.4 shows the interpretation of different PI values.

Table 1.4 Interpretation of PI values [11]

PI	**Interpretation**
< 1	Not acceptable
1-1.1	Poor
1.1-1.25	Questionable
1.25-2.0	Fair
> 2	Good

A distinct advantage of PI test over IR measurement is that, since it is a ratio based test, PI measurement is not influenced by temperature. Therefore, temperature correction is not necessary in a PI test. However, there are some defects like localized voids, pinholes etc., which are present in dry insulation system, but usually pass in PI test. Such defects can cause partial discharge to trigger at high voltage [17]. Besides, if the charging current of the insulation varies, then the interpretation of PI may be wrong. In that case, PI test provides incorrect information regarding the insulation condition.

1.5.3 C-tanδ test

Capacitance and dielectric dissipation factor (C-tanδ) measurement at power frequency is conducted to assess the condition of transformer insulation and bushings. The capacitance of the transformer and the bushings depend on the geometry of the insulation. Any change in capacitance value indicates the degradation of the insulation due to physical damage, or partial breakdown between the layers in the case of capacitance graded bushings. The concept of dielectric dissipation factor (tanδ) is briefly explained below.

The insulation system can be modeled using a resistance and a capacitance either in series or in parallel combination [47]. A parallel combination is widely used for modeling insulation at power frequency [11, 47]. When an alternating voltage $\bar{V}(\omega)$ is applied across any insulation, the current flowing through the insulation system has two components (see Fig 1.3). The resistive component ($\bar{I}_R$) is in phase with the supply voltage $\bar{V}(\omega)$, while the capacitive component ($\bar{I}_c$) is leading $\bar{V}(\omega)$ by 90°. The angle (δ) between the $\bar{I}_c$ and the resultant current $\bar{I}(\omega)$ is known as the loss factor angle and tangent of loss angle, i.e. (tanδ), is known as the dielectric dissipation factor, which can be expressed as the ratio of the resistive component to the capacitive component of the current as

$$\tan\delta = \frac{\bar{I}_R}{\bar{I}_C} = \frac{1}{\omega CR} \tag{1.5}$$

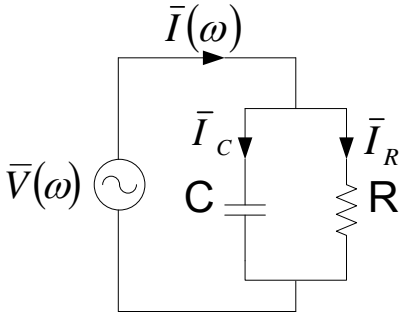

Figure 1.3:Electrical equivalent model of an insulation

C-tanδ measurement is performed on transformers at power frequency (50 or 60 Hz), by applying a test voltage typically between 10 kV-30 kV [17]. The core and the tank of the transformer must be kept earthed during measurement. The HV and LV bushing terminals are shorted and the capacitance (C_{HL}) is measured either in between two windings or between each winding and tank (C_H or C_L), respectively. During C-tanδ measurement, the excitation voltage is generally applied to one winding, while the response current is measured from the opposite winding (for C_{HL} measurement) or from the tank (in the case of C_H or C_L measurement). In the case of measurement on bushings, the test voltage is applied on the test conductor while the current is recorded from the measurement tap. Since both C and tanδ values are influenced by temperature, therefore C-tanδ measurement is often conducted at different temperatures [17]. One of the major limitations of C-tanδ measurement is that the complete frequency spectrum of the dielectric response is not available since the measurement is conducted at one frequency. The insulation condition can be better understood if C-tanδ measurement is conducted covering a wide frequency range. Such measurement is known as frequency domain spectroscopy (FDS), which is discussed extensively in Section 1.6.3.

1.6 Dielectric spectroscopy measurement

Conventional electrical based diagnostics fail to provide a comprehensive overview regarding the amount of moisture present in the paper insulation of the transformer. Since moisture accelerates the aging of the cellulosic paper insulation, therefore determination of *m.c* is important for proper evaluation of the insulation condition. Besides, it is also important to segregate the effects of moisture and other parameters like conductivity, insulation geometry etc. for proper assessment of insulation condition. In this context, dielectric spectroscopy measurement is a major non-invasive, electrical diagnostic technique widely used by electrical power utilities to evaluate the condition of the transformer insulation [48-52]. Dielectric spectroscopy measurement can be broadly classified into two types: (a) Time domain spectroscopy and (b) Frequency domain spectroscopy. Time domain spectroscopy includes Polarization and Depolarization current (PDC) measurement and Return Voltage measurement (RVM) [53-54]. Dielectric spectroscopy measurement in frequency domain is known as Frequency domain spectroscopy (FDS) [55]. A brief overview of both time and frequency domain dielectric spectroscopy measurements are given below.

The detailed theoretical background of dielectric spectroscopy measurement can be found in existing literatures [48-49, 51].

1.6.1 Polarization Depolarization current (PDC) measurement

When a dielectric is exposed to an electric field $E(t)$, a relative shift of positive and negative charges occur within the material. This phenomenon is known as dielectric polarization which results in the flow of displacement current in addition to the conduction current. According to Maxwell's equation, the total current density $J(t)$ generated by $E(t)$ can be expressed as the summation of conduction current and displacement current as

$$J(t) = \sigma_0 E(t) + \frac{\partial D(t)}{\partial t} \tag{1.6}$$

Here, σ_0 is the dc conductivity and D is the electric flux density, which is related to the applied electric field $E(t)$ and the macroscopic polarization $P(t)$ as

$$D(t) = \varepsilon_0 E(t) + P(t) \tag{1.7}$$

where, ε_0 is the permittivity of the vacuum. The total current density $J(t)$ can therefore be expressed as

$$J(t) = \sigma_0 E(t) + \varepsilon_0 \frac{\partial E(t)}{\partial t} + \frac{\partial P(t)}{\partial t} \tag{1.8}$$

Now, the polarization $P(t)$ is related to the dielectric response function $f(t)$ as

$$P(t) = \varepsilon_o \chi_\infty E(t) + \varepsilon_0 \int_{-\infty}^{t} f(t-\tau) E(\tau) d\tau \tag{1.9}$$

In the above equation, $\varepsilon_\infty = 1 + \chi_\infty$, where χ is the electric susceptibility and the index ∞ stands for instantaneous polarization which is very fast process and cannot be measured either in time or frequency domain

adequately. Considering $E(t)$ = constant, using equation (1.8) and (1.9), the current density $J(t)$ can be expressed as

$$J(t) = \sigma_o E(t) + \varepsilon_o[\varepsilon_\infty \delta(t) + f(t)]E(t) \tag{1.10}$$

Now, if a step voltage V_c is suddenly applied to an initially relaxed insulation, then the polarization current flowing through it can be expressed as

$$i_{pl}(t) = C_0 V_c \left[\frac{\sigma_0}{\varepsilon_0} + \varepsilon_\infty \delta(t) + f(t) \right] \tag{1.11}$$

In the above equation, C_0 denotes the geometric capacitance and $\delta(t)$ is the delta function coming from the applied step voltage V_c at $t=T_o$, where T_o is the starting time. It is evident from equation (1.11), that the polarization current consists of three terms. The first term is related to the intrinsic conductivity of the insulation under test, the second part term is the impulse function which cannot be recorded due to very fast polarization processes active at very short time and the last term represents the total polarization processes taking place due to the application of voltage V_c [48]. The polarization current can be eventually stopped if $i_{pl}(t)$ is either too low or becomes stable due to d.c conductivity [49].

Now, if the insulation under test is short circuited after $t=T_c$, where T_c is the charging time (time duration for which V_c is applied) then the depolarization or discharging current can be measured. Neglecting the contribution of $\delta(t)$ component of $i_{pl}(t)$ in equation (1.11), the depolarization current $i_{dpl}(t)$ can be expressed as

$$i_{dpl}(t) = -C_o V_c [f(t) - f(t + T_c)] \tag{1.12}$$

If the charging time T_c is of extremely long duration to complete all polarization processes, then the second term in equation (1.12) can be neglected [49]. Then the depolarization current $i_{dpl}(t)$ becomes directly proportional to the dielectric response function $f(t)$, but of opposite polarity. Figure 1.4 shows the typical nature of the polarization and depolarization currents (PDC) of an oil- paper insulation subjected to dc voltage V_c.

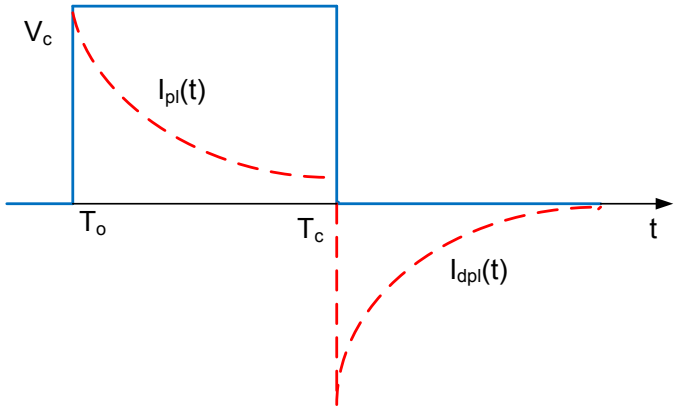

Figure 1.4: Typical nature of the polarization and depolarization currents (PDC) of an oil- paper insulation subjected to dc voltage V_c

The test circuit commonly used for PDC measurement of oil-paper insulation is shown in Figure 1.5.

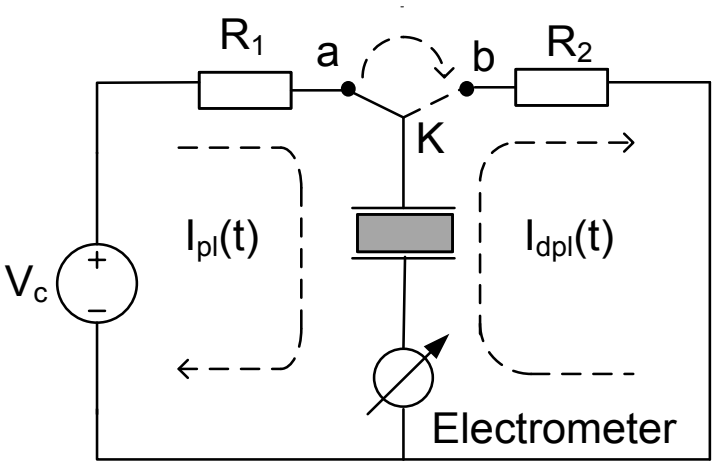

Figure 1.5: Test circuit commonly used for PDC measurement

The test circuit consists of two protective resistances (R_1 and R_2), which have negligible effect on recorded current data. The HV and LV bushings of the transformers are shorted individually prior to measurement. The shorted LV

end is always connected to the current measuring device (electrometer). The PDC measurements are generally conducted by applying a D.C voltage of magnitude typically 1kV for a sufficiently long time till no change in polarization current is observed. During recording of polarization current, the HV end is connected to position '*a*' via switch '*K*', so that the charging voltage V_c appears across the insulation. After polarization process is over, the switch '*K*' is moved to position '*b*' to record the depolarization current. During depolarization, the insulation is short circuited through the current measuring device.

Figure 1.6 shows the nature of polarization and depolarization current curve of an oil-paper insulation recorded from a power transformer [52, 56-58]. The recorded current data is plotted against time using a log-log scale. It depicts that different parts of the polarization current are sensitive to different parameters. The initial portion of the PDC curve (1-100 seconds) represents the condition of oil, while the tail of the polarization current is more sensitive to presence of moisture in the paper insulation [57]. The middle portion of the polarization curve is mainly dominated by insulation geometry and oil properties [52].

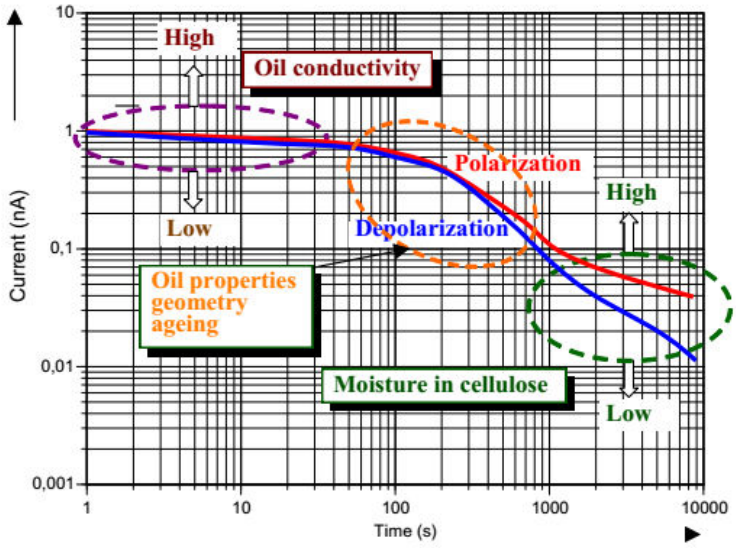

Figure 1.6: Interpretation of polarization and depolarization current curves [56]

An increase in oil conductivity causes the vertical shift of the polarization current curve and vice-versa [52, 58]. The PDC curve is almost insensitive to insulation geometry [52]. The presence of higher moisture causes the magnitude of both polarization and depolarization current to increase resulting in an upward shift of PDC curve [57-60]. The rate of decay of depolarization current due to increased moisture is steeper compared to the polarization current [52]. Therefore, using PDC analysis, effect of moisture in cellulose can be segregated from other parameters like oil conductivity, insulation geometry etc.

Temperature is an important parameter that influences the PDC results. Increase in temperature cause the conductivity of oil and paper insulation to increase, which results in faster polarization processes. As a consequence, the polarization current becomes stable at a much quicker time as the temperature increases [52, 61]. Besides, the magnitude of polarization current also increases with the increase in temperature [61]. Therefore, temperature correction is necessary during PDC measurement for accurate interpretation [17, 52].

1.6.2 Return Voltage Measurement (RVM)

Return voltage measurement (RVM) is the oldest method to measure the slow dielectric polarization processes in time domain. The basic theory of RVM measurement is similar to PDC measurement [48]. The insulation under test is subjected to a charging DC voltage V_c and the polarization current (i_{pl}) is measured for a fixed charging time T_c. Next the insulation is short circuited and the depolarization current (i_{dpl}) flows through the electrometer. However, in the case of RVM measurement, the entire i_{dpl} is not recorded. After a certain discharging time T_d (generally kept half of T_c), the short circuit is removed and the voltage across the unearthed sample is recorded under open circuit conditions [56]. This voltage is known as recovery voltage V_R. A typical nature of recover voltage waveform is shown in Figure 1.7.

During RVM measurement, due to insufficient discharging time T_d, the bound charges tend to become free in nature and appear as open circuit voltage in between two electrodes [48]. Typically V_R is the manifestation of all different active polarization processes which were not relaxed completely due to short discharging time T_d. The variation of peak value of recovery

voltage ($\hat{V}_R$) with T_c is known as recovery voltage spectrum (RVS) and the time instant corresponding to the peak of RVS is known as central time

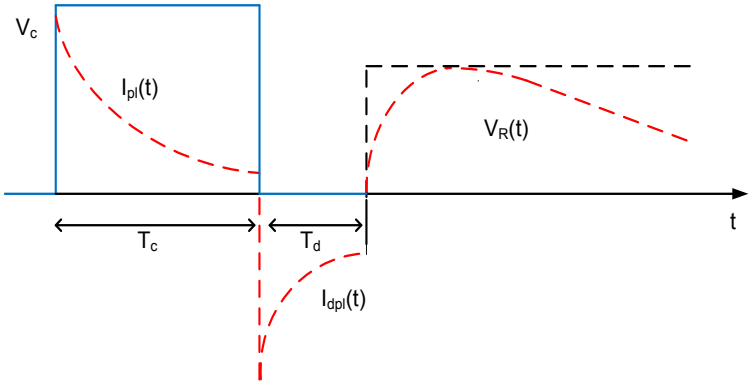

Figure 1.7: Typical nature of recovery voltage waveform

constant (CTC). The peak magnitude, initial slope and the CTC of the RVS were three important parameters mainly used to assess the insulation condition [56]. The effect of paper moisture on CTC of RVS is shown in Figure 1.8. Increased moisture causes RVS to shift towards the left resulting in lower CTC, and vice versa [62-63]. Therefore, CTC follows an inverse

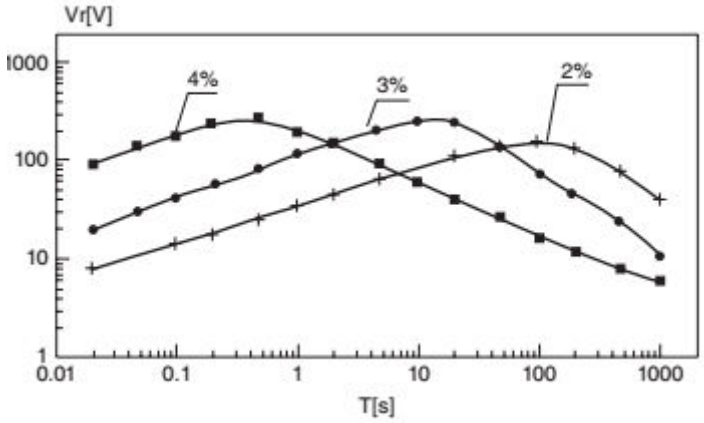

Figure 1.8: Variation of RVS for different moisture contents [62]

relationship with paper moisture. Increased oil conductivity causes $\hat{V}_R$ to rise faster and therefore the peak and the intial slope of RVS increases with the increase in oil conductivity [17]. Tempertaure also influences the RVS charcateristics of oil-paper insulation. As the tempearture increases, the RVS spectrum shifts towards lower CTCs, i.e towards left [61, 64]. This may be due to quick release of surface charges at increased temperature resulting in RVS peak to attain at lower CTCs.

Although parameters derived from RVS can be used to aseess the insulation condition, yet it has been reported in many existing litertures that the effect of moisture in paper insulation cannot be completely differentiated from other parameters (like oil and paper conductivity, insulation goemetry etc.) using RVM [56, 63]. Besides, the RVS peak and CTC cannot unambiguously separate the effect of aging and moisture of oil-paper insulation [65]. Therefore, RVM fails to provide accurate and reliable interpretation of insulation condition and is seldom used today for the purpose of insulation diagnosis.

1.6.3 Frequency domain spectroscopy (FDS) measurement

Frequency domain spectroscopy is the technique to measure dielectric response in frequency domain [66]. The basic theory behind FDS measurement is explained briefly.

The expression for current density $J(t)$ generated inside a dielectric subjected to a step excitation $E(t)$ was already described by equation (1.6) in section 1.5.1. The current density $J(t)$ in time domain can be converted into frequency domain by using either Laplace or Fourier transformation. The transformed current density in frequency domain $J(\omega)$ can be expressed as

$$J(\omega) = \sigma_0 E(\omega) + j\omega\varepsilon_o\varepsilon_\infty E(\omega) + j\omega\varepsilon_0 F(\omega)E(\omega)$$

$$= \sigma_0 E(\omega) + j\omega\varepsilon_o E(\omega)[\varepsilon_\infty + F(\omega)] \qquad (1.13)$$

From equation (1.13), it is evident that $F(\omega)$ is the Fourier transform of the dielectric response function $f(t)$, which can be also replaced with complex susceptibility $\overline{\chi}(\omega)$ as

$$\overline{F}(\omega) = \int_0^\infty f(t)e^{-j\omega t}\,dt = \overline{\chi}(\omega) = \chi'(\omega) - j\chi''(\omega) \qquad (1.14)$$

Combining equations (1.13) and (1.14), and rearranging all the terms, the current density $J(\omega)$ can be expressed as

$$J(\omega) = j\omega\varepsilon_0\left(\varepsilon_\infty + \chi'(\omega) - j[\frac{\sigma_0}{\omega\varepsilon_o} + \chi''(\omega)]\right)E(\omega) \qquad (1.15)$$

Now, if a sinusoidal voltage of $\overline{V}(\omega)$ is applied on the insulation and $\bar{I}(\omega)$ be the corresponding current flowing through it, then equation (1.15) can be rewritten as

$$\bar{I}(\omega) = j\omega C_0\left(\varepsilon_\infty + \chi'(\omega) - j[\frac{\sigma_0}{\omega\varepsilon_o} + \chi''(\omega)]\right)\overline{V}(\omega) \qquad (1.16)$$

$$= j\omega[C'(\omega) - jC''(\omega)]\overline{V}(\omega)$$

$$= j\omega\overline{C}(\omega)\overline{V}(\omega) \qquad (1.17)$$

In the above equation, $\overline{C}(\omega)$ represents the complex capacitance of the insulation. The real part of the complex capacitance $C'(\omega) = C_0[\varepsilon_\infty + \chi'(\omega)]$ represents the energy storage component. The imaginary part $C''(\omega) = C_0[\frac{\sigma_o}{\omega\varepsilon_0} + \chi''(\omega)]$ denotes the losses, which includes both resistive losses and dielectric losses occurring within the dielectric medium.

The dielectric dissipation factor $\tan\delta(\omega)$ can be expressed as the ratio of the imaginary part of the complex capacitance $C''(\omega)$ to the real part $C'(\omega)$ as

$$\tan\delta(\omega) = \frac{C''(\omega)}{C'(\omega)} = \frac{\frac{\sigma_o}{\omega\varepsilon_0} + \chi''(\omega)}{\varepsilon_\infty + \chi'(\omega)} \tag{1.18}$$

It is evident from equation (1.18), that $C''(\omega), C'(\omega)$ and $\tan\delta(\omega)$ are all frequency dependent parameters Therefore, unlike C-tanδ measurement, which is done at power frequency only, FDS measurement is done over a wide range of frequency [48]. The basic principle of FDS measurement is described below.

During FDS measurement, sinusoidal excitation is applied on the oil-paper insulation system for two cycles starting from 0.1mHz to 1kHz, and the corresponding response current flowing through it is recorded [66-70]. From the magnitude and the phase difference between the applied excitation voltage and the response current, dielectric dissipation factor, real and imaginary part of complex capacitance of the insulation system are computed over the frequency range from 0.1mHz to 1kHz [48,67-69]. Therefore, during FDS measurement, a complete frequency spectrum of the transformer insulation system is available, from which the insulation condition can be assessed. A typical circuit configuration used for FDS measurement is shown in Figure 1.9.

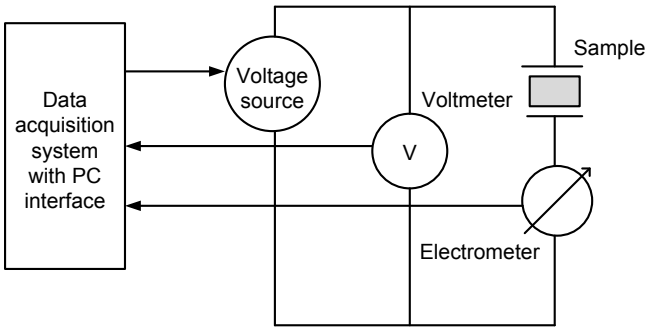

Figure 1.9: Circuit configuration used for FDS measurement

Unlike PDC measurement, which is conducted at high voltage, FDS measurement is usually conducted at a relatively lower voltage level. The amplitude of the excitation voltage varies between 5V-200V [11]. The

frequency sweep during FDS measurement is generally started from high frequency (1 kHz) down to low very frequency (0.1mHz) [71].The magnitude of the applied excitation voltage is increased with the decrease in measurement frequency to provide better anti-interference ability. In general, two cycles of sine wave at discrete measurement frequency points from 0.1mHz to 1kHz are applied on the test object during FDS measurement. For computation of real and imaginary part of complex capacitance and tanδ, the initial cycle is generally discarded to eradicate the transient effect due to excitation voltage switching at each individual measurement frequency.

Like PDC and RVM, FDS measurement on a transformer is also conducted offline, which requires shutdown of the transformer. The FDS measurement is generally performed using a 3 terminal device. The HV and LV windings are shorted separately and the transformer tank is kept earthed during the entire course of the measurement. The dielectric response measurement is done either in between HV and the LV winding (C_{HL}) or in between each winding (C_H or C_L) with the grounded tank [71]. In the case of C_{HL} measurement, the test voltage is usually injected on the HV terminal and the response currents are recorded from the LV terminal of the transformer. The third terminal acts as a guard electrode, which is used to divert the leakage current to ground to improve the measurement accuracy.

Figure 1.10 shows the nature of variation of tanδ with frequency for a practical transformer plotted in log-log scale. At low frequency, the tanδ value is high. As the measurement frequency increases, the tanδ value decreases to a minimum value and again increases slightly. Moreover, it can be also pointed out from Figure 1.10, that the different regions of tanδ curve are sensitive to different parameters. The moisture in cellulose insulation mainly affects the low frequency region (1mHz or below) and the high frequency region (above 100Hz) of the tanδ curve [52, 72]. Any increase in paper moisture causes the tanδ curve to shift upward due to increase in dielectric losses within the insulation at increased moisture [9]. Besides, as the paper moisture increases, $\tan\delta_{min}$ also shifts towards the higher frequencies. The mid-frequency region from 0.1Hz to 100 Hz is mainly influenced by oil conductivity [52, 72]. Increased oil conductivity cause the tanδ curve to shift towards the higher frequencies and vice-versa. The 'hump' in the tanδ curve at about 0.01Hz is mainly due to the effect of insulation geometry [52, 72]. Therefore, interpretation of tanδ versus frequency curve can separate the effect of moisture from several other parameters and therefore can be used for reliable assessment of insulation condition.

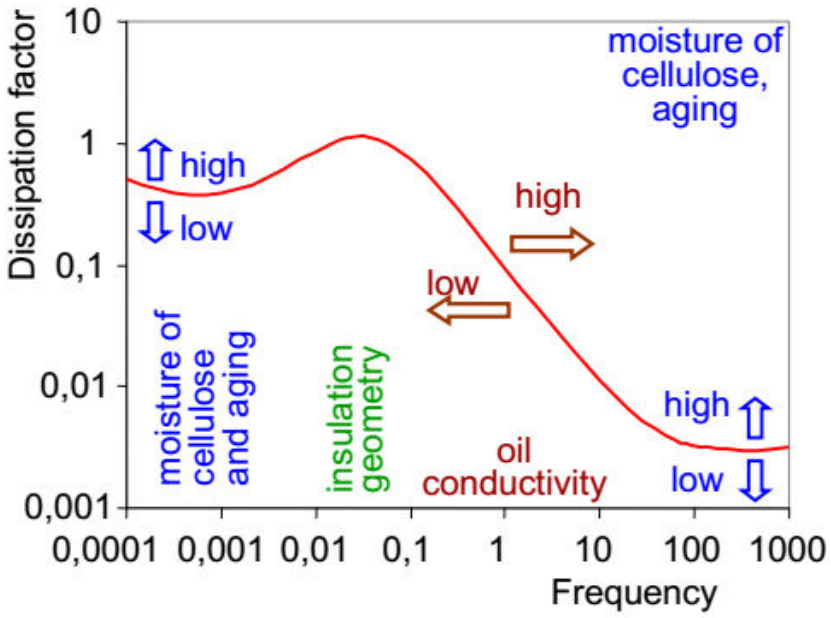

Figure 1.10: Interpretation of FDS results [52]

However, like PDC, FDS measurement is also not insensitive to temperature effect. Temperature effects the FDS measurement causing the tanδ curve to shift both horizontally and vertically along the frequency axis. The horizontal shift may be due to an increase in activation energy with the increase in temperature [73]. On the other hand, the vertical shift in tanδ may be due to increased oil conductivity at higher temperatures which causes the increment of ion mobility in the oil [73-74]. Therefore, FDS measurements are conducted long time after the transformer is de-energized from the service so as to ensure proper thermal equilibrium. On the other hand, proper temperature correction is necessary if FDS test is conducted on a power transformer immediately after taking shutdown.

1.7 Advantages of FDS measurement over time domain measurements

Over the past few years, both time and frequency domain spectroscopy measurements are widely used by electrical power utilities for condition

monitoring of transformer insulation. However, in comparison to time domain measurement, dielectric response measurement in frequency domain offers some distinct advantages, which are discussed below.

The magnitude of applied test voltage in the case of PDC measurement is relatively higher compared to FDS measurement. A high voltage source is not necessary to conduct FDS measurement, since FDS measurement can be conducted at low voltage level [11, 75]. Moreover, as the magnitude of excitation voltage being inversely proportional to the measurement frequency, therefore to conduct FDS test at 1kHz, amplitude of the applied sine wave excitation is about 5V or even lower [75]. So, in terms of hardware complexity, FDS test is superior compared to time domain measurements.

Another distinct advantage of FDS measurement is that it is robust against noise and interference compared to PDC measurement [76-77]. The dielectric response current recorded during PDC measurement in a noisy substation environment is often contaminated with different types of noise and interference from the mains [78]. Presence of noise may lead to wrong interpretation of the PDC data leading to an incorrect estimation of insulation condition. In the case of FDS measurement, any background noise present in the insulation response current can be eliminated using Fast Fourier Transform (FFT) and the fundamental component of voltage and current can be extracted to obtain the tanδ curve of the insulation. Since insulation condition is predicted from the tanδ curve and not from the response current directly, therefore FDS is more immune to noise compared to time domain measurements.

Estimation of moisture present in the paper insulation can be done directly from FDS measurement compared to PDC measurement. As reported by W.S.Zaengl, the paper *m.c* (%) at a particular temperature is empirically related to $\tan\delta_{min}$ using the following equation [79]

$$m.c\ (\%) = 15.297 + 2.53267 \times \ln(\tan\delta_{min}) \tag{1.19}$$

It is evident that if $\tan\delta_{min}$ value for any oil-paper insulation is known from FDS measurement, then the amount of moisture present in paper insulation can be directly estimated, which is not possible in the case of PDC measurement. Therefore, for condition assessment of transformer insulation, FDS is more preferred by electrical power utilities over PDC measurement, owing to its several advantages.

1.8 Practical issues related to conventional FDS measurement

Although FDS measurement offers distinct advantages over time domain measurements, yet from the practical point of view, some improvements over conventional FDS testing method is necessary for fast and reliable diagnosis of insulation condition.

In conventional FDS (cFDS) measurement, sinusoidal excitation voltage is applied on the transformer insulation at separate measurement frequency points from 0.1mHz to 1kHz for two cycles. Due to application of discrete sine waves at each individual measurement frequency points, cFDS measurement becomes lengthy and time consuming, which is a serious practical problem [48, 77-78].

Although in cFDS measurement it is recommended to apply pure sine wave as excitation voltage, yet in reality the transformer insulation throughout their service life is often stressed by voltage waveforms, which are significantly deviant from pure sinusoid [80-82]. Due to recent advances in high voltage power electronic converters and inverters, as a consequence of integration of renewable energy sources into grid, the voltage and the current waveforms often tend to become non-sinusoidal in nature. In that case, application of pure sine wave as excitation voltage may not provide reliable assessment of insulation condition. FDS measurement using non-sinusoidal excitation waveform has been reported in many existing literatures [80-84]. Besides, it was reported that the application of non-sinusoidal waveforms as excitation voltage provides better estimation of insulation condition compared to sinusoidal excitation voltage [81-83] Therefore, choice of excitation voltage is an important issue in cFDS measurement.

Another important issue in cFDS measurement is the non-linearity of oil-paper insulation system. The oil-paper insulation system measurement is considered to behave as a linear time invariant (LTI) system. But in reality, the transformer insulation system is highly complex in nature and manifests non-linear behavior [85-86]. Besides, the non-linearity increases with both aging and moisture content (i.e. degradation) of the insulation condition [87]. Therefore, non-linear modeling of oil-paper insulation system is an important aspect for reliable diagnosis of insulation.

1.9 Need for time reduction in FDS measurement

During cFDS measurement, series of sine waves at discrete measurement frequency points are applied on the composite oil-paper insulation system starting from 0.1mHz to 1kHz. However, the main problem in conducting a cFDS test lies in lower frequency range (from 0.1mHz to 1Hz). Since at least two cycles are needed to quantify the phase shift between the applied voltage and the response current at each measurement frequency, the net time required to perform the test goes up to a couple of hours especially during lower frequency measurement. It was reported by W. S. Zaengl that 2000 seconds are needed to quantify the phase shift between voltage and current at 1mHz [48]. From 1mHz to 1Hz, the overall test time is about 4000 seconds [88]. So the over-all test is quite lengthy to perform at site. Moreover, since the low frequency portion of the tanδ curve is mainly influenced by paper moisture, therefore, measurement on transformers are often done till 0.1mHz (instead of 1mHz) for proper estimation of moisture in cellulose [72]. The overall time required to conduct FDS test from 0.1mHz to 1Hz takes roughly 10.5-11 hours, considering 3 measurement frequencies per frequency decade. Increasing the number of measurement frequency per decade further increases the overall test time. Such a lengthy measurement is truly undesirable from the practical point of view [89]. Since, FDS is an off-line testing method till date, such a time consuming offline measurement inadvertently leads to an extended shutdown of a power transformer. The consequence is the huge loss of both time and money. From a power utility point of view, prolonged shutdown of a transformer incurs significant amount of financial loss. Besides, from the point of view of manpower and following proper maintenance schedule, such an abnormally long test on a power transformer is impractical.

Another important parameter that influences cFDS measurement is temperature. Due to offline nature of the measurement, several hours are needed to cool down a power transformer before cFDS test can be conducted on a power transformer, or else suitable temperature correction factors are needed to reduce the temperature error. During performing cFDS test for couple of hours at site, the ambient temperature changes very often. As a consequence, the relative position of dipoles present inside the dielectric medium is altered, because the moisture migration in composite oil-paper insulation is temperature dependent [90]. The change in relative arrangement of dipoles inside the insulation influences the frictional loss and hence the tanδ profile of the insulation [9, 81]. It may so happen that cFDS

measurement conducted on a power transformer insulation for such a long period of time may not give accurate results in estimation of insulation condition due to change in inter-dipolar arrangement with the change in temperature. Therefore, it is necessary to reduce cFDS measurement duration so that the change in ambient conditions has negligible effect on FDS results.

1.10 Scope of the thesis

The objective of the thesis is to reduce dielectric response measurement time for fast and reliable diagnosis of transformer insulation.

In ***Chapter 2***, a new FDS measurement technique based on mathematical regression approach was proposed to reduce cFDS measurement time. The main problem in conducting cFDS measurement is the application of two full cycle of sinusoidal excitation voltage at each measurement frequency from 0.1mHz to 1Hz. Due to application of two full cycles of sine wave during low frequency measurement, the overall cFDS test becomes extremely lengthy in nature. Moreover, the applied excitation voltage waveform during FDS measurement need not have to be pure sinusoidal in nature. Application of non-sinusoidal waveforms lead to more synchronized dipolar movements, yielding minimum inter-dipolar frictional losses. Therefore, use of non-sinusoidal excitations provides better estimation of insulation condition compared to sinusoidal excitation voltage. Hence, in ***Chapter 2***, a new method to conduct FDS measurement for condition assessment of oil–paper insulation was developed considering both sinusoidal as well as non-sinusoidal excitation voltage waveforms.

In ***Chapter 2***, it was observed that the regression approach can bring down cFDS measurement time significantly. However, the total FDS measurement time using regression approach depends on the number of measurement frequency points considered per decade. Moreover, the regression technique proposed in ***Chapter 2*** is also not independent of the initial transients which are present every time the excitation voltage is switched on. To eradicate the problem of switching transients and to make the measurement independent of measurement frequency, another technique for accelerated dielectric response measurement of oil-paper insulation was proposed in ***Chapter 3***. In ***Chapter 3***, chirp signals were proposed as broadband excitations to conduct FDS measurement on oil-paper insulation. Chirp waveforms with linear and exponential sweeps were used to conduct FDS measurement on several

laboratory prepared test samples with different moisture contents, within the frequency bandwidth from 0.1mHz to 1Hz. Practicability of the chirp waveforms for conducting fast and reliable assessment of insulation condition was also tested on a couple of real-life transformers.

Experimental investigations on FDS measurement using chirp signals with different sweeps revealed that chirps with exponential sweeps were capable of providing accurate information of insulation at a significantly reduced time. However, the influence of system non-linearity on the dielectric response measurement was not addressed in ***Chapter 3***. The oil-paper insulation system of the transformer is highly complicated which manifests non-linear behavior with increase in moisture content and aging. To highlight this issue, in ***Chapter 4***, a non-linear model of oil-paper insulation using chirp waveforms was developed based on system identification theory. Non-linearity due to increased paper moisture has been addressed for better assessment of insulation condition. Test on an aged power transformer was also conducted to characterize the aging related non-linearity.

In ***Chapter 5***, the conclusions and the scope of the future work have been discussed.

The variation of dielectric dissipation factor with frequency computed using regression approach for different non-sinusoidal waveforms is presented in ***Appendix.***

1.11 Originality of the thesis

To the best of author's knowledge, the original contributions of the thesis are as follows:

1 Development of a new measurement technique based on regression approach for fast dielectric response measurement considering both sinusoidal and non-sinusoidal excitation voltage waveforms.

2 Application of broadband excitation voltage in the form of chirp signals with different frequency sweeps for accelerating cFDS measurement of oil-paper insulation at low frequencies.

3 Development of a non-linear model of oil-paper insulation system based on system identification approach for reliable diagnosis of transformer insulation using chirp excitation voltage.

Chapter 2

Reducing Frequency Domain Spectroscopy Measurement Time: A Regression Based Approach

2.1 Introduction

During FDS measurement, sinusoidal excitation voltage is applied on the oil-paper insulation system at discrete measurement frequency points for a period of two cycles typically starting from 0.1mHz to 1kHz, and the corresponding dielectric response current flowing through the insulation system at each measurement frequency is measured. From the magnitude and the phase difference of the applied excitation voltage and the measured response current, several frequency dependent dielectric parameters like dielectric dissipation factor (tanδ), real and imaginary parts of complex capacitance etc. are computed over the frequency range from 0.1mHz to 1 kHz, from which the insulation condition is estimated. Although cFDS testing method suggests the application of only two cycles of pure sinusoidal excitation voltage at each individual measurement frequencies (from 0.1mHz to 1kHz), yet from the practical point of view, cFDS measurement has some major limitations which are stated below.

In the first case, application of sinusoidal voltage at each individual measurement frequency points to obtain the magnitude and the phase spectrum of the insulation from 0.1mHz to 1Hz makes FDS measurement inadvertently lengthy and time consuming. As highlighted earlier in Section 1.8, the major problem in conducting cFDS measurement lies in the lower frequency range, i.e. between 0.1mHz to 1Hz, where the overall measurement duration takes approximately 10-11 hours considering two cycles of applied sinusoidal excitation voltage at three measurement frequency points per decade. Such a lengthy measurement is quite unacceptable from the practical point of view. Since FDS is an offline testing method till date, such an extended test time means a prolonged shutdown of a power transformer, which is a huge loss of both time and money.

Another important issue concerning FDS measurement is the choice of excitation voltage waveform. Due to recent advances in high voltage power electronic converters and inverters and as a consequence of integration of renewable energy sources into grid, the insulation system of transformer throughout the period of operation is often stressed by voltage waveforms that deviate significantly from a pure sinusoid. Therefore, recently application of non-sinusoidal excitation signals in the place of conventional sine wave for conducting FDS measurement have been reported in many literatures [76, 80-85]. Besides, it has been also reported in [81-83], that use of non-sinusoidal excitation in the form of triangular wave shape provides better insight to insulation condition compared to sinusoidal excitation voltage.

Considering these two issues related to FDS measurement, in this chapter a method to reduce FDS measurement time is proposed taking into account both sinusoidal and non-sinusoidal (triangular) excitation voltage waveforms for fast and reliable assessment of insulation condition.

2.2 Theory behind FDS measurement using non-sinusoidal excitation voltage

When pure sinusoidal excitation voltage is applied on the oil-paper insulation system, different dipoles present in the composite insulation start oscillating in the direction of electric field. During oscillations, dipoles interact with each other, which result in frictional loss within the dielectric medium [91-94]. Since different dipoles present in composite oil-paper insulation have different oscillation frequencies, the application of pure sinusoidal excitation with a single frequency during FDS measurement results in unsynchronized movement of dipoles within the insulation [9,82]. As a consequence, the frictional loss increases further, which is mainly reflected in the corresponding tanδ profile obtained for oil-paper insulation subjected to pure sinusoidal excitation. For composite oil-paper insulation, the *m.c* of the paper insulation is usually evaluated using $\tan\delta_{min,}$ which reflects the actual insulation condition due to minimum frictional loss caused by inter dipolar interactions [83,89]. Now, $\tan\delta_{min}$ implies that the frictional loss due to inter dipolar interactions is minimum. Hence, it may be possible that the conventional testing method using pure sinusoidal excitation may not be accurate in estimating the actual condition of the insulation, since the presence of only one frequency component in the excitation voltage increases

the frictional loss inside the dielectric medium due to asynchronous movement of the dipoles.

The above fact inevitably gives rise to an opportunity of choosing an excitation voltage consisting of multiple frequencies (i.e. non-sinusoidal excitation) to conduct FDS measurements for better estimation of insulation condition. The presence of multiple frequencies in a non-sinusoidal waveform results in a more synchronized movement of dipoles inside the insulating medium. As a consequence, the frictional loss occurring due to inter dipolar interaction decreases, which in turn is reflected in the tanδ profile of the insulation system. Previous investigations in [81-83] revealed that the error in estimation of paper *m.c* using triangular waveform is less compared to cFDS using pure sinusoidal excitation. This reduction of estimation error may be due to additional information inherent to the dielectric response recorded for triangular excitation, which could be closely related to the non-linearity of the insulation system. Another distinct advantage of using triangular waveform is that along with the fundamental component, several harmonic components are also present in the waveform. Moreover, the harmonic components can be altered by varying the initial slope of the waveform [82]. Therefore in the present work, both triangular and sinusoidal excitation voltages are chosen as excitation voltage for conducting FDS measurement on oil-paper insulation.

2.3 Details of applied excitation voltage waveforms

Figure 2.1 shows the different triangular and sinusoidal excitation voltage waveforms used for the purpose of conducting FDS measurement. The peak value of the sinusoidal and different triangular excitation voltage waveforms were chosen as 100 V. The details of the triangular waveforms are tabulated below in Table 2.1. The detailed description of the different harmonics present in the different triangular waveforms was reported in [82].

Table 2.1: Types of triangular waveforms

Triangular Waveforms	**Initial slope in terms of (t/T)**
Tri1	0.0625
Tri2	0.1250
Tri3	0.2500
Tri4	0.3750
Tri5	0.4375

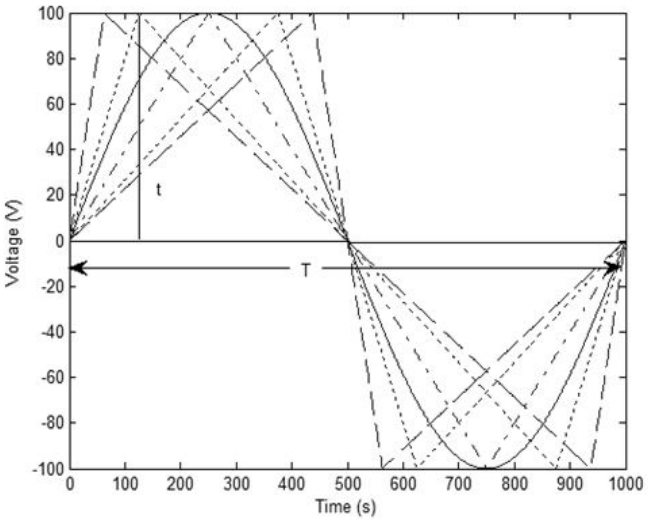

Figure 2.1: Sinusoidal and different triangular excitation voltage waveforms

2.4 Time Reduction of cFDS measurement

2.4.1 Dielectric response current at different frequencies

The investigation on cFDS measurement time reduction was started with the primary focus given on the response current waveform, since tanδ profile of the oil-paper insulation system is computed from the phase difference between the voltage and current waves at different frequencies. It has been reported in existing literatures that the oil-paper insulation system can be modelled as a linear dielectric which consists of a resistive capacitive (R-C) network [48, 63]. Therefore, when an alternating excitation voltage is impressed upon the insulation, the current at the lower frequencies is predominately resistive in nature with some phase shift, since the capacitive reactance is very high at low frequencies [76]. As the frequency of the excitation waveform increases to about 0.1Hz, the current tends to become capacitive in nature. Figure 2.2(a) and 2.2(b) shows the typical nature of dielectric response currents observed for an insulation subjected to triangular excitation (Tri3) recorded at 1mHz and 0.1Hz, respectively.

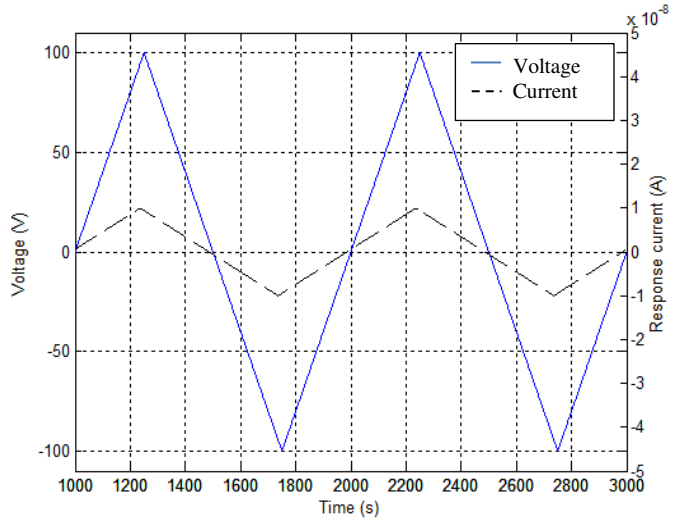

(a)

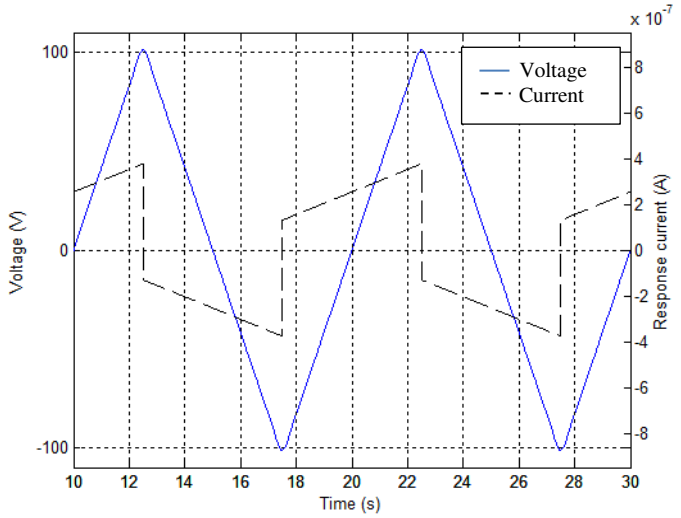

(b)

Similarly, Figures 2.2(c) and 2.2(d) show the insulation response currents subjected to sinusoidal excitation at 1mHz and 0.1Hz, respectively.

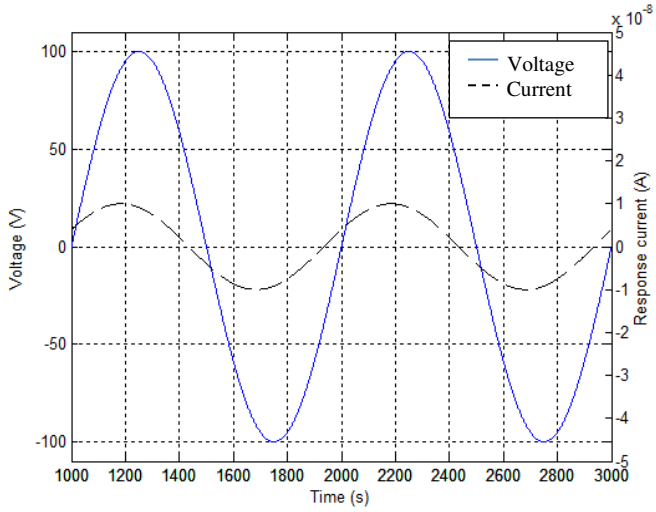

(c)

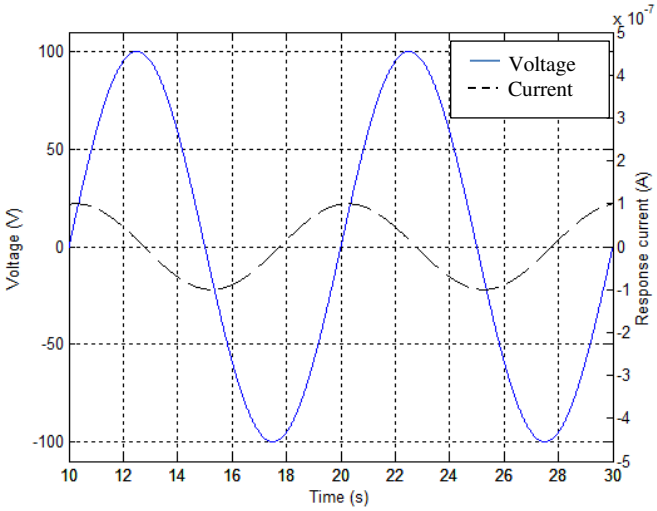

(d)

Figure 2.2: Typical nature of dielectric response current for Tri3 and sinusoidal excitation (a) 1 mHz Tri3 (b) 0.1 Hz Tri3 (c) 1 mHz sinusoidal (d) 0.1 Hz sinusoidal

It is evident from Figures 2.2(a) through 2.2(d) that the dielectric response currents measured over two cycles is periodic in nature and has definite correlation with the excitation voltage waveform. In the case of triangular (Tri3) excitation, both the excitation voltage waveform and response currents are periodic and symmetrical in nature. The response current rises linearly with a constant slope up to quarter cycle at 1mHz. As the excitation frequency increases (at about 0.1 Hz), the current stays symmetrical in nature, but the slope changes indicating the onset of the capacitive nature. Similar observations were also true for all triangular waveforms. Hence, in the case of triangular excitations, the response current up to quarter cycle can be predicted from some fraction (for e.g. one-tenth) of one full cycle by using suitable curve fitting technique. From quarter-cycle, the response current over two cycles can be easily constructed owing to the symmetry of the waveform.

In the case of sinusoidal excitation also as shown in Figure 2.2(c) and 2.2(d), the current remains sinusoidal in nature, with definite phase shift which increases with the increase in frequency of the excitation voltage. Hence, the response current over two cycles obtained by applying some fraction of sinusoidal excitation voltage waveform can also be estimated by using non-linear curve fitting technique. Therefore, instead of applying two full cycles of sinusoidal excitation voltage, application of some fraction of excitation of one full cycle especially at lower frequencies, may lead to significant reduction in measurement duration. In order to predict the response current over two cycles from some fraction of applied excitation voltage, a mathematical regression approach was used, which is discussed in the next section.

2.4.2 Mathematical Regression

Regression or fitting curve to a set of data points is a statistical tool that requires a parametric model, which relates the actual data to the predicted data by evaluating one or more parameters [76, 95]. The error e_k known as residual is the difference between the actual data and the predicted data. For k^{th} data point, the residual e_k is given by

$$e_k = y_k - \hat{y}_k \tag{2.1}$$

Where, y_k is the observed value and $\hat{y}_k$ is the fitted value. By using the method of least squares, the parameters are estimated that minimizes the summed square of the residuals, which is given by

$$SS_{res} = \sum_{k=1}^{n} e_k^{\,2} \tag{2.2}$$

If $\bar{y}$ is the mean of the actual data points then

$$\bar{y} = \frac{1}{N} \sum_{k=1}^{n} y_k \tag{2.3}$$

The total sum of the squares (SS_{tot}) is given by

$$SS_{tot} = \sum_{k=1}^{n} (y_k - \bar{y})^2 \tag{2.4}$$

The goodness of fit is measured by a statistical term known as coefficient of determination, R^2, which is an indicator of how well the regression line fits the data points. A value of R^2 close to unity indicates the best fit. R^2 is determined using the following equation

$$R^2 = 1 - \frac{SS_{res}}{SS_{tot}} \tag{2.5}$$

Table 2.2 shows the variation of R^2 performed by applying different fractions of one full cycle of response current for Tri3 and sinusoidal excitation.

Table 2.2: Variation of R^2 for different percentage of one full cycle of Tri3 and Sinusoidal excitation

Percentage of one full cycle of excitation	R^2 Tri3	R^2 Sinusoidal
5	0.974	0.968
10	0.991	0.986
15	0.996	0.992
25	0.998	0.996

It is imperative from the regression analysis that the increase in excitation span percentage of one full cycle leads to better estimation of dielectric response current. This is evident from R^2 value obtained in Table 2.2, which increases and approaches unity with the increase in excitation span percentage.

2.4.3 Effect of noise and interference

Measurement of FDS in laboratory is usually performed under controlled environmental conditions, where the background noise level and interference from mains are very low. However, during FDS measurement on transformers in a real life substation environment, various types of noise and interferences can creep in to the measurement system [76-77]. Although FDS has better noise immunity compared to PDC measurement [96], yet the presence of noise and interference may upset the proposed regression approach, leading to a complete wrong estimation of response current. Hence, for accurate estimation of dielectric response current, it is necessary that the proposed method should be robust against noise and interference. Considering the above said fact, white Gaussian noise at different signal to noise ratios (SNR) is mixed with the response current. Figure 2.3 shows the variation of R^2 for Tri3 and sinusoidal excitation for different values of SNR varying from 3 dB to 40 dB.

Along with noise, the effect of interference from mains is also investigated by varying different percentage of 50Hz interference. Figure 2.4 shows the variation of R^2 for different values of 50Hz interferences for Tri3 and sinusoidal excitation with interference level varying from 25 % to 0.5%. For this purpose, the SNR is kept fixed at 40 dB. It can be pointed out from the results obtained in Figures 2.3 and 2.4, that the higher values of SNR and lower interference from mains leads to better estimation of dielectric response current. Hence, the experimental set-up and the measurement

system should be prepared in such a way so that the background noise level and interference are kept within the tolerance limit.

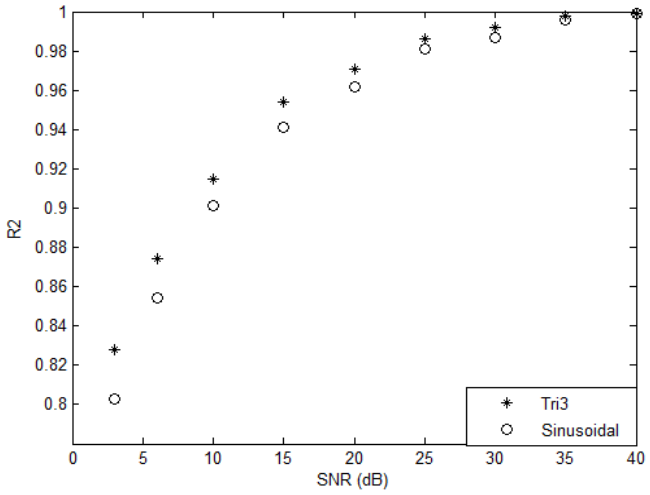

Figure 2.3: Variation of R^2 for Tri3 and sinusoidal excitation for different values of SNR

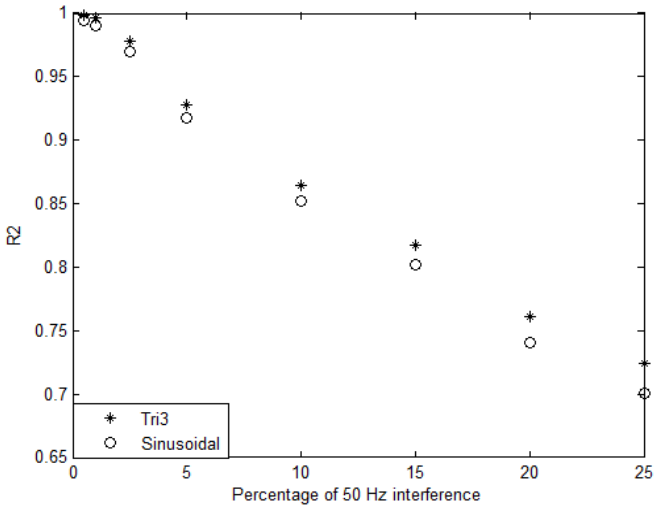

Figure 2.4: Variation of R^2 for Tri3 and sinusoidal excitation for different interference levels

2.5 Experimental validation

2.5.1 Preparation of Test Samples

Three test samples emulating the oil-paper insulation of a practical transformer were prepared in the laboratory for the purpose of validation of the proposed technique. A galvanized iron sheet A of dimensions 50 mm × 50 mm × 100 mm was used to form the core of the transformer. A pressboard cylinder B of 70 mm diameter was fitted over the galvanized iron (GI) sheet. A layer of unimpregnated kraft paper C was wrapped over B. A copper foil D was positioned over C, which formed the low voltage (LV) winding of the transformer, over which another layer of unimpregnated kraft paper E was placed. Pressboard strips F of 10 mm gap served as oil ducts, over which another layer of impregnated kraft paper G was wound. Another layer of copper foil H was placed over G, which represented the high voltage (HV) winding of the transformer. Finally, the sample preparation was completed by wrapping another layer of unimpregnated kraft paper over G. The cross section as well as the actual photograph of the samples is shown in Figures 2.5(a) and (b), respectively.

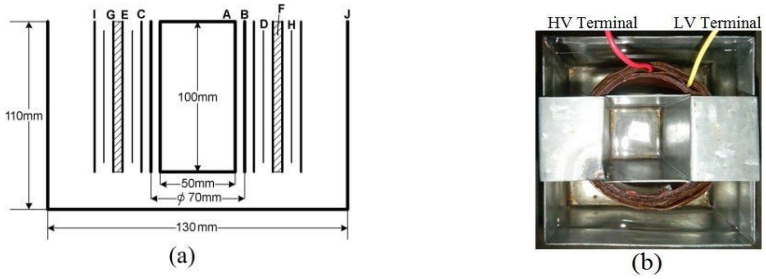

Figure 2.5: Prepared test sample in the laboratory (a) Cross-sectional drawing and (b) actual photograph

2.5.2 Moisture content setting by dry weight method

After the preparation of the samples, the moisture content of the samples were determined using dry weight method as reported in [82-83,89,97]. For this purpose, the prepared test samples were placed inside an environmental chamber (see Figure 2.6) and were heated at 90°C for several days to remove any moisture that might have penetrated during sample preparation process.

After heating for several days, the weight of the samples was measured using a precision weighing balance having a resolution of 10 µg. Then the samples were exposed to air for moisture absorption. The weight of the samples was again measured after exposure to air. Finally, percentage paper moisture (*m.c*) content of the samples at a fixed temperature was determined as follows:

$$\%m.c = (\frac{W_w - W_d}{W_d}) \times 100 \tag{2.6}$$

In the above equation, W_d and W_w represent the weight of the test samples before and after exposure to air, respectively.

Figure 2.6: Test sample inside the environmental chamber

Table 2.3 illustrates the paper moisture contents of the three test samples at 30°C prepared in the laboratory.

Table 2.3: Prepared samples with paper moisture content

Samples	Paper moisture content (%)
Sample-1	1.0
Sample-2	2.0
Sample-3	3.0

2.5.3 Oil impregnation procedure

Once the paper moisture content of the samples was set, oil impregnation was performed by immersing the prepared samples inside a GI tank filled with equal volume of fresh transformer oil of conductivity 0.05pS/m. The conductivity of the transformer oil was measured using a conductivity measuring probe before immersion of the test samples. The whole set up was thereafter kept again inside the chamber at 30°C, to ensure proper thermal equilibrium. Thereafter, FDS test was performed using both sinusoidal excitation as well as five triangular excitation voltage waveforms.

2.5.4 Experimental set-up

In order to conduct FDS measurement on test samples an experimental set up was developed in the laboratory. Figure 2.7 shows the schematic diagram of experimental set up.

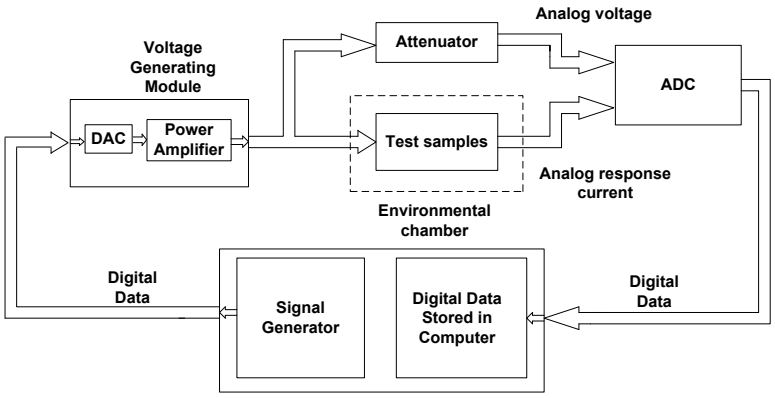

Figure 2.7: Schematic diagram of the experimental set-up

A signal generator was fabricated in the laboratory capable of generating sinusoidal and triangular waveforms as well as frequency sweep from 0.1mHz to 1kHz ideal for FDS measurement. The information about the amplitude and phase of the specified triangular waveform mentioned in Section 2.3 was stored in a file in the computer and are eventually passed through Digital to Analog Converter (DAC). An analog voltage amplifier was connected at the output of DAC that can amplify the output voltage from 0 to $200V_{peak}$. The amplified output voltage was applied across the three prepared samples and the corresponding dielectric response current is measured for each sample. The analog dielectric response current was measured using Keithley Electrometer (which can measure current of the order of pico-ampere).The measured analog response current was passed through a 2-channel high speed 100 MS/s digitizer for conversion to digital signal. The digital current data were finally stored in computer. The sampling frequency for acquiring the response current data was kept at 1000 times the fundamental frequency of the applied sinusoidal and triangular excitations, which was above the Nyquist frequency to prevent any aliasing.

2.5.5 Experimental procedure

At first, the dielectric response current for all 3 samples were measured using two full cycles of both sinusoidal and triangular excitations over the frequency range of 0.1mHz-1Hz. Measurements above 1Hz were not performed here since it takes very less measurement time to conduct FDS measurement from 1Hz-1kHz. During FDS measurement, the excitation voltages were applied on the emulated HV winding of the test samples and the response currents were measured from the emulated LV winding. After recording of dielectric response current at each measurement frequency, the emulated HV and LV terminals of the test samples were short circuited for a sufficient duration, before the next excitation voltage is applied. This was done to ensure the absence of any memory effect into the measurement system. Next, the three samples were subjected to some fraction of one full cycle of both sinusoidal and triangular excitations (typically starting with 5% of one full cycle) and the corresponding dielectric response currents were measured and were eventually stored in a PC for analysis.

2.5.6 Analysis of measured dielectric response current

The dielectric dissipation factors for all three test samples were initially computed for cFDS measurement by applying sinusoidal and triangular

excitation voltage waveforms for two cycles. For sinusoidal excitation, the tanδ profiles were calculated from the phase difference between the applied excitation voltage and the corresponding measured response current. In the case of triangular excitation voltage waveforms, the fundamental component of the applied excitation voltage and the response currents were extracted using Fast Fourier Transform (FFT). From the phase difference between the fundamental component of applied excitation voltage and the response current, the dielectric dissipation factors were computed from 0.1mHz to 1Hz, for all triangular waveforms. It is important to mention here that every time the new excitation is applied on test samples, it is made sure that the system is in steady state. This is important to avoid any transient effect at the start that may affect the measurement system. To ensure that the system is in steady state, the dielectric response current measurement is done for 3 cycles and for each measurement frequency the initial portion (e.g. typically first cycle) of the applied excitation voltages and the measured dielectric response currents were discarded for both sinusoidal and triangular excitation voltage waveforms.

After computation of tanδ profile of test samples for cFDS measurement is over, next, the fractional dielectric response currents (measured by applying some fraction of one full cycle of excitation voltage waveforms) were predicted upto two cycles using mathematical regression technique as described in Section 2.4.2. From the knowledge of voltage waveform and predicted response current for two cycles, dielectric dissipation factors were recalculated for both sinusoidal and triangular waveforms. The values of tanδ so obtained using some fraction of one full cycle of excitation were compared with the values obtained from application of entire two cycles of applied excitation and the percentage error in tanδ was calculated. To make the method practicable, an error band of $\pm$ 5% was fixed. If the error in tanδ measurement lies within the error band, then the optimum percentage of excitation span for a particular waveform at a particular measurement frequency was determined. Otherwise, the excitation span was increased to obtain the result within the error band. This algorithm was then applied for all three test samples and the optimum excitation spans at different frequencies were determined for five triangular as well as sinusoidal excitation voltage waveforms. The algorithm used for determination of optimum excitation span percentage is shown in a flowchart in Figure 2.8.

.

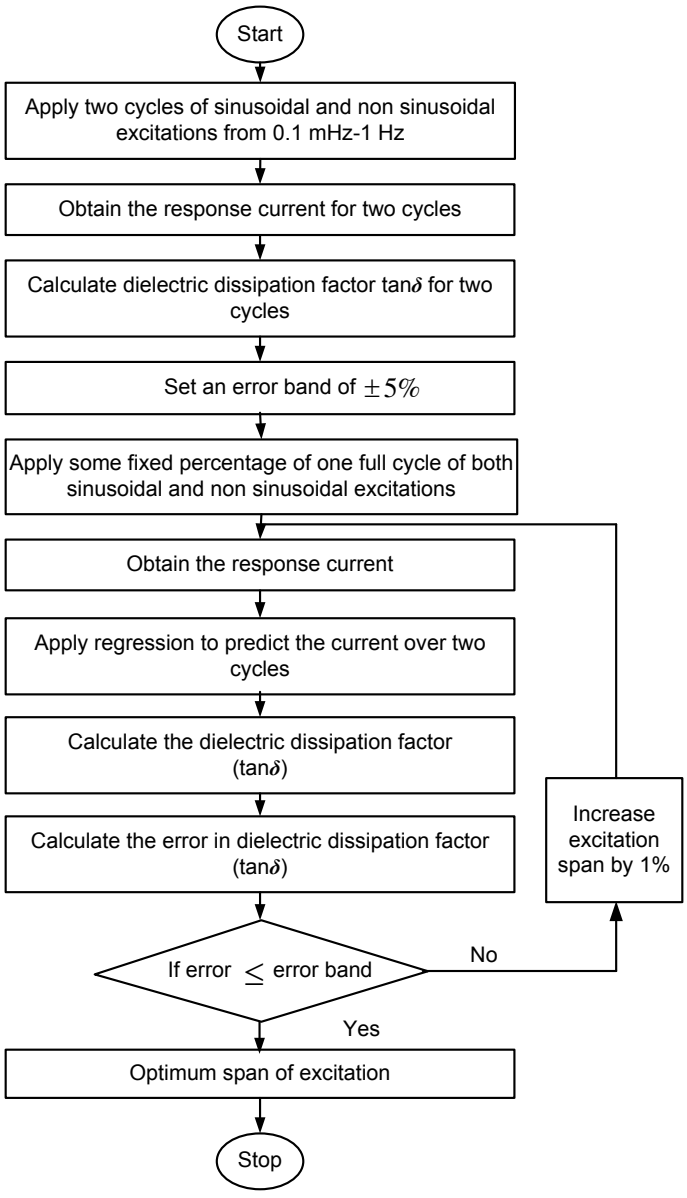

Figure 2.8: Flowchart showing determination of optimum excitation span (%) of one full cycle

2.6 Experimental results

2.6.1 Determination of optimum excitation span (%) for different waveforms

The optimum excitation span percentages for sinusoidal as wells as five triangular waveforms were determined using the procedure as depicted in Figure 2.8. Figures 2.9 (a) and 2.9 (b) illustrate the variation of optimum excitation span percentages for sinusoidal and triangular excitations at different frequencies for sample-1, 2 and 3, respectively.

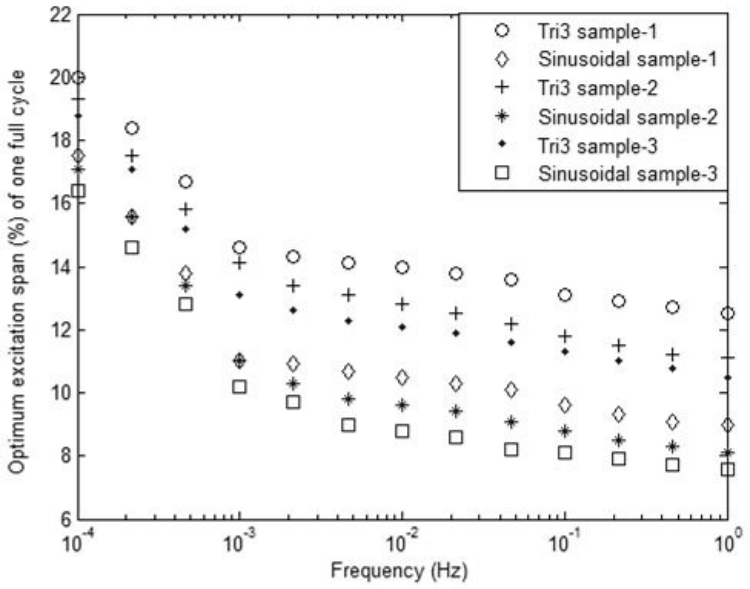

(a)

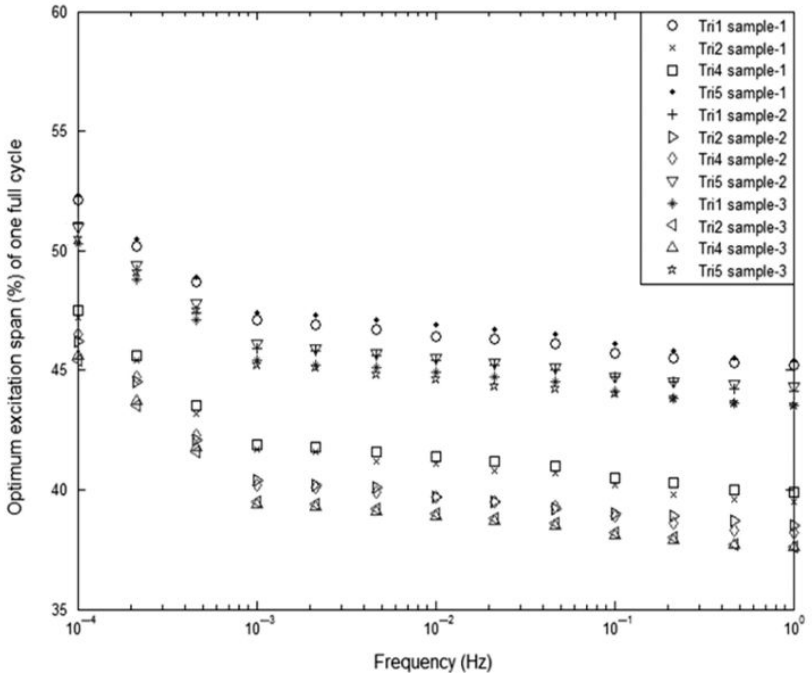

(b)

Figure 2.9: Variation of optimum excitation spans for triangular excitations for 3 samples at different frequencies (a) Tri3 and Sinusoidal (b) Tri1, Tri2, Tri4 and Tri5

From the results presented in Figures 2.9(a) and 2.9(b), it is evident that some of the factors like frequency of excitation voltage waveform, type of excitation voltage waveform, moisture content of the samples etc. play important role in proper estimation of the dielectric dissipation factor profile of the insulation, which are discussed below.

a) Frequency

The frequency of excitation voltage waveforms does play an important role in determination of optimum excitation span for successful estimation of tanδ profile of the insulation. From Figures 2.9(a) and 2.9(b), it can be observed that for all the three samples prepared in the laboratory, higher percentage of excitation span is necessary to correctly estimate the dielectric dissipation

factor at 0.1mHz. As the frequency of the applied excitation increases, lesser excitation span was necessary for proper prediction of the current waveform and hence the dissipation factor.

b) Type of applied excitation voltage waveform

Different types of excitation voltage (sinusoidal and triangular) waveforms were used for performing the FDS test in the laboratory. It can be noted from Figures 2.9 (a) and 2.9(b) that optimum excitation span varies with the nature of excitation voltage waveforms. Among different applied excitation voltage waveforms, it was found that Tri3 required the least excitation span. Considering different non sinusoidal excitations, Tri1 and Tri5 required almost identical spans. Similar was the case with Tri2 and Tri4, which required almost equal spans. Hence, it is evident that excitation voltage waveforms have a definite impact on determination of optimum excitation span for proper estimation of dielectric dissipation factor.

a) Moisture content of the samples

Another interesting observation from Figures 2.9(a) and 2.9(b) is that the optimum excitation span determined for all waveforms also depend on the moisture content of the samples. It can be observed that for samples with different moisture contents prepared in the laboratory, sample-1 with lowest *m.c* (1.0%) required a slightly higher excitation span percentage, compared to the sample-3 with highest *m.c* (3.0%). This was found to be true for all excitation voltage waveforms and at all measurement frequencies.

2.6.2 Determination of an applicable excitation span (%) of one full cycle

The optimum excitation spans determined for sinusoidal as well as for different triangular waveforms (in section 2.6.1) was found to vary with measurement frequency, type of excitation voltage waveform and moisture content of the samples. However, during onsite measurement, since the moisture content of a transformer is practically unknown, hence a suitable excitation span for different excitation voltage waveforms has to be determined that will be applicable for all cases in performing FDS measurement. This applicable excitation span was determined on the basis of highest excitation span required for different excitation voltage waveforms at all frequencies among all three samples. It can be seen that among all three

samples prepared in the laboratory, sample-1 requires highest excitation at 0.1mHz, which decreases with the increase in frequency as stated earlier in Section 2.6.1. Hence, the excitation span required for sample-1 at 0.1mHz was chosen as an applicable excitation span. Performing FDS test with this applicable span for all different excitation voltage waveforms will ensure proper estimation of dielectric dissipation factor within the frequency range of 0.1mHz to1Hz. The applicable excitation span percentage of one full cycle determined for sinusoidal and five triangular excitations are tabulated below in Table 2.4. In Table 2.4, an applicable excitation span percentage for different applied voltage waveforms considering a stop frequency of 1mHz have also been determined.

Table 2.4: Applicable excitation span (%) of one full cycle for different excitation voltage waveforms

Excitation Waveform	**Applicable excitation span (%) of one full cycle considering stop frequency of 0.1mHz**	**Applicable excitation span (%) of one full cycle considering stop frequency of 1mHz**
Tri1	54.1	47.1
Tri2	48.2	41.7
Tri3	17.5	11.0
Tri4	48.4	41.9
Tri5	54.3	47.4
Sinusoidal	20.0	14.6

2.6.3 Measured and predicted dielectric response current

Figures 2.10 (a) and 2.10 (b) shows the predicted response current over two cycles using the determined applicable excitation span (as obtained in Table 2.4 for stop frequency of 1mHz) for Tri3 and sinusoidal excitation, respectively. It is evident from Figures 2.10 (a) and 2.10 (b) that the measured and the predicted response currents for both Tri3 and sinusoidal excitation voltages almost coincides with each other, indicating the practicability of the proposed method for FDS measurement of oil-paper insulation.

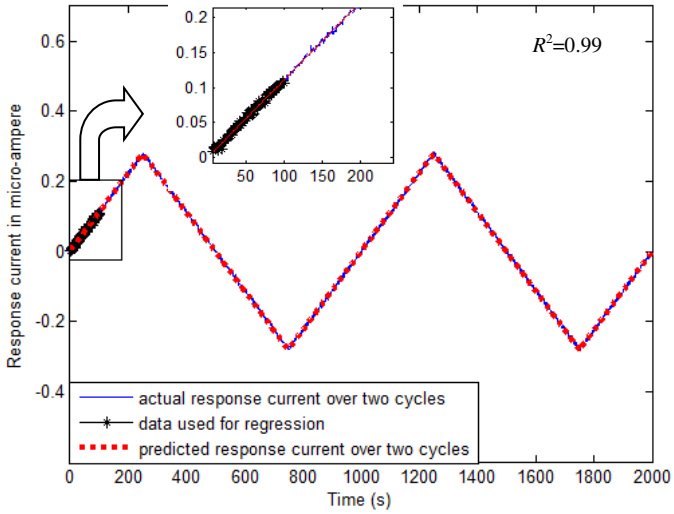

(a)

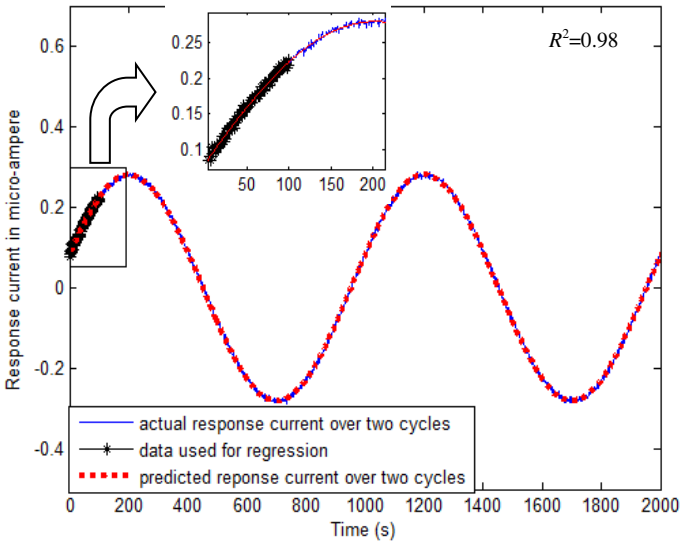

(b)

Figure 2.10: Predicted response current using 11.0% of Tri3 excitation and 14.6% of sinusoidal excitation

2.6.4 Variation of dielectric dissipation factor for test samples

Figures 2.11 (a) and 2.11 (b) show the variation of dielectric dissipation factor (tanδ) against frequency using 17.5% of one full cycle of Tri3 and 20% of one full cycle of sinusoidal excitation in comparison to two cycles. It can be pointed out from the results presented in Figures 2.11 (a) and 2.11 (b), the tanδ of test samples at each measurement frequency computed using conventional FDS method by applying sinusoidal excitation voltage for two cycles are almost similar with that obtained by proposed method. Therefore, it can be inferred that the proposed method is capable of providing similar results as that obtained by using cFDS measurement, but at a much reduced time. In the next section, the overall measurement FDS test time required by the proposed method is compared with measurement using two cycles of sinusoidal excitation voltage.

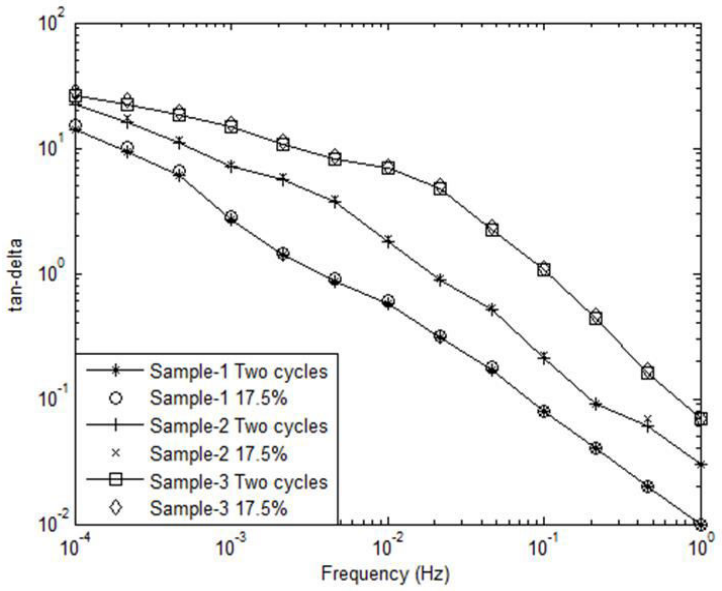

(a)

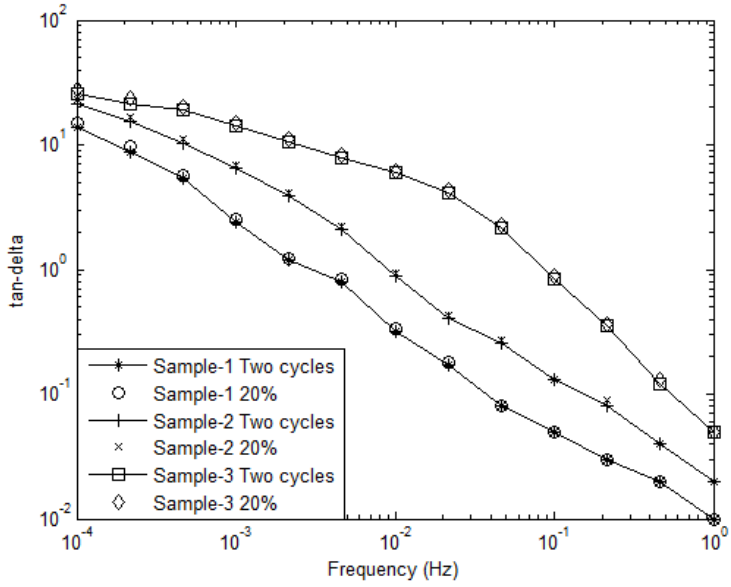

(b)

Figure 2.11: Variation of dielectric dissipation factor (tanδ) against frequency for (a) Tri3 excitation and (b) sinusoidal excitation in comparison to two cycles

The variation of dielectric dissipation factors with frequency for Tri1, Tri2, Tri4 and Tri5 waveforms computed by using applicable excitation span percentage of one full cycle (as given in Table 2.4) was compared with cFDS measurement and the results were presented in ***Appendix***.

2.7 Computation of overall FDS measurement time

The over-all test time was initially computed using conventional method by applying two cycles of sinusoidal excitation voltage. Then, the overall measurement time was calculated by applying the determined applicable excitation span (as determined in Table 2.4) for all different waveforms. Finally, the percentage reduction in overall test time is compared with conventional method. Tables 2.5 and 2.6 show the overall test time and percentage reduction in overall measurement time achieved using the proposed method in comparison with cFDS measurement considering stop frequency of 0.1mHz and 1mHz, respectively.

Table 2.5: Comparison of overall test time and percentage reduction in overall test time considering stop frequency of 0.1mHz

Excitation waveform	**Overall test time in hours (cFDS)**	**Overall test time (in hours) using proposed method**	**Percentage reduction in overall test time**
Tri 1	10.4	2.80	73.08
Tri 2		2.49	76.06
Tri 3		0.90	91.35
Tri 4		2.50	75.96
Tri5		2.81	72.98
Sinusoidal		1.03	90.10

Table 2.6: Comparison of overall test time and percentage reduction in overall test time considering stop frequency of 1mHz

Excitation waveform	**Overall test time in minutes (cFDS)**	**Overall test time (in minutes) using proposed method**	**Percentage reduction in overall test time**
Tri 1	62.2	14.7	76.37
Tri 2		13.0	79.10
Tri 3		3.5	94.37
Tri 4		13.1	78.94
Tri5		14.8	76.21
Sinusoidal		4.6	92.60

It can be observed from Tables 2.5 and 2.6 that there is a considerable reduction in overall test time using the proposed method compared to cFDS measurement. The overall measurement time required for Tri3 is minimum followed by sinusoidal excitation, compared to other excitation voltage waveforms. This may be due to the fact that, the dielectric response current measured under application of Tri3 waveform is most symmetrical in nature among different triangular excitation voltages used in the work. Therefore, the increasing and decreasing slope of Tri3 is constant throughout the entire time period. This symmetric property of Tri3 is also reflected in the measured dielectric response current. Hence, the measured dielectric response current shows the most symmetric nature compared to the other response current waveforms. This fact enables to retrieve the entire cycle data from least measurement data in comparison with the response currents under other excitation voltages used here. It is to be mentioned here that this comparison is done based on three measurement frequencies per decade.

The overall test time required by the regression approach is also compared with some existing methods proposed in [76, 77] and the results are presented in Table 2.7. It is evident that the proposed method can bring down FDS measurement time significantly in comparison with existing methods, thereby

enabling diagnosis of insulation condition at a significantly reduced time. It is to be mentioned here that in this comparative study overall measurement time and percentage reduction in measurement time is computed for only sinusoidal excitation voltage considering three measurement frequency points per decade.

Table 2.7: Comparison of overall test time and percentage reduction in overall test time with existing methods

Reference	Total measurement time (in hours)	Total measurement time (in hours) using regression approach (0.1mHz to 1Hz)	Percentage reduction in measurement duration
[76]	3.36	1.03	69.34
[77]	1.81		43.09

2.8 Conclusions

In this chapter, a technique to reduce cFDS measurement time has been proposed using sinusoidal and triangular excitations. At first, the insulation under test was subjected to two full cycles of excitations (sinusoidal and triangular) over a range of frequencies from 0.1mHz to1Hz, and the dielectric response currents were measured from which the dielectric dissipation factor were calculated. Next, instead of applying the excitations for two cycles, some fraction of one full cycle of sinusoidal and triangular excitations were applied separately on the same set of samples and the corresponding response currents were obtained. Using symmetry and periodic nature of the response current and by employing mathematical regression technique, the entire response current over two cycles were predicted from some fraction of one full cycle of response current. The dielectric dissipation factor of the test samples were thereby recalculated from the fundamental component of the excitation voltages and the predicted response currents for both sinusoidal and triangular excitation voltage waveforms. Finally, the results were compared with that obtained by using two full cycles of excitation voltages earlier, so that it lies within an error band of $\pm 5\%$. Satisfying the error constraint, optimum excitation span percentages of one full cycle of sinusoidal and different triangular excitations were determined, for all three test samples at different measurement frequencies. While evaluating the optimum excitation span for different waveforms, several factors were found to play pivotal role in estimation of tanδ profile of the insulation. Considering the effect of all these factors, finally an applicable excitation percentage has been determined from the obtained set of optimum span of excitation for

sinusoidal and all triangular excitation voltage waveforms. For validation purpose, three different test samples were tested in the laboratory. The dielectric dissipation factor of the test samples obtained with the determined applicable excitation span shows reasonably good agreement with the results obtained by using two cycles as in conventional method. Based on this applicable excitation span, the over-all time required to perform the test have been computed. Compared to cFDS measurement, it has been observed that there is a considerable reduction in the measurement time. Also, it has been found that for a typical triangular waveform (Tri3), the measurement time is lowest compared to sinusoidal and other triangular excitations.

Although the regression based method proposed in this chapter is capable of reducing cFDS measurement time appreciably, yet from the practical measurement point of view, it is difficult to apply fractional excitation waveform at each individual measurement frequency to conduct the dielectric response measurement from 0.1mHz to 1Hz. The first problem is the presence of initial transients, which are inadvertently present in the measured dielectric response current, every time the excitation voltage is switched on. The presence of switching transients at the start of the measurement may affect the accuracy of the dielectric response measurement using regression approach. Besides, the total measurement duration as well as the percentage reduction in overall measurement time computed in this chapter is also dependent on the number of measurement frequency points per decade. Increasing the number of frequency points especially during very low frequency measurement (0.1mHz to 1mHz) can lead to substantially longer measurement duration even by using fractional excitation voltage waveforms. Considering these two practical issues, in the next chapter broadband excitation voltage waveforms in the form of chirp signals are proposed to accelerate FDS measurement from 0.1mHz to 1Hz.

Chapter 3

Accelerating Frequency Domain Spectroscopy Measurement Using Chirp Excitations

3.1 Introduction

In Chapter 2, a method to reduce FDS measurement time based on mathematical regression technique was proposed for condition monitoring of oil-paper insulation system subjected to both sinusoidal and non-sinusoidal excitation voltage waveforms. It was observed that by applying regression technique on some fraction of one full cycle of excitation voltage waveforms, it was possible to predict the response current for two full cycles, which led to a significant reduction in measurement duration, since the necessity of applying two full cycles of excitation voltage was eliminated. However, from the practical point of view, accelerating FDS measurement using the regression based approach has certain limitations, which are briefly elucidated below.

The first problem related to regression based approach proposed in Chapter 2 is the presence of initial transients, which influence the measurement system every time the excitation voltage is switched on. Since the oil-paper insulation system of a transformer can be represented by a linear dielectric model consisting of parallel R-C branches, hence a transient current always flows through the insulation system each time the excitation voltage is applied on it. Now for the purpose of regression in Chapter 2, the initial transient part of the response current was neglected and the regression process started after the current attained a steady state value. This procedure was repeated at each measurement frequency points to nullify the effect of initial transients on measurement system. During calculation of reduction in measurement time also (in Tables 2.5 and 2.6), the influence of current settling time on overall test duration was not considered. However, if the settling time of the dielectric response current at each measurement frequency is considered, then the overall FDS measurement duration even by regression approach can be much longer, which was not considered in Chapter 2.

Another important issue related to regression based approach is that the overall measurement duration and the percentage reduction in measurement time both depends on the number of measurement frequency points per decade. In chapter 2, it was observed that for less number of measured frequency points per decade (only 3 per decade), the regression approach worked reasonably well leading to a significant reduction in overall measurement time. But as the number of measurement frequency points per decade increases (5-8 per decade), FDS measurement time also increases even by applying regression technique, since the fractional excitation voltage has to be applied on the insulation system for more number of times, which leads to an overall increase in measurement duration. For better understanding, the overall FDS measurement time computed by applying 20% of one full cycle of sinusoidal excitation (applicable excitation span as determined in Chapter 2) for 5 as well as 8 number of measurement frequency points per decade from 0.1mHz to 1Hz is shown in Table 3.1.

Table 3.1: Total FDS measurement duration for 5 and 8 measurement frequency points/decade

Measurement frequency points/decade	**Test time in hours (applying 20% of one full cycle) for sinusoidal excitation**
5	1.70
8	2.68

It is evident from the results presented in Table 3.1 that the overall FDS measurement time needed for regression based approach is influenced by the number of measurement frequency points per decade and increases with the increase in number of measurement points per decade. Therefore, accelerating FDS measurement using regression technique on some fraction of one full cycle of applied excitation has certain practical problems, which inadvertently call for an improved measurement approach for reliable diagnosis of transformer insulation at a much reduced time.

Considering the aforesaid facts, in this chapter another method of accelerating FDS measurement at low frequencies is proposed using broadband excitation voltage waveforms in the form of chirp signals. In this study, chirp signals having both linear and exponential frequency sweeps are used as excitation voltage waveforms to conduct FDS measurement on oil-paper insulation from 0.1mHz to 1Hz. The advantages of using chirp excitations are twofold. Since, chirp signals are non-stationary in nature, i.e. whose frequency and phase vary with time, it is possible to measure dielectric response current simultaneously at several measurement

frequencies [86, 98]. Therefore, it is not necessary to apply a series of excitation voltages at each individual frequency points to obtain the dielectric response, thereby eliminating the problem of initial switching transient at each measurement frequency. Besides, being a broadband excitation [86, 99-100], the tanδ value at any frequency within the measurement frequency bandwidth (from 0.1mHz to 1Hz) can be computed, thereby imposing no restriction on the number of measurement frequency points per decade. The mathematical details of the chirp waveforms including different parameters designed for the purpose of FDS measurement on oil-paper insulation are discussed hereafter.

3.2 Details of Chirp Waveforms

Mathematically, a chirp signal can be expressed as

$$V_{ch}(t) = A\sin(\phi(t)) = A\sin\left(2\pi\int_0^t f_i(t)dt\right) \tag{3.1}$$

Here, '*A*' is the amplitude and $f_i(t) = \frac{1}{2\pi}\left(\frac{d\phi(t)}{dt}\right)$ is the instantaneous frequency of the chirp signal. For a linear chirp (LC) waveform, instantaneous frequency $f_i(t)$ varies linearly with time

$$f_i(t) = f_I + \beta t \tag{3.2}$$

Here, β is the chirp rate, which is given by $\beta = \frac{f_F - f_I}{T_{ch}}$, f_I is the initial frequency, T_{ch} is the duration of the chirp signal and f_F is the final frequency at $t=T_{ch}$. Substituting the equation (3.2) in equation (3.1), the LC waveform can be expressed as

$$V_{ch}(t) = A\sin\left(2\pi f_I t + \frac{\beta t^2}{2}\right) \tag{3.3}$$

Another type of chirp excitation exists where the instantaneous frequency $f_i(t)$ varies exponentially with time.

$$f_i(t) = f_I \beta^t \tag{3.4}$$

This type of chirp waveform is known as logarithmic chirp (LGC) signal. Putting equation (3.4) in equation (3.1), mathematically, a logarithmic chirp waveform can be expressed as

$$V_{ch}(t) = A\sin\left(2\pi f_I\left(\frac{\beta^t - 1}{\ln(\beta)}\right)\right) \tag{3.5}$$

In the present work, chirp waveforms with both linear and logarithmic frequency sweeps are used as excitation voltage signals for conducting FDS measurement on oil-paper insulation. The initial f_I and the final frequency f_F of the sweep were set at 0.1mHz and 1Hz, respectively, thereby covering the entire low frequency range from 0.1mHz to 1Hz. The final frequency of the sweep was fixed at 1Hz, because the time taken to conduct FDS measurement from 1Hz to 1kHz is very small. The total time duration T_{ch} required by the chirp waveforms to cover the frequency range from 0.1mHz to 1Hz is 5000 seconds. Figure 3.1 (a) and 3.1 (b) shows the typical LC and LGC excitation voltage waveforms used for FDS measurement, respectively.

Along with the chirp waveforms, cFDS measurement using conventional sine wave excitation covering the same frequency range (0.1mHz to 1Hz) was performed for the purpose of comparison. The amplitude of both sinusoidal as well the chirp excitations were kept fixed at 200V. For better understanding of the amplitude spectrum of different chirp waveforms, the spectral analysis of both LC and LGC waveforms is done in the following section.

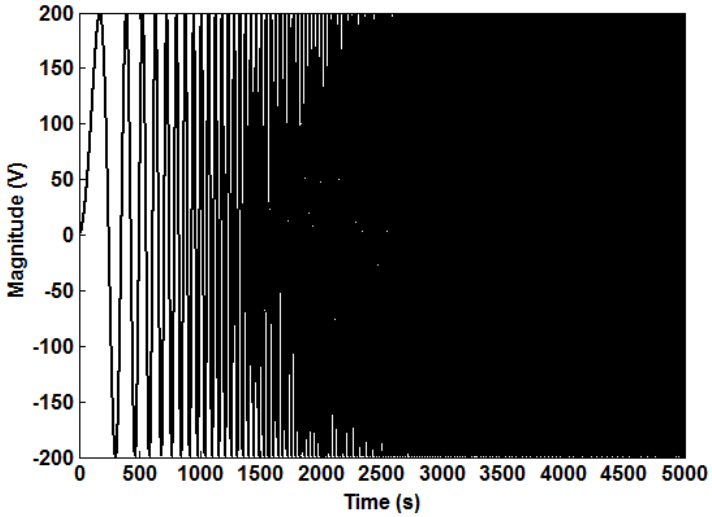

(a)

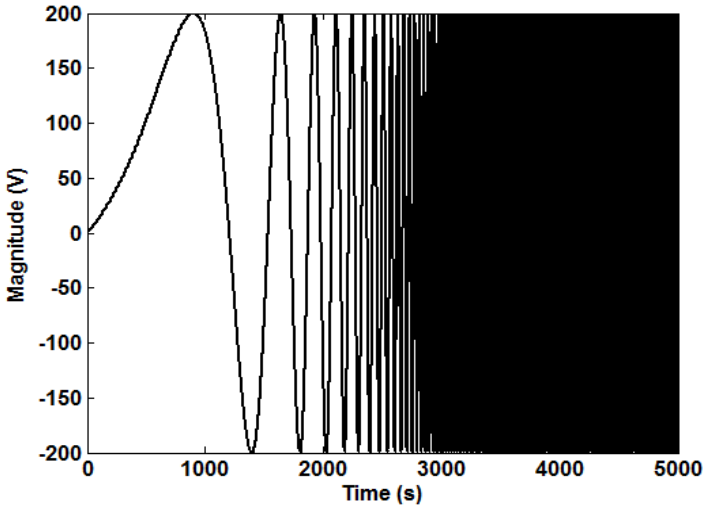

(b)

Figure 3.1: Typical (a) LC (b) LGC excitation voltage waveforms

3.3 Spectral analysis of chirp waveforms

In order to compute the amplitude spectrum of LC and LGC signals, Fast Fourier Transform (FFT) was performed separately on equation (3.3) and (3.5), respectively. Figure 3.2 shows the amplitude spectrum of both types of chirp waveforms within the frequency range from 0.1mHz to1Hz.

It can be observed from Figure 3.2, that the amplitude spectrums of both LC and LGC waveforms are different from each other. For linear chirp waveform, the spectrum is almost flat, whereas for logarithmic chirp signal, the magnitude of excitation voltage decreases with the increase in frequency. Moreover, the amplitude spectra of both types of chirp waveforms are ripple free, with very little fluctuations and having steep drop down outside

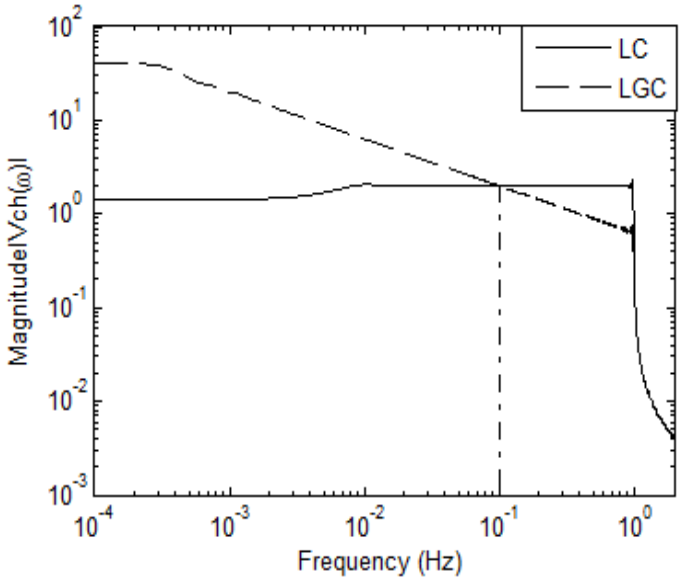

Figure3.2. Amplitude spectrum of different chirp waveforms

the measurement range (0.1mHz to 1Hz), which are ideal for broadband measurement. It can be further pointed out from Figure 3.2, that the amplitude spectra of both linear and logarithmic chirp signals intersect at about 0.1Hz. From 0.1mHz to 0.1Hz, the magnitude of logarithmic chirp waveform is higher than a linear chirp waveform. Since, the energy content of the signal is directly proportional to the signal magnitude, therefore, it is

evident that the logarithmic chirp signal possesses more energy within the frequency range from 0.1mHz to 0.1Hz, compared to linear chirp. In order to calculate the energy E_{ch} of the chirp waveforms over the frequency range from 0.1mHz to 0.1Hz, Parseval's theorem, was used, which is given by [101]

$$E_{ch} = \frac{1}{2\pi} \int_{0.1mHz}^{0.1Hz} \left| V_{ch}(\omega) \right|^2 d\omega \tag{3.6}$$

Here, $\left| V_{ch}(\omega) \right|$ denotes the amplitude spectrum of the chirp waveforms. The computation of E_{ch} is important, because the magnitude of dielectric response current within the frequency range from 0.1 mHz to 0.1Hz being very low (of the order of several nano-amperes), there is every possibility that the recorded response current will be affected by the presence of background noise. Therefore, it is desirable that the excitation signals must possess significant amount of energy to ensure high SNR, so that the measured response current is not affected by noise especially during low frequency measurement [102]. Since, tanδ is computed mainly from the phase response of the applied excitation voltage and the response current, presence of noise may lead to error in computation of tanδ profile of the insulation. As the measurement frequency increases above 0.1Hz, the magnitude of response current also increases. In that case, the measured dielectric response current becomes less sensitive to noise. Therefore it is necessary to compute the energy content of chirp waveforms over the frequency range from 0.1mHz to 0.1Hz. The signal energies for both LC and LGC waveforms computed using equation (3.6) are presented in Table 3.2.

Table 3.2: Energy of different chirp waveforms

Type of chirp waveform	E_{ch} **(Joules)**
LC	31.83
LGC	64.28

It can be observed from Table 3.1, that the logarithmic chirp waveform has approximately 50.48% more energy than a linear chirp waveform within the frequency range from 0.1mHz-0.1Hz. Hence, from the spectral analysis of chirp waveforms, it is clear that LGC waveform offers better SNR than LC waveform during FDS measurement at low frequencies.

3.4 Advantage of chirp waveforms over existing broadband excitations

In existing literatures, application of several broadband excitations like DC [75, 103] and 'multisine' [71, 76] signals etc have been reported by the researchers to reduce cFDS measurement time. The pros and cons of different broadband excitations proposed for accelerating cFDS measurement are explained briefly.

In the case of DC excitation, the dielectric response current is measured in time domain and is converted to frequency domain using Fast Fourier Transform (FFT) technique, to obtain the frequency spectrum of the insulation over the frequency range from 0.1mHz to 0.1Hz. Although this hybrid method of combining time and frequency domain measurement can bring down cFDS measurement time considerably, but as reported in [77], the method has inherent complexities related to measurements in time domain. Moreover, the method requires additional hardware and software requirements in order to perform measurements in both time and frequency domains [98].

A more probable solution to this problem was proposed in [76], where another broadband excitation in the form of multiple frequency sinusoids (also known as 'multisine signal), was proposed to conduct FDS measurements from 0.1mHz to 0.1Hz. However, a major issue in designing a 'multisine' excitation signal is the crest factor (CF). Since, a 'multisine' consists of several sinusoids of different frequencies, the resultant waveform have inevitably high CF values. High CF is responsible for poor signal to noise ratio (SNR) during acquisition of response current, which affects FDS measurement at very low frequencies [76, 102]. To eradicate the problem of CF, phase shifts are introduced in the sinusoids and the 'multisine' excitation with optimum CF is designed using an optimization algorithm [76]. Even then, the CF of an optimized 'multisine' waveform is always higher than that of a pure sinusoid, which may influence dielectric response current measurement at low frequency [104].

In the case of chirp signals proposed in this chapter, because of the broadband nature of the excitation signal, the entire spectrum the insulation response from 0.1mHz to 1Hz is available from a solitary measurement. Therefore, there is no need of converting time domain dielectric response current to frequency domain. Besides, use of chirp signals also eliminates the problem of CF optimization, since the CF of a chirp signal is essentially same as that of a sinusoid, thereby making signal processing much simpler and suitable for on chip

implementation [102]. Therefore, in comparison with existing broadband excitations, chirp waveforms have distinct advantages in terms of both software and hardware implementation and were therefore used for FDS measurement of oil-paper insulation in this work.

3.5 Frequency response measurement using chirp excitations

Figure 3.3 shows the typical nature of dielectric response current obtained by using LGC on oil-paper insulation. It can be observed from Figures 3.1 and 3.3, that both the applied excitation and the measured response current are typically non-stationary in nature. Therefore, the magnitude and the phase response cannot be correctly obtained by direct application of FFT algorithm. In order to obtain magnitude and phase spectrum accurately from chirp signals, a different methodology was adopted in this work.

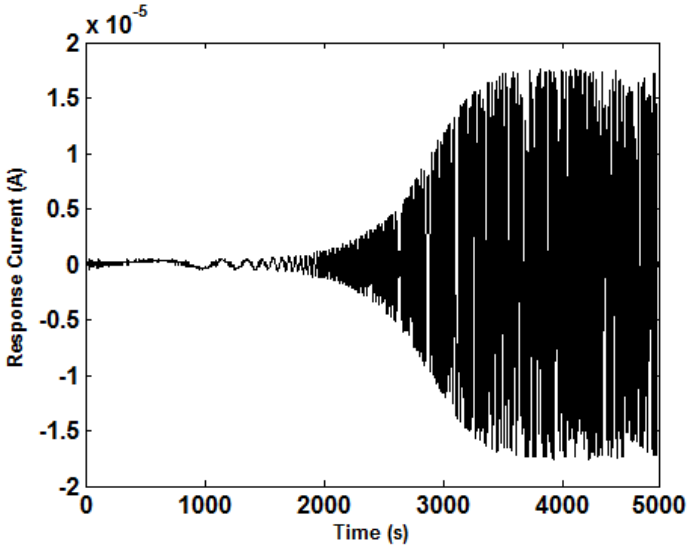

Figure 3.3: Dielectric response current of an oil-paper insulation subjected to LGC excitation voltage

Instead of directly applying FFT, a correlation technique is applied at first on both excitation voltage and the response current to obtain the impulse response of the oil paper insulation system. For any linear discrete time system, if $c(n)$ is the output of the system, with $r(n)$ being the input to the

system, then the impulse response $G(n)$ of the system can be obtained by equation (3.7) [101]

$$S_{cr} = G(n)S_{rr} \tag{3.7}$$

where, S_{cr} is the cross correlation between the output and the input sequence and S_{rr} is the autocorrelation of the input sequence. A distinct advantage of the correlation technique is that it requires minimum computational burden. Moreover, it also minimizes the effect of external random noise present in the signal while obtaining the dielectric response of the composite oil paper insulation system at low frequencies [102]. Now, if the input is perfect white noise, autocorrelation sequence S_{rr} yields a perfect delta function [104]. In that case, the impulse response $G(n)$ is given by equation (3.8)

$$G(n) = S_{cr} \tag{3.8}$$

Since, S_{rr} is not a perfect delta function, for chirp signals, hence the impulse response in time domain was obtained using equation (3.9) [104]

$$G(n) = \frac{S_{cr}}{S_{rr}} \tag{3.9}$$

Finally, applying FFT on equation (3.9), the impulse response in frequency domain can be expressed as

$$G(j\omega) = \frac{FFT(S_{cr})}{FFT(S_{rr})} = |G(j\omega)|\angle G(j\omega) \tag{3.10}$$

where, $FFT(S_{cr})$ and $FFT(S_{rr})$ are the Fast Fourier transform performed on the correlation sequences S_{cr} and S_{rr}, respectively. From the magnitude and phase responses, parameters like dielectric dissipation factor, real and imaginary parts of complex capacitance etc were calculated for chirp signals over the frequency range from 0.1mHz to 1Hz.

3.6 Experimental set-up

3.6.1 Sample preparation

Three fresh samples with different paper moisture contents were prepared in the laboratory for the purpose of the experiment. The moisture content of the test samples at 30°C was set at 0.8%, 1.5% and 2.5%, respectively which are shown in Table 3.3. The details of the sample preparation were reported in Chapter 2.

Table 3.3: Test samples with different moisture content

Sample Number	***m.c* (%)**
Sample-4	0.8
Sample-5	1.5
Sample-6	2.5

The whole set up (test samples immersed in transformer oil) was kept inside the environmental chamber at 30°C for several days to ensure proper thermal equilibrium. Thereafter, FDS tests were performed using both sinusoidal excitation as well as chirp excitation voltage waveforms. Along with three samples, experiments were also conducted on two real-life transformers. The details of the investigated transformers are given in Table 3.4.

Table 3.4: Details of investigated transformers

Transformer	**Transformer Rating**
Trf-1	Single phase, 250 kVA, 400 V/40 kV
Trf-2	Single phase, 200 kVA, 400 V/50 kV

3.6.2 Experimental procedure

The FDS measurement was performed by keeping the test samples within an environmental chamber with the leads being taken outside for connection to the measurement unit. At first, cFDS measurement was performed on both test samples and transformers over the frequency range of 0.1mHz to 1Hz. During measurement, the excitation voltage was applied to the HV bushing and the response current was measured from the LV bushing for the transformers and the emulated HV and LV bushings in the case of test samples. After conducting cFDS measurement, the terminals of the transformers and the test samples were kept short circuited to eliminate any memory effect. After sufficient time duration, the short circuit was removed, and the experiment was repeated by applying LC and LGC chirp signals on

the samples as well the transformers. During the entire course of measurement, the transformer tank and the GI tank in the case of samples were earthed in order to nullify the effect of stray capacitances. Besides, a separate earth connection was also provided to protect the measuring equipment. A photograph of the FDS measurement on real-life transformers is shown in Figure 3.4.

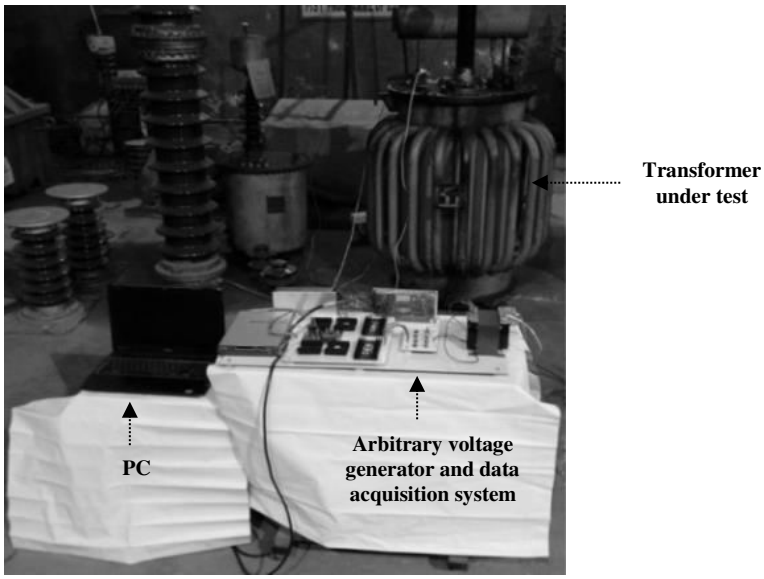

Figure 3.4: FDS measurement on real-life transformers

3.7 Experimental results

3.7.1 Results on test samples

The dielectric dissipation factor (tanδ) for three samples were initially calculated from the phase difference between the applied sinusoidal excitation voltage and the dielectric response current in the frequency range from 0.1mHz to 1Hz. Following this, using equation (3.10), the magnitude and phase response of the same samples were computed from the applied chirp excitation voltages and the corresponding response currents. Finally, from the phase response, tanδ values at each measurement frequency (over

the frequency range from 0.1mHz to 1Hz) were recalculated for both LC and LGC excitation voltage waveforms and were compared with that obtained by applying sinusoidal excitation voltage. The variations of tanδ with frequency for three test samples computed using sinusoidal as well as chirp excitation voltages are shown in Figure 3.5 (a) and Figure 3.5 (b), respectively.

It can be pointed out from Figure 3.5 (a) and Figure 3.5 (b) that the nature of variation of tanδ against frequency computed using sinusoidal as well as chirp excitation voltage waveforms for three samples are almost similar. Moreover, the values of tanδ computed at each measurement frequency for three samples are almost identical for both sinusoidal and LC as well as LGC excitation voltages. Hence, from the experimental results on test samples, it can be concluded that the chirp signals are capable of providing almost identical

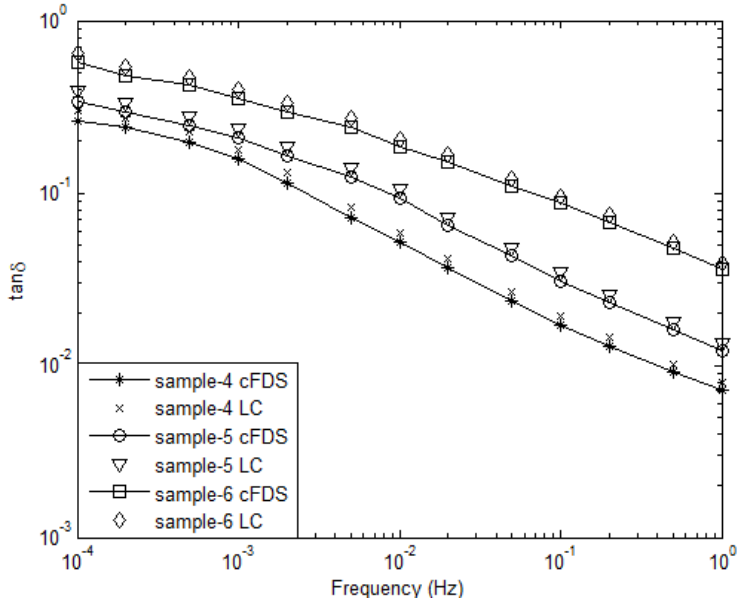

(a)

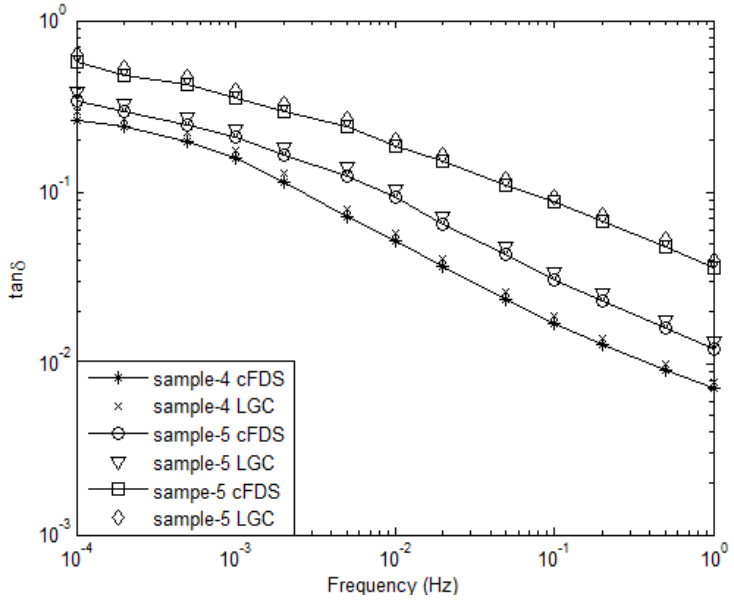

(b)

Figure 3.5: Variation of *t*an*δ* with frequency for three samples subjected to (a) LC and (b) LGC signal in comparison with cFDS measurement

information regarding the condition of transformer insulation as that obtained by using sinusoidal excitation. However, to have a better insight into the experimental results, the percentage error in estimation of tan*δ* profile (with respect to cFDS measurement) obtained using LC and LGC waveforms, are computed as discussed in next section.

3.7.2 Error analysis

The percentage error in tan*δ* at i^{th} measurement frequency is calculated using the following formula

$$Error(\%) = \frac{\left|\tan\delta_{Ch_i} - \tan\delta_{cFDS_i}\right|}{\tan\delta_{cFDS_i}} \times 100 \tag{3.11}$$

In the above equation, $\tan\delta_{cFDS_i}$ indicates the value of tan*δ* value at i^{th}

measurement frequency obtained during cFDS measurement by applying sinusoidal excitation voltage from 0.1mHz to 1Hz. Similarly, $\tan\delta_{Ch_i}$ denotes the tanδ values computed at corresponding measurement frequencies using chirp signals (LC and LGC). Figure 3.6 shows the variation of percentage error (with respect to cFDS measurement) with frequency under the application of LC and LGC excitations for all three test samples.

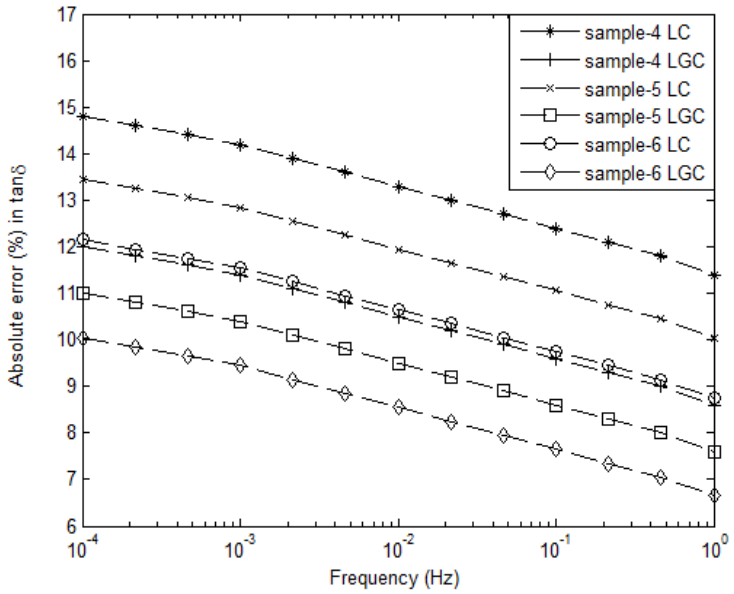

Fig.3.6. Variation of absolute percentage error (with respect to cFDS) with frequency for three samples for LC and LGC signals

It can be seen from Figure 3.6 that the percentage errors are different for LC and LGC waveforms. Besides, the percentage error also varies with both measurement frequency and the paper moisture content of the test samples. The highest absolute percentage error of almost 14.8% is observed in the case of LC waveform at 0.1mHz for sample-4 with *m.c* 0.8%. The corresponding value for LGC waveform is 12%. As the frequency and the *m.c* increases, the percentage error decreases for both waveforms. The lowest absolute percentage error of about 6.8 % is observed in the case of LGC waveform at 1Hz for sample-6 with *m.c* 2.5%. This nature of variation of error percentage with *m.c* and frequency

may be explained as follows.

In the case of sample-4 which has lowest *m.c* of 0.8%, the magnitude of the measured dielectric response current is very low during low frequency measurement. Therefore, for accurate estimation of tanδ profile it is necessary that the excitation signal must have higher signal energy and better noise rejection ability. From the spectral analysis of chirp signals (in section 3.3), it is evident that LGC signal has more signal energy than LC waveform at 0.1.mHz. Therefore, the percentage error in estimation of tanδ profile is less in the case of LGC signals compared to LC signals. As the moisture content and the measurement frequency increases, the magnitude of the dielectric response current also increases. In that case, the measured dielectric response current becomes less sensitive to the presence of noise, so the percentage error decreases for both LC and LGC signals. The variation of mean absolute error *MAE* (%) with paper *m.c* computed for LC and LGC waveforms is shown in Figure 3.7.

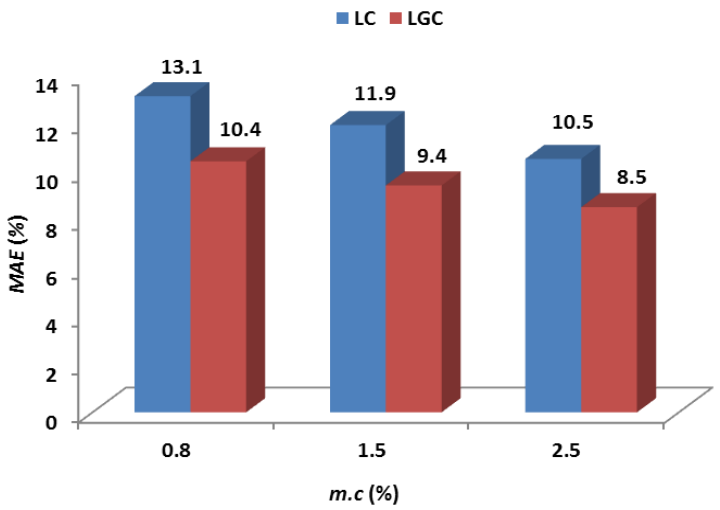

Figure 3.7: Variation of mean absolute error (*MAE*) percentage with *m.c* for LC and LGC signals

The *MAE* (%) was calculated by taking the mean of percentage errors computed for *N* number of measurement frequency points over the frequency range from 0.1mHz to 1Hz. The *MAE* (%) is calculated using equation (3.12)

$$MAE(\%) = \frac{1}{N}\sum_{i=1}^{N}\frac{\left|\tan\delta_{Chi} - \tan\delta_{cFDS_i}\right|}{\tan\delta_{cFDS_i}} \times 100 \tag{3.12}$$

In this study, since, three measurement frequency points are chosen therefore, in (3.12) N=13. From Figure 3.7, it can be pointed out that *MAE* (%) computed for LC and LGC waveforms are found to decrease with the increase in *m.c* of the test samples. Moreover, between LC and LGC waveforms, *MAE* (%) is found to be lowest in the case of LGC waveforms. On the basis of experimental results, it can be said that between LC and LGC signals, LGC waveform provides minimum error percentage in estimation of tanδ profile of the insulation. Therefore, LGC signals are more suitable for FDS measurement of transformer insulation compared to linear sweep. In order to verify the practicability of the proposed accelerated FDS measurement using LGC excitation, additional experiments were conducted on two real-life transformers, which are discussed in the next section.

3.7.3. Test results on transformers

The dielectric dissipation factor and the real part of complex capacitance of two transformers were computed for cFDS measurement as well as by applying chirp signals over the frequency range from 0.1mHz to1Hz. Figures 3.8 (a) and 3.8 (b) show the variation of dielectric dissipation factor and real part of complex capacitance against frequency for *Trf*-1 and *Trf*-2. It is to be noted here that during measurements on real life transformers, experiments were conducted using LGC waveforms only, since LGC waveform is found to provide better results compared to LC waveform in the case of test samples.

It can be seen from Figure 3.8 (a) and Figure 3.8 (b) that the nature of variation of tanδ and real part of complex capacitance against frequency evaluated using cFDS and LGC waveform are almost similar for both transformers. Moreover, the values of tanδ and real part of complex capacitance of *Trf*-1 and *Trf*-2, evaluated at each measurement frequency, are almost same for both cFDS measurement and LGC waveform, which further indicates the feasibility of application of chirp signals in the case of real-life FDS measurements.

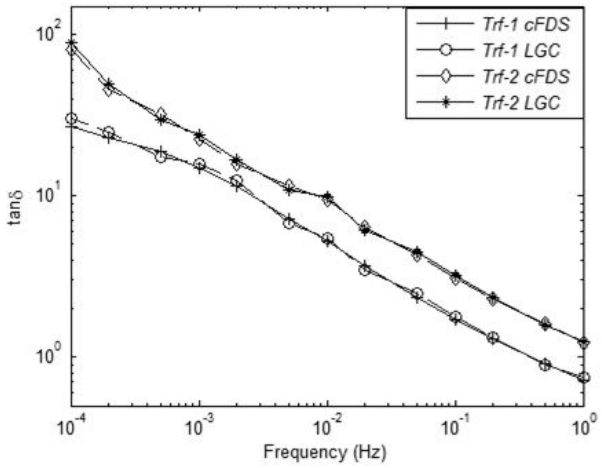

(a)

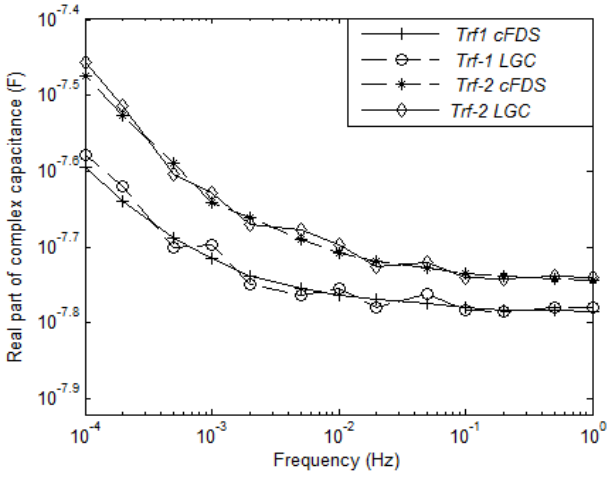

(b)

Figure 3.8: Variation of (a) tanδ and (b) real part of complex capacitance of two transformers for cFDS measurement and LGC excitation voltage

3.8 FDS Measurement time duration: A comparative study

3.8.1 Comparative study of measurement time with cFDS

The measurement time was initially computed for cFDS measurement by applying sinusoidal excitation voltage within the frequency range from 0.1mHz to1Hz. Next, the measurement time was recalculated by using chirp excitation voltage waveforms and the percentage reduction in measurement time with respect to cFDS measurement was computed and the results are reported in Table 3.5. It is important to mention here that, this comparative study is based on different measurement frequency points per decade and also considering both single as wells as two cycles of sinusoidal excitation voltage.

Table-3.5: Comparative study of measurement time with cFDS

Number of measurement frequency points / decade	**Total Measurement duration (hours)**		**Percentage reduction in measurement duration**
	cFDS (sinusoidal)	**Proposed method (chirp excitations)**	
3	10.4 (Two cycles)	1.38	86.73
	5.2 (One cycle)		73.46
5	17 (Two cycles)		91.88
	8.5 (One cycle)		83.76
8	26.8 (Two cycles)		94.85
	13.4(One cycle)		89.70

It can be observed from Table 3.5, that the total test time using chirp waveforms are significantly less compared to cFDS measurement. Considering the effect of number of cycles, the percentage reduction of measurement time is found to be higher in the case of two cycles of sinusoidal excitation compared to single cycle. Another interesting observation from Table 3.5 is that the net measurement duration in the case of cFDS measurement increases with more number of measurement frequency points per decade. But, in the case of chirp excitations, the total measurement time is found to be independent of the number of measurement frequency points per decade. This is due to the fact that the chirp signals being broadband excitations, all desired frequency points can be measured using a single measurement, thereby eliminating the influence of initial switching transients on measurement system. Hence, the frequency domain spectrum of the oil paper insulation system can be measured at a much reduced time using chirp waveforms, in comparison with cFDS measurement.

3.8.2: Comparative study of measurement time with existing methods

In this section, the total measurement time as well as the percentage time reduction using chirp signals is compared with some of the existing broadband excitations and the results are presented in Table 3.6.

Table 3.6:.Comparative study of measurement time with existing methods

Type of Excitations	**Total measurement time (in hours)**	**Total measurement time (in hours) using chirp excitations (0.1mHz to 1Hz)**	**Percentage reduction in measurement duration**
DC [75, 103] (0.1mHz to 0.1Hz)	2.54	1.38	45.66
'multisine' [71, 76] (0.1mHz to 1Hz)	3.36	1.38	58.92

It can be observed from Table 3.6 that the use of chip excitations provide fastest FDS measurement compared to both 'multisine' excitation (0.1mHz to 1Hz) and DC excitation (0.1mHz to 0.1Hz), respectively. Hence, it is evident that the chirp excitations have the potential of saving substantial amount of measurement time compared to both cFDS and existing methods.

3.9 Conclusions

In the present work, an application of non-stationary and broadband excitation using chirp signals is presented for condition assessment of oil-paper insulation. Chirp signals having both linear and logarithmic frequency sweeps band limited from 0.1mHz to1Hz, were used in this study for the purpose of FDS measurement. A comparative study of the proposed method with cFDS measurement is also reported. To validate the proposed method, experiments were conducted on a few laboratory prepared samples and also on two real life transformers. As outcome of the investigations, the following inferences can be drawn.

(i) Use of chirp excitations provided similar information regarding insulation condition in comparison with cFDS measurement.

(ii) Between LC and LGC excitations used in this study, logarithmic chirp provided better information regarding insulation condition compared to linear chirp signals offering minimum *MAE* (%) in estimation of dielectric dissipation factor with respect to cFDS measurement.

(iii) The total measurement duration using chirp signals was found to be significantly lower compared to cFDS measurement.

(iv) Compared to existing broadband excitations, the use of chirp excitations required much lower measurement time.

Therefore, it can be concluded that FDS measurement using chirp excitations offer reliable assessment of insulation condition at a much reduced time compared to cFDS measurement.

However, one important issue, which is not discussed in this chapter, is the effect of non-linearity of oil-paper insulation system during FDS measurement using chirp excitations. During computation of the magnitude and phase response of oil-paper insulation using logarithmic chirp excitation, it was assumed that the oil-paper insulation system behaves as a linear system. However, in reality, as the condition of the oil-paper insulation system degrades (increase in *m.c*), it no longer behaves like a linear system. Considering the above said fact, in the next chapter, a non-linear model of transformer insulation using chirp excitation is proposed based on system identification theory for more reliable assessment of insulation condition at reduced measurement time.

Chapter 4

Non-Linear Modeling of Oil-paper insulation Using Chirp excitation- A System identification Approach

4.1 Introduction

In Chapter-3, it was observed that the application of chirp signals as excitation voltage in place of traditional sine wave is capable of reducing cFDS measurement time significantly. Besides, experimental investigations on several test samples and also on two real-life transformers also confirmed that among different type of chirp perturbations LGC waveform is better suited for cFDS measurement compared to LC waveform. Moreover, application of chirp waveforms also eliminate the problem of both hardware and software complexity owing to its ease of implementation compared to several other broadband excitations. Moreover, being a broadband signal, cFDS measurement using chirp signal is independent of the number of measurement frequency points per decade. As a consequence the problem of initial transients due to switching on the excitation voltage at each measurement frequency is also eliminated. Hence, from the point of view of practical measurement, application of LGC waveform as a broadband excitation voltage for conducting FDS measurement on transformers over the frequency range from 0.1mHz to 1Hz is a feasible option.

However, one important aspect of FDS measurement which was not considered in Chapter-3 is the influence of non-linearity of the oil-paper insulation system during FDS measurement using chirp excitation. In the earlier chapter, during frequency response measurement using LGC signal, the oil-paper insulation was assumed to behave as a linear system. But in reality, the transformer insulation system is highly complex in nature and manifests non-linear behavior as reported in many existing literatures [81, 85-87]. It was reported in [81, 87], that the non-linearity of oil-paper insulation increases with the increase in moisture and aging (i.e. degradation) of the cellulose insulation. Ojha et al. have investigated the non-linearity of oil-paper insulation based on PDC and RVM measurements [105, 106]. The presence of non-linearity in the dielectric response of the transformer insulation based on

PDC measurement was also reported in [106]. Pradhan et al. have reported the presence of non-linearity in oil-paper insulation system and subsequently developed a non-linear model for insulation based on FDS measurement [81]. Zhang et al. have investigated the non-linear phenomenon in oil-paper insulation due to the presence of impurity ions at different moisture levels by conducting FDS test at different voltage levels [108]. Therefore, it is evident from the existing literature survey that the oil-paper insulation system possesses inherent non-linear characteristics and the tanδ profile of the oil-paper insulation assuming linear model (LM) of the insulation may not be accurate enough in the case of samples with higher moisture content and also for aged transformers. Considering the above fact, a non-linear model of oil-paper insulation based on system identification theory using chirp excitation is proposed in this chapter for having better information regarding the insulation condition.

Existing literatures reveal that the oil-paper insulation system can be considered to be a black-box. Hence for any given input perturbation to the system, the mathematical model of the black-box can be obtained based on the input-output data. In this chapter, LGC waveform is chosen as an input perturbation, because it has superior spectral properties and offers minimum *MAE* (%) in estimation of the dielectric dissipation factor profile of the oil-paper insulation compared to linear sweep as reported in Chapter 3. Moreover, because of the broadband nature of the applied excitation, the total insulation response can be obtained from a single measurement. Hence, it is possible to develop a mathematical model of the insulation based on the measured response current and the applied excitation voltage. For the purpose of non-linear modeling, system identification approach was used, which provides an equivalent model of any unknown system based on its input and output relationship. The steps involved in non-linear modeling of oil-paper insulation based on system identification theory are described below.

4.2 Non-Linear modeling of transformer insulation system

4.2.1 System Identification: A brief overview

In system identification, an equivalent mathematical model of any unknown test system is determined based upon input and output measurements [81, 86, 109]. The equivalent model can be identified by using either time domain or frequency domain data. In the present study, time domain data is used for modeling, since it is readily available from the measurement. The test system in this study is the composite oil-paper insulation system of the transformer.

A block diagram of system identification is shown in Figure 4.1.

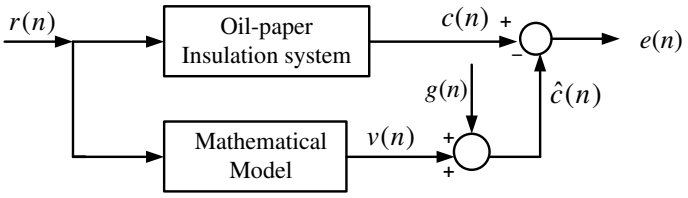

Figure 4.1: Block diagram of system identification

In Figure 4.1, $r(n)$ is the applied input excitation, $c(n)$ is the output of the test system, $\hat{c}(n)$ is the response of the predicted mathematical model under the application of same excitation $r(n)$, and $g(n)$ is the added noise. The error $e(n)$ is the difference between the actual system response and the equivalent model. When $e(n)$ tends to zero, a model is said to be correctly identified [81,109]. The equivalent model of the test system in Figure 4.1 can be represented by either linear or non-linear model depending on the type of the system. Due to the presence of non-linearity in the oil-paper insulation system, a non-linear model is selected as an equivalent model in this study for the purpose of modeling. In system identification there exist different types of non-linear models like autoregressive model, Hammerstein model, Wiener model etc. In this study a Wiener model (WM) is proposed for non-linear modeling of oil-paper insulation, since it was found to yield least error $e(n)$, compared to other models. The basic structure of Wiener model is explained in the next subsection.

4.2.2 Wiener Model

Figure 4.2 shows the block diagram of the Wiener model (WM). The structure of the WM consists of a discrete time linear system $G(n)$ in cascade with a static non-linear element $f(.)$. If the static nonlinearity $f(.)$ at the output is set to 1, it represents a linear model (LM) [110]. Therefore, WM is a more generalized model as both linear and non-linear system can be represented using a WM.

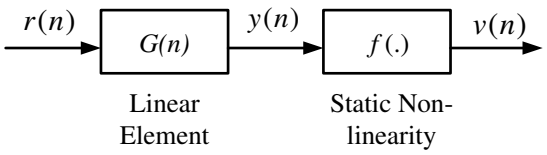

Figure 4.2: Block diagram of Wiener Model

The discrete time transfer function $G(z)$ of the linear element is expressed as the ratio of the Z-transform of the output $y(n)$ to the input $r(n)$ as follows

$$G(z) = \frac{Y(z)}{R(z)} \tag{4.1}$$

where

$$Y(z) = y_1 z^{-1} + y_2 z^{-2} + ... + y_p z^{-p}$$
$$R(z) = r_0 + r_1 z^{-1} + r_2 z^{-2} + ... + r_q z^{-q} \tag{4.2}$$

Here 'p' and 'q' denotes number of zeros and poles of the discrete time transfer function $G(z)$, respectively. The static non linearity function $f(.)$ at the output is generally represented as polynomial function. The output of the WM is expressed as

$$v(n) = a_0 + a_1 y_1(n) + a_2 y_2(n)^2 + ... + a_m y_m(n)^m \tag{4.3}$$

Here, 'm' is the index of the polynomial. The goal is to find the optimum value of $y=[y_1,y_2……..,y_p]$, $r=[r_1,r_2……..,r_q]$ and $a=[a_0,a_1……,a_m]$, for a given value of $r(n)$, $c(n)$, p, q and m such that $e(n)$ is minimum [81, 86]. Once the optimum values of the parameters were determined they were substituted in equation (4.1), (4.2) and (4.3) to obtain the equivalent WM of the insulation system. In order to test the accuracy of the equivalent WM model, a statistical parameter known as goodness of fit percentage was calculated using equation (4.4)

$$fit(\%) = 100 * \left(1 - \left(\frac{|c(n) - \hat{c}(n)|^2}{|c(n) - \bar{c}(n)|^2} \right) \right) \tag{4.4}$$

Here, $c(n)$ and $\bar{c}(n)$ represents the output and the mean output of the oil-paper insulation system, respectively and $\hat{c}(n)$ denotes the output of the equivalent WM. A higher value of fit (%) in equation (4.4) signifies that the equivalent model is almost identical with the actual insulation system [81, 87]. In system identification, the choice of suitable excitation voltage as an input perturbation to the test system is very important. The design of input excitation signal is described in the following section.

4.2.3 Brief description of design of excitation signal

In the present study, a LGC waveform is used as an excitation signal for identification of oil-paper insulation system, since it offers some distinct advantages over existing broadband excitations commonly used for system identification. The detailed mathematical description of LGC waveform and its relative advantages over other broadband signals were discussed in Chapter 3. The amplitude of the LGC excitation was kept fixed at 200V, and the total duration required by the chirp waveform to cover the frequency sweep from 0.1mHz to 1kHz is 5000 seconds. In order to compare the proposed non-linear model with the conventional model, cFDS measurement was also conducted from 0.1mHz to 1Hz. The amplitude of the sine wave excitation was also kept fixed at 200V. It is to be noted here that the amplitude of the excitation voltage was kept fixed at 200V because it was observed that the oil-paper insulation system exhibits non-linear behavior when the magnitude of the applied voltage is high. Experimental results showing the non-linear dielectric response of oil-paper insulation system is presented later in section 4.5.

Along with the detailed mathematical description, the spectral property of a LGC signal was also discussed in Chapter 3 (section 3.3). It was observed from Figure 3.2 that the amplitude spectrum of the logarithmic chirp signal decreases with the increase in frequency. Now, as the transformer insulation exhibits resistive behavior at low frequencies and capacitive behavior at the higher frequencies, choosing an excitation voltage waveform having almost constant amplitude spectrum is not advantageous [76]. This is because the magnitude of the response

current then becomes very high with the increase in frequency. To eliminate this problem, amplitude scaling is generally done to reduce the magnitude of excitation voltage, as the frequency increases [76]. However, in the case of a LGC signal, due to the decaying nature of the amplitude spectrum, amplitude scaling is not required. Moreover, it was reported earlier in Chapter-3, Table 3.2, that the LGC possesses more signal energy compared to LC within the low frequency range from 0.1mHz to 0.1Hz, thereby offering a better SNR during FDS measurement at low frequencies. Therefore, a logarithmic chirp signal was chosen in this chapter as an excitation voltage for the purpose of non-linear system identification of transformer insulation.

4.2.4 Response current data acquisition

After the design of excitation signal, next step is to acquire the response current data. Along with the three samples (prepared in chapter 3) a new sample with *m.c* 4% is prepared in the laboratory for the purpose of non-linear modeling of oil-paper insulation. Table 4.1 shows the prepared samples with different paper *m.c* (%) at 30°C. This additional sample was prepared to vary the *m.c* of the samples in a wide range to have a better idea regarding the non-linear dielectric response of oil-paper insulation.

Table 4.1: Test samples with different moisture content

Sample Number	***m.c* (%)**
Sample-4	0.8
Sample-5	1.5
Sample-6	2.5
Sample-7	4.0

Along with moisture, another important factor that contributes to the non-linearity of the oil-paper insulation system is the aging state of the insulation. It has been reported in existing literature that the aged transformer insulation also manifests non-linear behavior [86]. In order to investigate whether the aging related non linearity can be characterized using WM, a separate test was conducted on an aged real-life transformer to investigate the influence of aging related non-linearity. The detail of the aged transformer tested in laboratory is given in Table 4.2.

Table 4.2: Transformer details

Rating	**Age**
Single phase, 75 kVA, 400V/50 kV	30-35 years

The applied excitation voltage and the recorded current waveforms were divided into two parts. Initial part of the database was used to develop the equivalent WM and the later part was used for the purpose of validation.

4.2.5 Non-linear dielectric response of oil-paper insulation

It is well known that the non-linearity of the oil-paper insulation system depends on the magnitude of the applied excitation voltage. In order to prove the prepared test samples indeed produce the non-linear dielectric response, the amplitude of the applied excitation voltage was initially varied from $50V_p$ to $200V_p$ in steps of $50V_p$, and for each applied voltage the corresponding response currents of the different test samples were measured. The volt ampere (V-I) characteristics (at 1mHz) of two test samples sample-4 with *m.c* (0.8%) and sample-7 with *m.c* (4.0%), respectively are shown in Figure 4.3. Besides, the measured dielectric response current waveforms for two samples

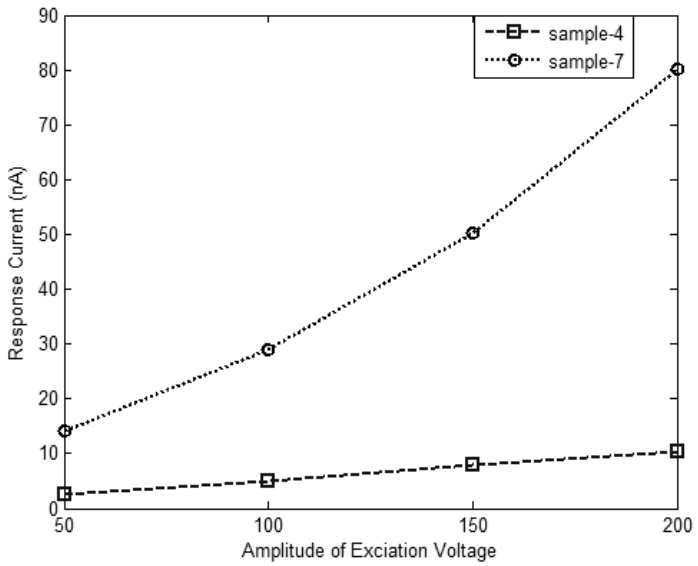

Figure 4.3. V-I characteristics of test samples

From Figure 4.3, it can be observed that the magnitude of the response current increases with the increase in magnitude of the applied excitation

voltage. For sample-4 with *m.c* (0.8%), the V-I characteristics is almost linear (satisfying superposition theorem), whereas for the wet sample, sample-7 with *m.c* 4.0%, (as the magnitude of the excitation voltage is increased), the V-I characteristics deviate from the linear one indicating that the degraded insulation can no longer can be approximated as a linear system. Another important observation is that for sample-7, the deviation from the linear characteristics starts at about 150V, indicating that the magnitude of the excitation voltage should be high to trigger the non-linear dielectric response.

Based on the experimental observations, it can be inferred that the conventional Debye model of oil-paper insulation, which assumes the insulation system to behave as pure linear dielectric, cannot be applied to the wet and degraded insulation. Therefore, a more generalized non-linear WM model of the insulation is proposed in this chapter, which can take into account both linear as well as non-linear behavior of the insulation. The determination of WM parameters for non-linear model of oil-paper insulation is discussed below.

4.2.6 Determination of model order

The determination of WM model order is the first task in successful identification of the mathematical model. Unfortunately, there was no prior information regarding the order of the system for identification of equivalent model. Therefore, in the present work, the number of zeros 'p' and poles 'q' of the discrete time transfer function $G(z)$ were determined using trial and error method. For this purpose, the value of 'p' and 'q' was varied from 1 to 5 starting from p=1, q=2 (with $p < q$). The fit (%) corresponding to each value of 'p' and 'q', was calculated using (4.4). Finally, the lowest model order was selected based on the value of 'p' and 'q' yielding best fit (%). The variation of fit (%) using different combinations of 'p' and 'q' for a particular sample (sample-7) is reported in Table 4.3.

Table 4.3: Variation of fit (%) for different values of 'p' and 'q'

'p'	**'q'**	**fit (%)**
1	2	96.25
2	3	97.82
3	4	96.54
4	5	95.47

It can be pointed out from Table 4.3, that the fit (%) initially increases with the increase in model order, but thereafter decreases. The highest fit (%) was observed for '*p*'=2 and '*q*'=3. Similar observation was also found for other three test samples. Therefore, the oil-paper insulation system was modeled using a third order system. The discrete time transfer function $G(z)$ of the insulation system can thus be represented as

$$G(z) = \frac{y_1 z^{-1} + y_2 z^{-2}}{r_o + r_1 z^{-1} + r_2 z^{-2} + r_3 z^{-3}} \tag{4.5}$$

The next task is to determine the polynomial index '*m*' of the static non-linear polynomial function at the output in equation (4.3). The order of the polynomial index was determined by varying '*m*' from 1 to 5, keeping the predetermined model order fixed at '*p*'=2 and '*q*'=3, respectively. It was observed for '*p*'=2 and '*q*'=3, the highest fit (%) was obtained for '*m*'=4. Hence, the static non-linearity at the output was modeled using a 4th order polynomial function. The output of the WM can now be expressed as

$$v(n) = a_0 + a_1 y_1(n) + a_2 y_2(n)^2 + a_3 y_3(n)^3 + a_4 y_4(n)^4 \tag{4.6}$$

After determination of WM order, the next step is to determine the coefficients of the transfer function $G(z)$ and that of the static polynomial non-linearity at the output. The variation of WM parameters with paper moisture are described below.

4.2.7 Variation of WM parameters with paper moisture

The optimum values of numerator and denominator coefficients of $G(z)$ were computed using Newton's iterative grid search algorithm [81, 109]. The variation of absolute values of numerator and denominator coefficients of $G(z)$ with paper *m.c* is reported in Tables 4.4 and 4.5.

Table 4.4: Variation of numerator coefficients with *m.c*

***m.c* (%)**	**$y_1 \times 10^{-6}$**	**$y_2 \times 10^{-6}$**
0.8	0.55	0.55
1.5	0.807	0.806
2.5	1.142	1.142
4.0	1.877	1.88

Table 4.5: Variation of denominator coefficients with *m.c*

***m.c* (%)**	r_o	r_1	r_2	r_3
0.8	1	0.3068	0.3067	0.99
1.5	1	0.3158	0.3158	0.99
2.5	1	0.3217	0.3216	0.99
4.0	1	0.3349	0.3349	0.99

It can be observed from Tables 4.4 and 4.5 that both numerator and the denominator coefficients show an increasing tend with the increment in paper *m.c*. However, the coefficients r_o and r_3 are almost insensitive to the change in *m.c*. Therefore, in comparison with denominator coefficients, the numerator coefficients are more sensitive to change in *m.c*. It can be further pointed out that the absolute values of the numerator coefficients for a fixed paper *m.c* are almost equal. Similar behavior was observed in the case of denominator coefficients too (r_1 and r_2). Now, in order to have a better understanding of the variation of transfer function coefficients with *m.c*, the numerator and denominator of equation (4.5) were multiplied by z^3. The modified discrete time transfer function *G*(z) can thus be expressed as

$$G(z) = \frac{y_1 z^2 + y_2 z^1}{r_0 z^3 + r_1 z^2 + r_2 z^1 + r_3} \tag{4.7}$$

Now, from the results presented in Tables 4.6 and 4.7, it can be observed that for the oil-paper insulation system, $y_1 \approx y_2 = y$, $r_o \approx r_3 = 1$ and $r_1 \approx r_2 = r$. The modified transfer function can therefore be written as

$$G(z) = \frac{y(z^2 + z^1)}{z^3 + r(z^2 + z^1) + 1} \tag{4.8}$$

$$= \frac{\frac{y}{r}(z^2 + z^1)}{\frac{1}{r}(z^3 + 1) + z^2 + z^1}$$

$$= \frac{\alpha(z^2 + z^1)}{\beta(z^3 + 1) + z^2 + z^1}$$

where, $\alpha = \frac{y}{r}$ and $\beta = \frac{1}{r}$. The variation of α and β with paper *m.c* for different test samples are presented in Figure 4.4.

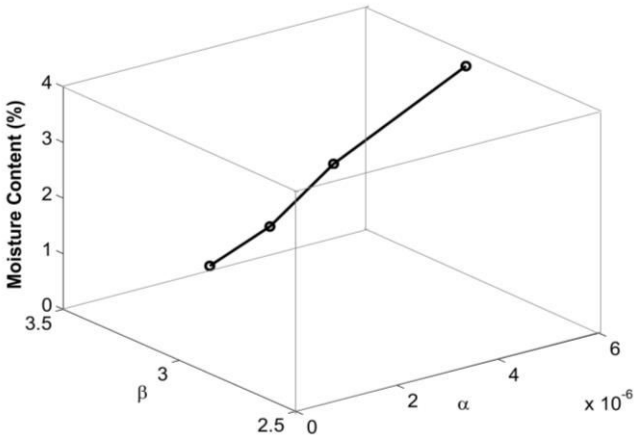

Figure 4.4: Variation of α and β with paper *m.c*

It is evident from Figure 4.4, that both α and β varies with the change in moisture content of the samples. As the paper *m.c* increases, α shows an increasing trend while a decreasing trend is observed for β. Therefore, if a large number of test samples are available, then an empirical relationship between α, β, and *m.c* can be derived from which the condition assessment of insulation system is possible.

The variation of absolute values of polynomial coefficients (for static output non-linearity) with paper *m.c* is presented in Table 4.6

Table 4.6: Variation of polynomial coefficients with *m.c*

***m.c* (%)**	$\mathbf{a_o}$	$\mathbf{a_1}$	$\mathbf{a_2}$	$\mathbf{a_3}$	$\mathbf{a_4}$
0.8	0.45	0.64	1.25	2.56	1.71
1.5	1.32	1.04	1.82	0.65	2.15
2.5	1.41	3.24	4.56	2.41	6.43
4.0	1.25	2.78	3.57	1.23	5.34

It can be observed from Table 4.6 that the polynomial coefficients of the non-linearity function also varies with the *m.c* of the test samples. However, unlike the numerator and the denominator coefficients, the polynomial

coefficients do not follow any distinct pattern with the change in *m.c*. Therefore, based on experimental results, it is not possible to establish any relationship between the polynomial coefficients with the *m.c* of the insulation.

4.3 Model validation

4.3.1 Variation of time domain dielectric response current

After determination of the model parameters, the next step in system identification is to validate the proposed model. In order to validate the proposed WM of the insulation, a section of the experimental data which was kept for the purpose of validation, was used. The time variation of the experimentally obtained dielectric response current (a section of validation data) and that obtained by WM simulation for sample-7 with *m.c*-4% is

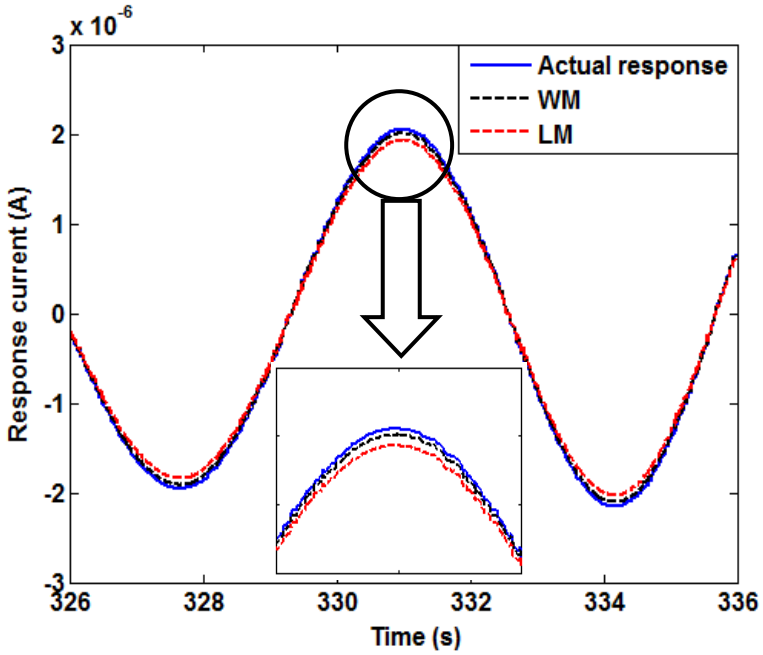

Figure 4.5: Time variation of response current (a section of validation data) computed using LM and WM

shown in Figure 4.5. Along with WM, equivalent LM response is also plotted in the same graph for the purpose of comparison. In order to simulate the equivalent LM of the oil-paper insulation system, the non-linearity function $f(.)$ at the output WM is set to 1. It can be noted from Figure 4.5, that in the case of LM, a notable deviation between simulated response current and the actual measured current data is observed, but the WM response is very close to the actual response of the insulation system. This is indicative of the fact that the non-linearity present in the oil-paper insulation system can be captured accurately by the proposed WM. The variation of the fit (%) accuracy of the validation data computed for four samples with different moisture contents evaluated using LM and WM are shown in Table 4.7.

Table: 4.7: Variation of fit (%) computed using WM and LM

m.c (%)	**LM**	**WM**
0.8	94.05	94.10
1.5	94.37	95.75
2.5	94.51	96.88
4.0	94.64	97.82

Observations from Table 4.7 reveal several interesting facts. For sample with lower *m.c* there is little difference in fit (%) between LM and the WM response, indicating that the system almost behaves almost like a LTI system and the system dynamics can be correctly modeled by LM. However, as the *m.c* increases, a significant difference in fit (%) was observed between LM and WM response. This can be explained by the fact that as the moisture content of the sample increases, non-linear characteristics of the oil-paper system are more prominent, which is not reflected in the LM response, but can be effectively characterized using WM. Another interesting observation is that with the increase in *m.c*, the WM fit (%) accuracy is also improved, indicating the fact that non linearity increases with the increase in *m.c*. Best WM fit (%) of 97.82 is obtained for sample-7 with *m.c*-4%. Thus, from the time domain response current analysis, it is conclusive that the proposed WM is capable of capturing the inherent non linearity present in the oil-paper insulation system more accurately compared to LM.

4.3.2 Frequency response analysis

The dielectric dissipation factor ($\tan\delta$) of the test samples were computed by conducting cFDS measurement and with LGC waveform from 0.1mHz to 1Hz were plotted against frequency and the variation is shown in Figure 4.6.

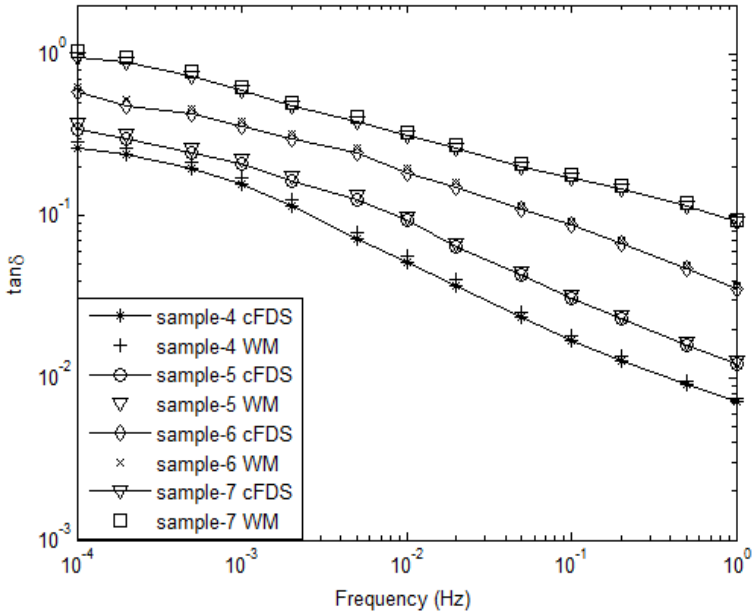

Figure 4.6: Variation of tanδ with frequency for test samples computed using WM and cFDS measurement

It can be seen from Figure 4.6, that the frequency response of the predicted WM and the actual frequency response of the test samples are consistent with each other. Besides, the values of tanδ, at each individual frequency computed using cFDS measurement and that obtained from WM almost coincides with each other, which further validate the accuracy of the proposed nonlinear WM identification for estimation of moisture present in the oil-paper insulation system.

In addition to WM, the tanδ values at each measurement frequency points from 0.1mHz to 1kHz for four test samples were also computed considering the LM of the insulation. Finally, the mean absolute *MAE* (%) percentage in tanδ (for both WM and LM) with respect to cFDS measurement is computed using equation (4.9) for all four samples.

$$MAE(\%) = \frac{1}{N}\sum_{i=1}^{N}\frac{\left|\tan\delta_{M_j} - \tan\delta_{cFDS_j}\right|}{\tan\delta_{cFDS_j}} \times 100 \tag{4.9}$$

In the above equation, $\tan\delta_{cFDS_j}$ indicates the value of tanδ value obtained from cFDS measurement by applying sine wave at j^{th} measurement frequency point within 0.1mHz to 1Hz. Similarly, tanδ_{Mi} denotes the tanδ values computed at the same frequency points from the proposed model (WM and LM) using LGC excitation voltage waveform. Here also, (N=total number of measurement frequency points) N=13, considering 3 measurement frequency points per decade.

Figure 4.7 shows the variation of *MAE* (%) in tanδ (with respect to cFDS measurement) for different test samples computed by considering both LM and WM of the insulation.

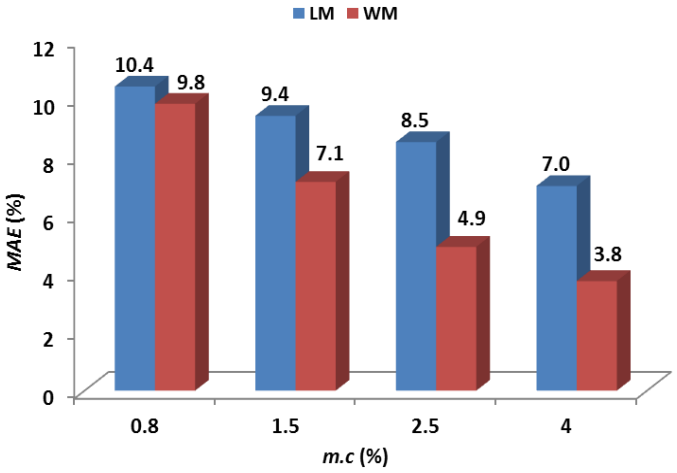

Figure 4.7: Variation of mean absolute error (*MAE*) percentage with *m.c* for LM and WM

It is evident from Figure 4.7 that the *MAE* (%) for both WM and LM is found to decrease with the increase in paper *m.c*. Moreover, between WM and LM response, *MAE* (%) is found to be lowest in the case of WM. This observation was found to be true for all test samples. For sample-4 with lowest *m.c* of 0.8%,

there is little difference in *MAE* (%) between LM and WM response which further indicates that the insulation system with less moisture behave almost like a LTI system. But as the *m.c* increases, the difference in *MAE* (%) between LM and WM also increases. For a wet insulation, sample -7 with *m.c*-4%, the *MAE* (%) in the case of WM is found to be significantly lower compared to LM indicating that the non-linear phenomenon of the wet and degraded insulation system can be better characterized using WM which was not reflected in the LM response. Therefore, based on time and frequency domain analysis on test samples, it is evident that the WM can be used as more generalized model of insulation system for reliable diagnosis of transformers. In the next section, an experiment is conducted on aged transformer insulation to verify whether the aging related non linearity can be quantified using WM.

4.3.3 Test on a real-life transformer

Figure 4.8 shows the time variation of a section of the response current data measured for an aged insulation and that obtained from the equivalent WM.

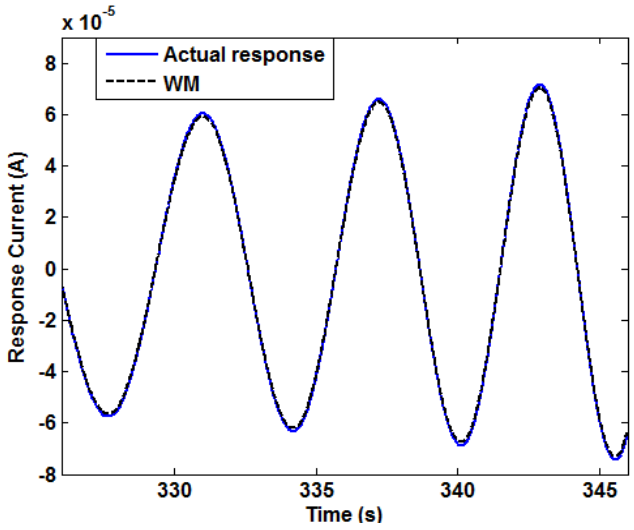

Figure 4.8: Time variation of response current (a section of validation data) of transformer insulation computed using WM

It can be seen from Figure 4.8 that the measured response current of the

transformer and the simulated WM response exactly matches with one another. A fit accuracy of 98.05% was achieved indicating that the non-linearity related to aged insulation response in time domain can also be effectively characterized using WM. It is to be mentioned here that compared to test samples, a higher model fit (%) is obtained in case of transformer insulation. This may be explained as follows. The magnitude of the measured dielectric response current in case of transformer is higher i.e. about 80 micro-ampere (see Figure 4.8) compared to the test samples which is only 2.5 micro-ampere (see Figure 4.5). Due to increased magnitude of dielectric response current, a better SNR is offered by the aged transformer insulation system, which leads to a higher fit (%) using WM. In Figure 4.9 (a) and 4.9 (b), the equivalent frequency response of the WM is compared with the frequency response of the original aged insulation derived from cFDS measurement.

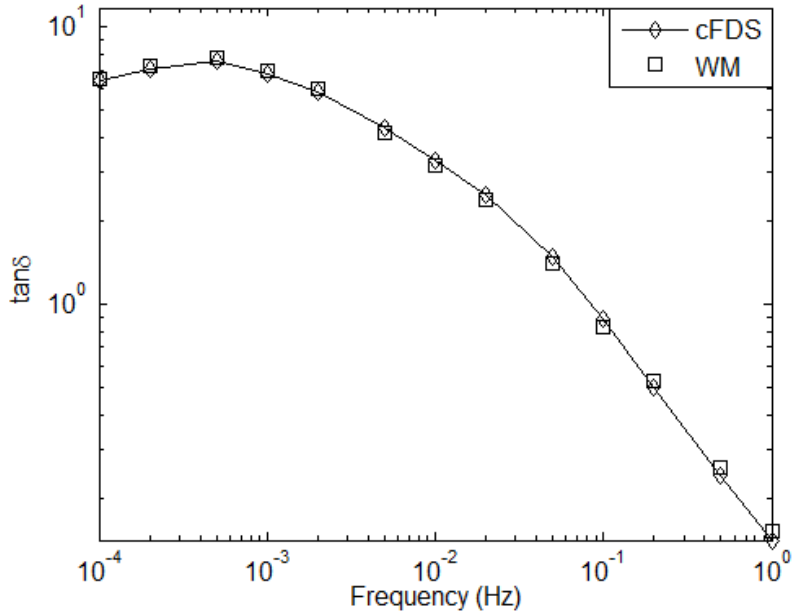

(a)

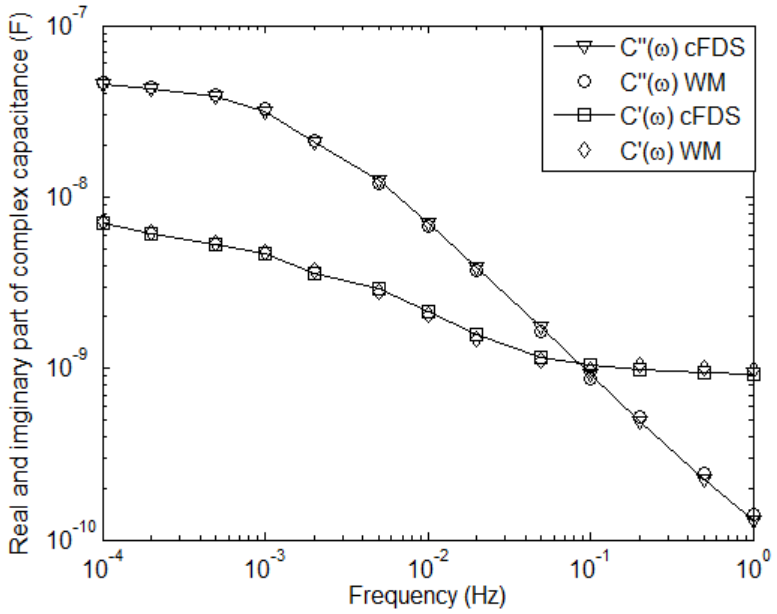

(b)

Figure 4.9: Variation of (a) tanδ (b) real and imaginary part of complex permittivity with frequency computed using WM and cFDS measurement

It is evident from Figure 4.9 (a) and Figure 4.9 (b), that the frequency response of the WM and the aged transformer insulation are also similar to each other. Moreover, tanδ, $C'(\omega)$ and $C''(\omega)$ of the transformer insulation system computed at each measurement frequency point using cFDS measurement are almost identical to that obtained by WM. Therefore, the proposed WM can also provide similar information regarding the aging status of the insulation in comparison with cFDS measurement.

4.4 Conclusions

In this chapter, a non-linear WM of oil-paper insulation system based on system identification theory is proposed for reliable diagnosis of transformer insulation. The proposed model was experimentally validated on a few laboratory prepared test samples and also on an aged insulation system of a

real-life transformer. Instead of conventional sine wave, a LGC excitation voltage was used for the purpose of experiment. The dielectric response (in both time and frequency domain) of different test samples computed from the proposed WM using chirp waveform was also compared with cFDS measurement. Besides, for better understanding of the insulation condition, separate relationships were established between the transfer function coefficients of the WM with *m.c*. The main outcomes of the experimental investigations are briefly highlighted below.

(i) The insulation system with less *m.c* behaves almost like an LTI system which can be characterized by both LM and WM. As the *m.c* increases, the non-linearity of oil-paper insulation system increases and the insulation can no longer be treated as a linear system. The non-linearity of the oil-paper insulation system due to increased moisture content can be effectively characterized using WM.

(ii) The coefficients of discrete time transfer function of the WM are sensitive to the change in paper *m.c*.

(iii) Investigations into time and frequency domain responses reveal that the proposed WM response is in well accordance with the actual response of the insulation system.

(iv) Between WM and LM, the *MAE* (%) in estimation of tanδ profile of the insulation is found to be lowest in the case of WM, indicating that the non-linear model can be implemented for reliable moisture estimation in transformers.

(v) Practical test on an aged real-life transformer insulation system also confirms the validation of the proposed WM for identification of aged oil-paper insulation system.

Hence, it can be inferred that the proposed LGC chirp signal aided non-linear WM provides very reliable information regarding the insulation condition at a significantly reduced time in comparison with the linear model. Hence, the proposed non-linear model of oil-paper insulation can be implemented for fast and reliable diagnosis of oil-paper insulation system.

Chapter 5

5. Conclusions

In this thesis, a couple of new measurement techniques to reduce FDS test time are proposed for fast and reliable assessment of condition of oil-paper insulation of transformers. All the proposed techniques were experimentally validated on several laboratory prepared test samples emulating the oil-paper insulation of a practical transformer. Besides, experiments were also conducted on a few real-life transformers to validate the practicability of the proposed measurement techniques. Experimental investigations revealed that the proposed methods can be satisfactory implemented in practice for diagnosis of transformer insulation at a significantly reduced time. A summary of the research work reported in this thesis along with advantages and limitations are given below.

A method to reduce FDS measurement duration based on regression approach was proposed for diagnosis of oil-paper insulation considering both sinusoidal and non-sinusoidal (triangular) excitation voltage waveforms. Since the oil-paper insulation exhibits resistive behavior at low frequencies and capacitive behavior at high frequencies, therefore, during FDS measurement it was observed that the dielectric response current are periodic and symmetrical in nature and are having a definite correlation with the applied voltage waveform. Therefore, instead of carrying out conventional measurement for two cycles, some fraction of one full cycle of excitation voltage at each measurement frequency was applied on the insulation and the corresponding dielectric response currents flowing through the insulation were measured. From the recorded fractional cycle response current, the complete dielectric response over two cycles was predicted using mathematical regression technique. From the knowledge of the applied excitation voltage and the predicted dielectric response currents, tanδ profile of the insulation was computed from 0.1mHz to 1Hz and the results were compared with cFDS measurement. An error band of ± 5% in estimation of tanδ value (with respect to cFDS) was fixed and it was observed that an optimum excitation span percentage of one full cycle is necessary to be applied to satisfy the error criterion. The optimum excitation span percentages were thereafter determined for both sinusoidal and triangular excitation voltage waveforms. Based on the determined optimum excitation span percentage of one full cycle, the total measurement duration was

calculated for both sinusoidal and triangular waveforms. It was observed that the proposed measurement technique based on regression approach can bring down FDS measurement time appreciably enabling transformer diagnosis to be conducted at a much shorter time compared to cFDS measurement. Besides, experimental observations also revealed that for a particular triangular excitation (Tri3) the total measurement duration was found to be somewhat lesser than the sinusoidal excitation.

Although the regression approach of FDS measurement can provide reliable information regarding the condition of oil-paper insulation at a significantly reduced time, yet from the practical measurement point of view FDS measurement using fractional excitation voltage at each measurement frequency is problematic. This is because of the presence of transients, which influence the FDS measurement, when the excitation voltage is switched on at each measurement frequency. Besides, the total FDS measurement time using regression approach also increases with the increase in number of measurement points per decade. To find a pragmatic solution to these two aforesaid problems, another new measurement technique to reduce FDS measurement time was proposed. A wideband excitation in the form of chirp signal was used to conduct FDS measurement on oil-paper insulation from 0.1mHz to 1Hz. Chirp signals having both linear and exponential frequency sweeps were designed for the purpose of experiment and FDS measurements were conducted using both type of chirp waveforms. The tanδ profile of the oil-paper insulation calculated using both type of chirp waveforms were compared with cFDS measurement. The *MAE* (%) in estimation of tanδ (with respect to cFDS) was also computed. It was observed that the *MAE* (%) decreased with the increase in *m.c* indicating that the condition of the more degraded insulation can be better estimated using chirp waveforms. Besides, it was observed that the LGC waveform offered better information regarding insulation condition offering minimum *MAE* (%) compared to LC signal. Comparative study of measurement duration with cFDS measurement revealed that the use of chirp excitations required least overall measurement time. Besides, it was also observed that in comparison with existing wideband excitations, chirp signals proposed in this chapter takes much less amount of time to cover the entire frequency range from 0.1mHz to 1Hz, thereby providing fastest FDS measurement compared to existing methods. The advantage of using chirp waveform is that since it is a non stationary excitation, the total frequency spectrum of the oil-paper insulation can be obtained from a single measurement. Therefore, it is not necessary to apply a series of excitation voltages at each individual frequency points, which eliminaties the problem of initial switching transient at each measurement

frequency. Besides, being a wideband excitation, the tanδ value can be computed at any measurement frequency from 0.1mHz to 1Hz, thereby imposing no restriction on the number of measurement frequency points per decade.

Although chirp signals provided reliable information regarding the condition of oil-paper insulation at a significantly reduced time, yet the influence of non-linearity of insulation system was not considered earlier. The insulation system of transformer exhibits non-linear behavior, which increases with the increase in degradation (*m.c* and aging) of the insulation. Therefore, the assumption that the transformer insulation behaves as a linear system may lead to incorrect information of the insulation condition, especially when the insulation is deteriorated. To address this issue, a non-linear Wiener model of oil-paper insulation system using chirp excitation was developed based on system identification theory. Experiments were conducted on different test samples by varying the paper *m.c* over a wide range. Investigations revealed that insulation with less *m.c* behaves almost like a linear system. However, as the paper *m.c* increases, the insulation tends to behave more like a non-linear system, which can be better represented by Wiener model. Besides, the coefficients of the transfer function of the Wiener model were found to be sensitive to the change in *m.c* which can be used to predict the amount of moisture present in the paper insulation. Besides, investigations into both time and frequency domain responses revealed that the Wiener model response is more close to the actual response of the insulation system. The *MAE* (%) in tanδ profile (with respect to cFDS measurement) computed using Wiener model and linear model showed that for insulation with higher *m.c*, the *MAE* (%) is minimum in the case of Wiener model compared to linear model. Therefore, in the case of degraded insulation, Wiener model provides more accurate information, which was not revealed by linear model. Experiment on the insulation of an aged real-life transformer also confirmed that the Wiener model response is in well accordance with the actual response of the insulation system, indicating that the aging related non-linearity can also be characterized by Wiener model. Therefore, the chirp signal based Wiener model of insulation can be considered a more generalized model which can be used for diagnosis of oil-paper insulation accurately at a relatively lesser amount of time.

5.1 Future Works

The measurement techniques proposed in this thesis for accelerating FDS measurement can be extended in future in different directions some of which are discussed below.

The regression approach proposed in this thesis has been experimentally validated on a few test samples with different moisture contents. However, the influence of aging on determination of optimum excitation span for different waveforms is not considered in the present work. It would be interesting to investigate the feasibility of regression approach of time reduction on samples with different aging rates and DP values. A relationship between the optimum applicable excitation span with DP value can be established in future. Besides, only triangular waveform has been considered in this thesis for the purpose of experiment. In future feasibility of using regression approach for FDS measurement time reduction using other non-sinusoidal waveforms (e.g. square wave) will also be investigated.

Similarly, in the case of chirp excitations, the influence of aging has not been taken into consideration in this thesis. In future, the *MAE* (%) in estimation of tanδ profile (with respect to cFDS) using chirp signals for samples with different aging state can be computed for better assessment of insulation condition. Moreover, the influence of measurement temperature on FDS measurement using chirp signals could also be investigated in future. Besides, only sine wave chirp signals were used for the purpose of experiment. In future, the feasibility of accelerating FDS measurement using non-sinusoidal chirp signals could also be investigated.

In the case of non-linear modeling of insulation, it was observed that the coefficients of transfer function of Wiener model were sensitive to the change in *m.c* of the samples. In future, more number of samples with different *m.c* will be prepared in order to establish a relationship between transfer function coefficients with paper *m.c* for further improving the estimation of moisture in transformer insulation. Although the influence of aging on non-linear modeling of transformer insulation was investigated for single transformer insulation, yet for better understanding further investigations are necessary before the transfer function coefficients of WM and the aging state of the insulation can be correlated. Moreover, the effect of temperature on WM identification of oil-paper insulation system is not considered in this thesis. In future work, the effect of temperature related non-linearity of oil-paper

insulation system could be investigated in order to develop a more robust model for fast and reliable determination of oil-paper insulation system condition.

References

[1] T. K. Saha, "Review of modern diagnostic techniques for assessing insulation condition in aged transformers," IEEE Transaction on Dielectric and Electrical Insulation, vol. 10, no. 5, pp. 903-917, 2003.

[2] X. Yang, "Enhancements to dielectric response measurements of oil-paper insulation for online and offline applications," Phd Thesis, Queensland University of Technology, Australia, 2015.

[3] M. Wang, A.J. Vandermaar and K.D. Srivastava, "Review of condition assessment of power transformers in service", IEEE Electrical Insulation Magazine, vol.18, no.6, pp.12–25, 2002.

[4] D. Linhjell, L. Lundgaard and U. Gafvert, "Dielectric response of mineral oil impregnated cellulose and the impact of aging", IEEE Transactions on Dielectrics and Electrical Insulation, vol. 14, no. 1, pp. 156-169, 2007.

[5] I. Fofana, H. Hemmatjou, F. Meghnefi, M. Farzaneh, A. Setayeshmehr, H. Borsi and E. Gockenbach, "On the Frequency Domain Dielectric Response of Oil-paper Insulation at Low Temperatures", IEEE Transactions on Dielectrics and Electrical Insulation, vol. 17, no. 3, pp. 799-807, 2010.

[6] IS-335:1993, Fourth Revision "New Insulating Oils-Specification", Indian Standard 1993.

[7] M. Schaible, "Electrical insulating papers–an overview", IEEE Electrical Insulation Magazine, vol.3, no.1, pp.8–12, 1987.

[8] T. V. Oommen and L. N. Arnold, ''Cellulose Insulation Materials Evaluated by Degree of Polymerization Measurements'', Proceedings of 15th IEEE Electrical and Electronics Insulation Conference (EIC), Chicago, IL, USA, pp. 257261, 1981.

[9] A. K. Pradhan, "Condition Monitoring of Transformer Insulation by Frequency Domain Spectroscopy using Non-sinusoidal Excitation", Phd Thesis, Jadavpur University, Kolkata, India, 2016.

[10] M. Duval, "A review of faults detectable by gas-in-oil analysis in transformers", IEEE Electrical Insulation Magazine, vol. 18, no.8, pp.8-17, 2002.

[11] T. K. Saha and P. Purkait, "Transformer Ageing: Monitoring and Estimation Techniques", (1st Edition) John Wiley and Sons, 2017.

[12] N. Lelekakis, J. Wijaya, D. Martin, and D. Susa, "The effect of acid accumulation in power-transformer oil on the aging rate of paper insulation", IEEE Electrical Insulation Magazine, vol. 30, no. 3, pp. 19-26, 2014.

[13] Y. Du, M. Zahn, B. C. Lesieutre, A. V. Mamishev and S. R. Lindgren, "Moisture equilibrium in transformer paper-oil systems", IEEE Electrical Insulation Magazine, vol. 15, no. 1, pp. 11-20, 1999.

[14] D. J. T. Hill, T. T. Le, M. Darveniza and T.K. Saha, "A study of the degradation of cellulosic insulation materials in a power transformer. Part III: Degradation products of cellulose insulation paper", Polymer Degradation and Stability, vol. 51, no. 2, pp. 211-218, 1996.

[15] D .H. Shroff and W. Stannett, "A review of paper aging in power transformers", IEE proceedings C-Generation, Transmission and Distribution, vol.132, no.6, pp.312-319, 1985.

[16] T. V. Oommen and T. A. Prevost, "Cellulose insulation in oil-filled power transformers: part II maintaining insulation integrity and life," IEEE Electrical Insulation Magazine, vol. 22, no. 2, pp. 5-14, 2006.

[17] S. Chakravorti, D. Dey and B. Chatterjee," Recent Trends in the Condition Monitoring of Transformers-Theory, Implementation and Analysis", (1st Edition) Springer-Verlag London, 2013.

[18] A. M. Emsley, X. Xiao, R. J. Heywood and M. Ali, "Degradation of cellulosic insulation in power transformers. Part 3: effects of oxygen and water on ageing in oil", IEE Proceedings-Science, Measurement and Technology, vol. 147, no. 3, pp. 115-119, 2000.

[19] M. Mirzaie, A. Gholamil and H. Tayyebi, "Thermal degradation of cellulose paper insulation in power transformers", Proceedings of

IEEE International Conference on Solid Dielectrics, ICSD '07, Winchester, UK, July 8–13, pp. 673–676, 2007.

[20] L. E. Lundgaard, W. Hansen, D. Linhjell and T. J. Painter, "Aging of oil-impregnated paper in power transformers", IEEE Transactions on Power Delivery, vol.19 no.1, pp. 230–239, 2004.

[21] I. Hohlein and A. J. Kachler, "Aging of cellulose at transformer service temperatures. Part 2. Influence of moisture and temperature on degree of polymerization and formation of furanic compounds in free-breathing systems," IEEE Electrical Insulation Magazine, vol. 21, no. 5, pp. 20-24, 2005.

[22] D. Martin, C. Perkasa and N. Lelekakis, "Measuring Paper Water Content of Transformers: A New Approach Using Cellulose Isotherms in Non equilibrium Conditions," IEEE Transactions on Power Delivery, vol. 28, no. 3, pp. 1433-1439, 2013.

[23] R. J. Liao, M. Z. Zhu, L. J. Yang, X. Zhou and C. Y. Gong, "Molecular dynamics study of water molecule diffusion in oil–paper insulation materials", Physica B: Condensed Matter, vol. 406, no. 5, pp. 1162-1168, 2011.

[24] Y. Du, M. Zahn, B. C. Lesieutre, A. V. Mamishev and S. R. Lindgren, "Moisture equilibrium in transformer paper-oil systems", IEEE Electrical Insulation Magazine, vol. 15, no. 1, pp. 11-20, 1999.

[25] IEEE Std. C57.104-2008 (Revision of IEEE Std. C57.104-1991). "IEEE Guide for the Interpretation of Gases Generated in Oil-Immersed Transformers".

[26] IEC 60567 Ed. 4.0 (Bilingual 2011). "Oil-filled electrical equipment – Sampling of gases and analysis of free and dissolved gases– Guidance".

[27] IEC 60599 Ed. 2.1 (Bilingual 2007). "Mineral oil-impregnated electrical equipment in service–Guide to the interpretation of dissolved and free gases analysis".

[28] A. de Pablo, "Gassing in mineral insulating oils. Abnormal hydrogen production", CIGRE Task Force 15/12-01-11, 2001.

[29] M. Duval and J. Dukarm, "Improving the reliability of transformer gas in oil analysis", IEEE Electrical Insulation Magazine, vol.21, no 4, pp.21-27, 2005.

[30] A. M. Emsley and G. C. Stevens, "Review of chemical indicators of degradation of cellulosic electrical paper insulation in oil-filled transformers", IEE Proceedings, Science Measurement Technology vol.141, no.5, pp.324–334, 1994.

[31] IEC 60450:2004. "Measurement of the average viscometric degree of polymerization of new and aged cellulosic electrically insulating materials".

[32] ASTM D 4243. "Standard Test Method for Measurement of Average Viscometric Degree of Polymerization of New and Aged Electrical Papers and Boards".

[33] I.A.R Gray, "A guide to transformer oil analysis", pp. 1-12, 2009. https://www.satcs.co.za/Transformer_Oil_Analysis.pdf.

[34] A. M. Emsley and G. C. Stevens, "A reassessment of the low temperature thermal degradation of cellulose", Proceedings of 6th IEEE International Conference on Dielectric Materials, Measurements and Applications, Manchester, UK, pp. 229–232,1992.

[35] T. B. Zhilyaev, L. S. Linova, V. N. Granovskaya and N. I. Golovan, "Investigation of ageing of cellulose electrical insulation materials in transformer oil", Electrotechnika, vol. 54, no.10, pp.74–77, 1983.

[36] W. J. Mcnutt, G .H. Kaufmann, A. P. Vitols and J. D. Mcdonald, "Short-time failure mode considerations associated with power transformer overloading", IEEE Transactions on Power Apparatus and Systems, vol.99, no. 3, pp.1186-1197, 1980.

[37] J. Unsworth and F. Michell, "Degradation of electrical insulation paper monitored by high performance liquid chromatography", IEEE Transactions on Electrical Insulation, vol. 25, no.4, pp.737–746, 1990.

[38] A. M. Emsley, X. Xiao, R. J. Heywood and M. Ali, "Degradation of cellulosic insulation in power transformers. Part 2: formation of furan products in insulating oil", IEE Proceedings, Science Measurement and Technology, vol.147, no.3, pp.110–114, 2000.

[39] IEC 61198: "Mineral Insulating Oils - Methods for the Determination of 2-Furfural and Related Compounds".

[40] R. Blue, D. Uttamchandani and O. Farish, "The determination of FFA concentration in transformer oil by fluorescence measurements", IEEE Transactions on Dielectrics and Electrical Insulation, vol.5, no.6, pp. 892–895, 1998.

[41] R. D. Stebbins, D. S. Myers and A. B. Shkolnik, "Furanic compounds in dielectric liquid samples: review and update of diagnostic interpretation and estimation of insulation ageing" Proceedings of IEEE 7th International Conference on Properties and Applications of Dielectric materials (ICPADM), vol 3, pp. 921–925, Nagoya, Japan, 2003.

[42] Z. Poniran and Z. A. Malek, "Life assessment of power transformers via paper ageing analysis", Proceedings of IEEE International Conference on Power Engineering, Setubal, Portugal, pp. 460–465, 2007.

[43] I. Chendong, "Monitoring paper insulation ageing by measuring furfural contents in oil", Proceedings of 7th International Symposium on High Voltage Engineering (ISH), Dresden, Germany, 1991.

[44] CIGRE Brochure 494. "Furanic Compounds for Diagnosis Working Group (D1.01.Task Force 13), April 2012.

[45] IEEE Std. 62-1995 (Revision of IEEE Std. 62-1978). "IEEE Guide for Diagnostic Field Testing of Electric Power Apparatus Part 1: Oil Filled Power Transformers, Regulators, and Reactors".

[46] IEEE Std. 43-2000 (2000). "IEEE recommended practice for testing insulation resistance of rotating machinery".

[47] ASTM D D150-11. “Standard Test Methods for AC Loss Characteristics and Permittivity (Dielectric Constant) of Solid Electrical Insulation”.

[48] W.S. Zaengl, “Dielectric spectroscopy in time and frequency domain for power equipment - theoretical considerations”, IEEE Electrical Insulation Magazine, vol. 19, no. 5, pp. 5-19, 2003.

[49] W. S. Zaengl, "Dielectric Spectroscopy in Time and Frequency Domain for HV Power Equipment (Transformers, Cables etc.)", Proceedings of 12th International Symposium on High Voltage Engineering (ISH), Bangalore, India, 2001.

[50] M. Gubanski, P. Boss, G. Csepes, V.D. Houhanessian, J. Filippini, P. Guuinic, U. Gafvert, V. Karius, J. Lapworth, G. Urbani, P. Werelius and W. S. Zaengl, “Dielectric Response Methods for Diagnostics of Power Transformers” CIGRE Task Force 15.01, Technical Brochure 254, Paris, 2004.

[51] T. K. Saha, "Review of Time-Domain Polarization Measurements for Assessing Insulation Condition in Aged Transformers", IEEE Transactions on Power Delivery, vol. 18, no. 4, pp. 1293-1301, 2003.

[52] M. Koch, "Reliable moisture determination in power transformers”, Ph.D. Thesis, Institute of energy transmission and high voltage engineering (IEH), University of Stuttgart, Germany, 2008.

[53] T. K. Saha and P. Purkait, “Investigation of polarization and depolarization current measurements for the assessment of oil–paper insulation of aged transformers”, IEEE Transactions on Dielectrics and Electrical Insulation, vol. 11 no.1, pp.144–154, 2004.

[54] T. Leibfried and A.J. Kachler, “Insulation diagnostics on power transformers using the polarisation and depolarisation current (PDC) analysis”, Proceedings of IEEE International Symposium on Electrical Insulation, Boston, USA, pp. 170–173, 2002.

[55] U. Gafvert, L. Adeen, M. Tapper, P. Ghasemi and B. Jonsson, “Dielectric spectroscopy in time and frequency domain applied to diagnostics of power transformers", Proceedings of the 6th IEEE

International Conference on Properties and Applications of Dielectric Materials, Xi'an, China, 2000.

[56] I. Fofana and Y. Hadjadj, "Electrical-Based Diagnostic Techniques for Assessing Insulation Condition in Aged Transformers", Energies, vol.9,679, pp.1-26, 2016.

[57] T. K. Saha, P. Purkait and F. Muller, "Deriving an Equivalent Circuit of Transformers Insulation for Understanding the Dielectric Response Measurements", IEEE Transactions on Power Delivery, vol. 20, no. 1, pp.149-157, 2005.

[58] M. Koch, S. Tenbohlen, M. Kruger and A. Kraetge, "Improved Moisture Analysis of Power Transformer using Dielectric Response Methods", (MatPost07) Proceedings of 3rd European Conference on HV and MV Substation Equipment, Lyon, France, 2007.

[59] I. Fofana, H. Hemmatjou and M. Farzaneh, "Low Temperature and Moisture Effects on Polarization and Depolarization Currents of Oil-Paper Insulation", Electric Power Systems Research, vol. 80, pp. 91–97, 2010.

[60] V. Der Houhanessian, "Measurement and Analysis of Dielectric Response in Oil-Paper Insulation Systems", Ph. D. Dissertation, No. 12832, ETH Zurich, Switzerland,1998.

[61] T. K. Saha and P. Purkait, "Investigations of temperature effects on the dielectric response measurements of transformer oil–paper insulation system", IEEE Transactions on Power Delivery, vol.23, no.1, pp. 252–260, 2008.

[62] G. Csepes, I. Hamos, R. Brooks and V. Karius, "Practical foundations of the RVM (recovery voltage method) for oil paper insulation diagnosis", IEEE Annual Report–Conference on Electrical Insulation and Dielectric Phenomena (CEIDP), pp. 345–355. Atlanta, USA, 1998.

[63] T. K. Saha and P. Purkait, "Investigation of an Expert System for the Condition Assessment of Transformer Insulation Based on Dielectric

Response Measurements", IEEE Transactions on Power Delivery, vol. 19, no.3, pp. 1127-1134, 2004.

[64] A. Kozlovskis and J. Rozenkrons, “Temperature dependence of return voltage characteristics”, IEEE Transactions on Power Delivery, vol.14, no.3, pp.705–708, 1999.

[65] M. Hassig, R. Braunlich, R. Gysi, J. J. Alff, V. Der Houhanessian and W. S. Zaengl, “On-site applications of advanced diagnosis methods for quality assessment of insulation of power transformers,” Proceedings of IEEE International Conference on Electrical Insulation and Dielectric Phenomena (CEIDP), Kitchener, Canada, pp. 441–447, 2001.

[66] C. Ekanayake, “Application of Dielectric Spectroscopy for Estimating Moisture Content in Power Transformers", Thesis for the Degree of Licentiate of Engineering, Chalmers University of Technology, Goteborg, Sweden, 2003.

[67] D. Linhjell, O. L. Hestad, U. Gafvert and L. E. Lundgaard, “Dielectric Response of Oil-impregnated Cellulose from 0.1 mHz to 3 MHz", Proceedings of IEEE International Conference on Dielectric Liquids (ICDL), Coimbra, Portugal, 2005.

[68] C. Ekanayake, S. M. Gubanski, A. Graczkowski and K. Walczak, “Frequency response of oil impregnated pressboard and paper samples for estimating moisture in transformer insulation”, IEEE Transactions on Power Delivery, vol. 21, no.3, pp.1309–1317, 2006.

[69] J. Blennow, C. Ekanayake, K. Walczak, B. Garcia and S. M. Gubanski, “Field experiences with measurements of dielectric response in frequency domain for power transformer diagnostics”, IEEE Transactions on Power Delivery, vol.21, no.2, pp. 681–688, 2006.

[70] M. Jaya, T. Leibfried and M. Koch, “Information within the dielectric response of power transformers for wide frequency ranges”, Proceedings of IEEE International Symposium on Electrical Insulation (ISEI), San Diego, USA, 2010.

[71] "IDAX300/350 and IDAX5.0 User's manual", Megger, Sweden, 2013.

[72] M. Koch and T. Prevost, "Analysis of Dielectric Response Measurements for Condition Assessment of Oil-Paper Transformer Insulation", IEEE Transactions on Dielectrics and Electrical Insulation, vol. 19, no. 6, pp. 1908-1915, 2012.

[73] A. Seytashmehr, I. Fofana, C. Eichler, A. Akbari, H. Borsi and E. Gockenbach, "Dielectric Spectroscopic Measurements on Transformer Oil-Paper Insulation under Controlled Laboratory Conditions", IEEE Transactions on Dielectrics and Electrical Insulation, vol. 15, no. 4, pp. 1100-1111, 2008.

[74] A. K. Pradhan, B. Chatterjee and S. Chakravorti, "Effect of Temperature on Frequency Dependent Dielectric Parameters of Oil-paper Insulation under Non-sinusoidal Excitation", IEEE Transactions on Dielectrics and Electrical Insulation, vol. 21, no. 2, pp. 653-661, 2014.

[75] DIRANA Brochure, "Dielectric response analysis and moisture in oil-paper dielectrics", OMICRON L2277, 2016.

[76] M. Jaya, D. Geißler and T. Leibfried, "Accelerating Dielectric Response Measurements on Power Transformers—Part I: A Frequency-Domain Approach", IEEE Transactions on Power Delivery, vol. 28, no. 3, pp. 1469–1473, 2013.

[77] M. S. Jaya, D. Geissler and T. Leibfried, "Accelerating Dielectric Response Measurements on Power Transformers-Part-II: A Regression Approach", IEEE Transactions on Power Delivery, vol. 29, no. 5, pp. 2095-2100, 2014.

[78] D. Dey, B. Chartterjee, S. Chakravorti and S. Munshi, "Hybrid Filtering Scheme for Proper Denoising of Real-Time Data in Dielectric Spectroscopy", IEEE Transactions on Dielectrics and Electrical Insulation, vol. 14,no.5, pp. 1323-1331, 2007.

[79] W. S. Zaengl, "Applications of dielectric spectroscopy in time and frequency domain for HV power equipment", IEEE Electrical Insulation Magazine, vol. 19, no. 6, pp. 9-22, 2003.

[80] B. Sonerud, T. Bengtsson, J. Blennow and S. M. Gubanski, “Dielectric Response Measurements Utilizing Semi-Square Voltage Waveforms", IEEE Transactions on Dielectrics and Electrical Insulation, vol. 15, no.4,pp. 920-926, 2008.

[81] A. K. Pradhan, C. Koley, B. Chatterjee and S. Chakravorti, “Non-linear modeling of oilpaper insulation for condition assessment using non-sinusoidal excitation”, IEEE Transactions on Dielectrics and Electrical Insulation, vol.22, no.4, pp. 2165–2175, 2015.

[82] A. K. Pradhan, B. Chatterjee and S. Chakravorti, “Estimation of Paper Moisture Content based on Dielectric Dissipation Factor of Oil-paper Insulation under Non-sinusoidal Excitations", IEEE Transactions on Dielectrics and Electrical Insulation, vol. 22, no. 2, pp. 822-830, 2015.

[83] A. K. Pradhan, C. Koley, B. Chatterjee and S. Chakravorti, “Determination of Optimized Slope of Triangular Excitation for Condition Assessment of Oil-paper Insulation by Frequency Domain Spectroscopy", IEEE Transactions on Dielectrics and Electrical Insulation, vol.23, no. 3, pp. 1303-1312, 2016.

[84] B. Sonerud, T. Bengtsson, J. Blennow and S. M. Gubanski, "High and low voltage dielectric response measurements utilizing arbitrarily shaped waveforms", International Symposium on High Voltage Engineering (ISH), Ljubljana, Slovenia, 2007.

[85] S.D.Nielsen, and G. F. Ledwich, "Non-linear effects in dielectric response measurements on oil paper insulated power transformers" Proceedings of IEEE International Conference on Properties and Applications of Dielectric Materials (ICPADM), Sydney, Australia, pp. 72-75, 2015.

[86] X.Yang, S.Nielsen and G.Ledwich, “Frequency Domain Spectroscopy Measurements of Oil-paper Insulation for Energized Transformers”, IEEE Transactions on Dielectrics and Electrical Insulation, vol. 24, no. 3, pp.1657-1664, 2017.

[87] L.Yang, J. Chen, J. Gao, H. Zheng and Y.Li, "Accelerating frequency domain dielectric spectroscopy measurements on insulation of

transformers through system identification", IET, Science Measurement and Technology, vol. 12, no.2, pp. 247-254, 2018.

[88] U. Gafvert, L. Adeen, M. Tapper, P. Ghasemi and B. Jonsson, "Dielectric Spectroscopy in Time and Frequency Domain Applied to Diagnostics of Power Transformers", Proceedings of 6th IEEE International Conference on Properties and Applications of Dielectric Materials,(ICPADM), Xi'an, China, 2000.

[89] S. Chatterjee, A.K. Pradhan, B. Chatterjee and S. Chakravorti, "Reducing Frequency Domain Spectroscopy Measurement Time for Condition monitoring of Oil-Paper Insulation using Non-sinusoidal Excitations", IET Science, Measurement & Technology, vol.11, no.2, pp. 204–212, 2017.

[90] B. Garcia, J. C. Burgos, A. M. Alonso and J. Sanz, "A moisture-in-oil model for power transformer monitoring - Part II: Experimental verification," IEEE Transactions on Power Delivery, vol. 20, no. 2, pp. 1423-1429, 2005.

[91] D. R. Askeland and P. P. Phul, "The Science and Engineering of Materials", 5th edition, Thomson, Toronto, Canada. ISBN 0-534-55396-6, 2006.

[92] K. G. Budinski and M. K. Budinski, "Engineering Materials: Properties and Selection", (9th edition), Prentice Hall, Upper Saddle River, New Jersey, USA. ISBN-10:0137128428, ISBN-13: 9780137128426, 2009.

[93] W. D. Callister, "Materials Science and Engineering: An Introduction" (8th edition) John Wiley and Sons, New York, USA. ISBN 978-0-470-41997-7, 2010.

[94] J. G. Powles, "Dielectric Relaxation and the Internal Field", Journal of Chemical Physics, vol. 21, no. 4, pp. 633-637, 1953.

[95] N. R. Draper and H. Smith. "Applied Regression Analysis." Wiley Series in Probability and Statistics; 1998.

[96] U. Pliquett, "Time –Domain based impedance measurement: strengths and drawbacks", Journal of Physics: Conference Series 434, 2013.

[97] S. Chatterjee, A.K. Pradhan, B. Chatterjee and S. Chakravorti, "An Advanced Technique for Frequency Domain Spectroscopy of Oil-paper Insulation at Reduced Time using Triangular Excitation", Proceedings of 1st IEEE International Conference on Energy, Economics and Environment, Noida, India, 2015.

[98] A. K. Pradhan, B. Chatterjee, D. Dey and S. Chakravorti, "Time Growing Frequency Sweep Signal based Insulation Condition Monitoring for Time Reduction in Frequency Domain Spectroscopy ", IEEE Transactions on Dielectrics and Electrical Insulation, vol. 23, no. 4, pp. 1898-1906, 2016.

[99] M. Min, U. Pliquett, T. Nacke, A. Barthel, P. Annus and R. Land, "Broadband excitation for short-time impedance spectroscopy", Physiological Measurement, vol.29, no.6, pp.185–192, 2008.

[100] B. Sanchez, G. Vandersteen, R. Bragos and J. Schoukens, "Basics of broadband impedance spectroscopy using periodic excitations", Measurement Science and Technology, vol. 23, no. 10, pp. 105501-1–105501-14, 2012.

[101] J. G. Proakis and D. G. Manolakis, "Digital signal processing, Principles algorithms and applications", (3rd edition.).Prentice-Hall, New Delhi, India 1997.

[102] S. Chatterjee, S. Dalai, S. Chakravorti and B. Chatterjee "Use of Chirp Excitations for Frequency Domain Spectroscopy Measurement of Oil-paper Insulation," IEEE Transactions on Dielectrics and Electrical Insulation, vol.25, no.2, pp. 1103–1111, 2018.

[103] M. Koch and M. Krüger, "A fast and reliable dielectric diagnostic method to determine moisture in power transformers", Proceedings of IEEE International Conference on Condition Monitoring and Diagnosis (CMD), Beijing, China, 2008.

[104] S. Chatterjee, S. Dalai, B. Chatterjee and S. Chakravorti, "A Method to Reduce FDS Measurement Time Using Logarithmic Chirp

Excitation Voltage", Proceedings of 3rd IEEE International Conference on Condition Assessment Techniques in Electrical Systems (CATCON), Rupnagar, Punjab, India, pp.248-252,2017.

[105] S. Ojha, P. Purkait and S. Chakravorti "An attempt to identify temperature dependent non-linear insulation characteristics from dielectric response measurement", Proceedings of 16th IEEE National Power Systems Conference (NPSC), Hyderabad, India, December, 2010.

[106] S. Ojha, P. Purkait and S. Chakravorti, "An attempt to identify voltage related non-linearities of transformer insulation from dielectric response measurements", Proceedings of IEEE Region 10 Conference, (TENCON), Bali, Indonesia, 2011.

[107] A. D. Ashkezari, H. Ma, T.K. Saha, and C. Ekanayake, "Investigation of non-linearity in dielectric response measurements for transformer insulation diagnosis", Proceedings of IEEE Innovative Smart Grid Technologies Asia (ISGT), Perth, Australia, pp. 1-7, 2011.

[108] D. Zhang, H. Zhao, J. Zhan, K. Tang, X. Sun, W. He, C. Niu, H. Mu and G. Zhang, "A non-linear phenomenon in dielectric response used for insulation diagnosis of oil-immersed paper", Proceedings of 12th International Conference on the Properties and Applications of Dielectric Materials (ICPADM), Xi'an, China May, 2018.

[109] L. Ljung, "System Identification: Theory for the User", (2nd edition). Prentice-Hall, Inc., New Jersey, 1999.

[110] D. Wang and F. Ding, "Least squares based and gradient based iterative identification for Wiener nonlinear systems", Signal Processing, vo.91, no.5, pp.1182-1189, 2011.

Appendix

Variation of dielectric dissipation factor for different triangular waveforms

In this section, the variation of dielectric dissipation factor (tanδ) with frequency for different triangular waveforms (as described in Chapter 2), for three test samples is shown. The tanδ values for Tri1, Tri2, Tri4 and Tri5 waveforms were initially computed by applying respective triangular excitation voltages for two full cycles from 0.1mHz to 1Hz. Following this, the dissipation factors for three test samples were recalculated by applying optimum excitation span percentages (as determined in Table 2.4, Chapter 2) for different triangular waveforms. The variation of tanδ with frequency for Tri1, Tri2, Tri4 and Tri5 waveforms are shown in Figures A.1, A.2, A.3 and A.4, respectively.

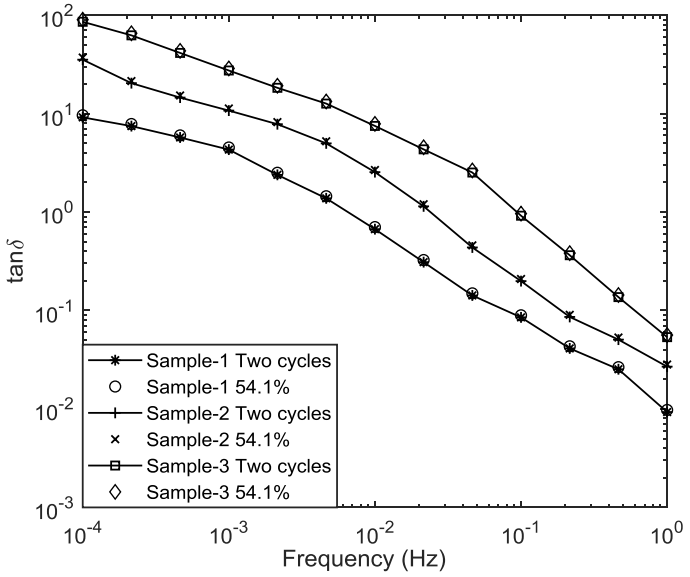

Figure A.1 Variation of tanδ with frequency for Tri1 excitation

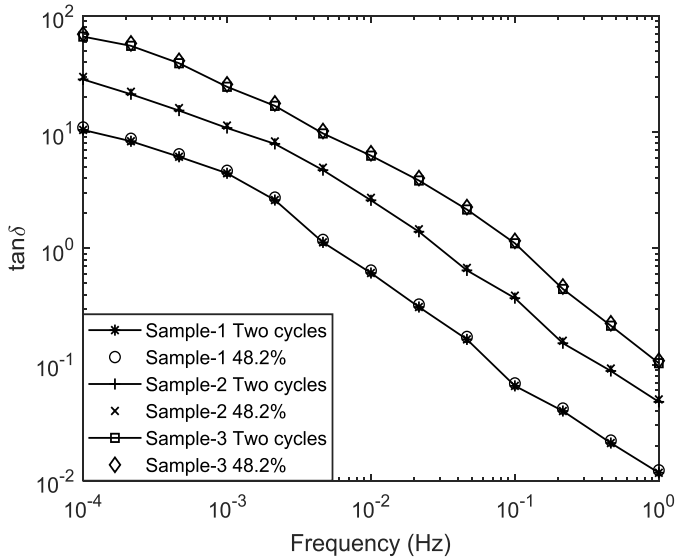

Figure A.2 Variation of tanδ with frequency for Tri2 excitation

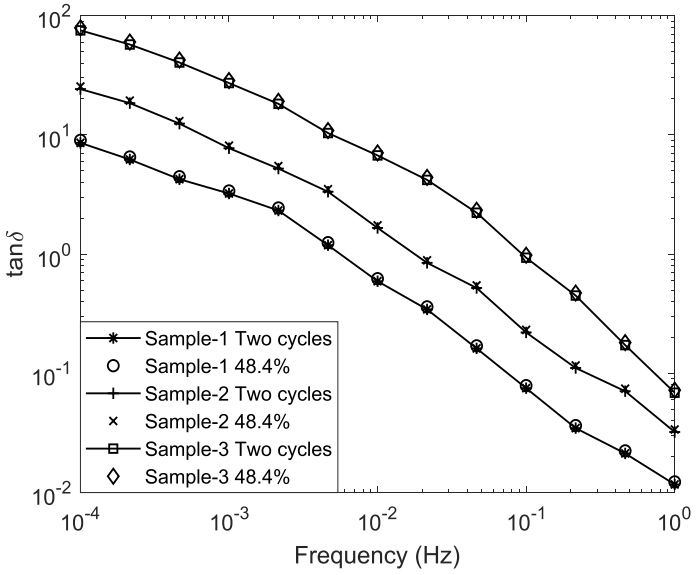

Figure A.3 Variation of tanδ with frequency for Tri4 excitation

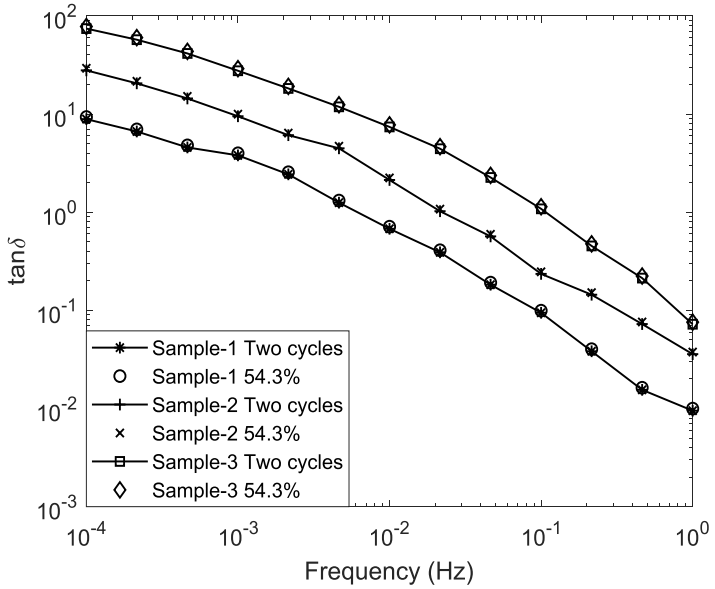

Figure A.4 Variation of tanδ with frequency for Tri5 excitation

It can be observed from Figures A.1, A.2, A.3 and A.4 that the tanδ for different triangular waveforms obtained by applying applicable excitation span percentage of one full cycle, almost coincides with that obtained by using two full cycles of excitation voltage. Hence, it can be inferred that the condition of the oil-paper insulation can be accurately monitored by applying fractional excitation span percentage instead of two full cycles, thereby saving a substantial amount of measurement time enabling transformer diagnosis to be conducted much quicker compared to conventional measurement.